Capacity Analysis in Different Systems Exploiting Mobility of VANETs

by

Miao Wang

A thesis
presented to the University of Waterloo
in fulfillment of the
thesis requirement for the degree of
Doctor of Philosophy
in
Electrical and Computer Engineering

Waterloo, Ontario, Canada, 2015

I hereby declare that I am the sole author of this thesis. This is a true copy of the thesis, including any required final revisions, as accepted by my examiners.

I understand that my thesis may be made electronically available to the public.

Abstract

Improving road safety and traffic efficiency has been a long-term endeavor for not only government but also automobile industry and academia. After the U.S. Federal Communication Commission (FCC) allocated a 75 MHz spectrum at 5.9 GHz for vehicular communications, the vehicular ad hoc network (VANET), as an instantiation of the mobile ad hoc network (MANET) with much higher node mobility, opens a new door to combat the road fatalities. In VANETs, a variety of applications ranging from safety related (e.g. emergency report, collision warning) to non-safety-related (e.g. infotainment and entertainment) can be enabled by vehicle-to-vehicle (V2V) and vehicle-to-roadside (V2R) communications. However, the flourish of VANET still hinges fully understanding and managing the challenges that the public concerns, for example, capacity and connectivity issues due to the high mobility of vehicles.

In this thesis, we investigate how vehicle mobility can impact the performance in three important VANET-involved systems, i.e., pure VANET, VANET-enhanced intelligent transportation systems (ITS), and fast electric vehicle (EV) charging systems. First, in pure VANET, our work shows that the network data-traffic can be balanced and the network throughput can be improved with the help of the vehicle mobility differentiation. Furthermore, leveraging vehicular communications of VANETs, the mobility-aware real-time path planning can be designed to smooth the vehicle traffic in an ITS, through which the traffic congestion in urban scenarios can be effectively relieved. In addition, with the consideration of the range anxiety caused by mobility, coordinated charging can provide efficient charging plans for electric vehicles (EVs) to improve the overall energy utilization while preventing an electric power system from overloading. To this end, we try to answer the following questions:

Q1) How to utilize mobility characteristics of vehicles to derive the achievable asymptotic throughput capacity in pure VANETs?

Q2) How to design path planning for mobile vehicles to maximize spatial utility based on mobility differentiation, in order to approach vehicle-traffic capacity in a VANET-enhanced

ITS?

Q3) How to develop the charging strategies based on mobility of electric vehicles to improve the electricity utility, in order to approach load capacities of charging stations in VANET-enhanced smart grid?

To achieve the first objective, we consider the unique features of VANETs and derive the scaling law of VANETs throughput capacity in the data uploading scenario. We show that in both free-space propagation and non-free-space propagation environments, the achievable throughput capacity of individual vehicle scales as $\Theta(\frac{1}{\log n})$[1] with n denoting the population of a set of homogenous vehicles in the network. To achieve the second objective, we first establish a VANET-enhanced ITS, which incorporates VANETs to enable real-time communications among vehicles, road side units (RSUs), and a vehicle-traffic server in an efficient way. Then, we propose a real-time path planning algorithm, which not only improves the overall spatial utilization of a road network but also reduces average vehicle travel cost for avoiding vehicles from getting stuck in congestion. To achieve the third objective, we investigate a smart grid involved EV fast charging system, with enhanced communication capabilities, i.e., a VANET-enhanced smart grid. It exploits VANETs to support real-time communications among RSUs and highly mobile EVs for real-time vehicle mobility information collection or charging decision dispatch. Then, we propose a mobility-aware coordinated charging strategy for EVs, which not only improves the overall energy utilization while avoiding power system overloading, but also addresses the range anxieties of individual EVs by reducing the average travel cost.

In summary, the analysis developed and the scaling law derived in $Q1$ of this thesis is practical and fundamental to reveal the relationship between the mobility of vehicles and the network performance in VANETs. And the strategies proposed in $Q2$ and $Q3$ of the thesis are meaningful in exploiting/leveraging the vehicle mobility differentiation to improve the system performance in order to approach the corresponding capacities.

[1]Note that we define two functions $f(x) \geq 0$ and $g(x) \geq 0$: $f(x) = o(g(x))$ means $\lim_{x\to\infty} f(x)/g(x) = 0$; $f(x) = O(g(x))$ means $\limsup_{x\to\infty} f(x)/g(x) = c < \infty$; $f(x) = o(g(x))$ means $\mathrm{g(x)} = \omega(\mathrm{f(x)})$; $f(x) = O(g(x))$ means $\mathrm{g(x)} = \Omega(\mathrm{f(x)})$; $f(x) = \Theta(g(x))$ means $f(x) = O(g(x))$ and $g(x) = O(f(x))$.

Acknowledgement

There are many people I wish to express my sincere gratitude and appreciation who have made this thesis successful and meaningful. First of all, I wish to express my sincere gratitude to my supervisor, Professor Xuemin (Sherman) Shen, for his invaluable and constant guidance through out my graduate studies in University of Waterloo. During years of extensive training he provided me, he not only inspired me to do cutting-edge research, but also profoundly influenced my thinking to be precise, logic, and sharp.

I am grateful to have an examining committee with distinguished scholars. I would like to thank Professor Wei-Chau Xie, Professor Otman Basir, and Professor Liangliang Xie for their helpful comments and insightful questions. I would like to thank Professor Xianbin Wang from University of Western Ontario for his commitment and serving as my external examining committee member.

I would like to thank all my friends and colleagues in the Broadband Communications Research Group, University of Waterloo. My sincere appreciation is extended to all friends and co-workers for their friendship and interaction. Special thanks go to Professor Hangguan Shan from University of Zhejiang, Professor Tom H. Luan from Deakin University, Professor Hao Liang from University of Alberta, and Professor Rongxing Lu from Nanyang Technological University for their great encouragement and constructive discussions along the way. I am also grateful to Professor Cai Lin, Dr. Muhammad Ismail, Dr. Ning Lu, Dr. Ruilong Deng, Dr. Hassan Omar, Dr. Zhongming Zheng, Qinghua Shen, Ning Zhang, Nizar H. Alsharif, Nan Cheng, and Kuan Zhang for their expertise and friendship.

Last, but not the least, I am much obliged to my parents, Zhanqi Wang and Wei Jiang, and my husband, Ran Zhang, for their unconditional love, understanding and support in my life.

To my parents and my husband

Contents

List of Tables

List of Figures

Chapter 1

Introduction

Vehicular ad hoc networks (VANETs) have recently emerged as a promising technology for providing revolutionized broadband services to vehicles. By deploying wireless gateways (e.g., road side units (RSUs)) along highways/sidewalks and equipping vehicles with on-board communication facilities (e.g., on-board units (OBUs)), two communication modes are enabled for vehicles on the move: vehicle-to-RSU (V2R) communications and vehicle-to-vehicle (V2V) communications, alternatively known as vehicle-to-infrastructure communications and inter-vehicle communications, respectively. In this framework, some applications can be supported, e.g., road safety applications (e.g., incident warning, traffic alerts), the traffic monitoring/management, and infotainment delivery (e.g., video streaming, online gaming) [1] [2].

For the exclusive use of automotive applications for VANETs, the program, Vehicle-Infrastructure Integration (VII) [3], alternatively called IntelliDrive by the U.S. Federal Communications Commission (FCC), has dedicated a 75 MHz spectrum in the 5.9 GHz band. This spectrum became known as Direct Short-Range Communications (DSRC)[1] [1]. The permissible power levels give DSRC signals a range of 1 km with data rates from 6 to 27 Mbps. The community also sets the accordingly developing DSRC standards, including the

[1]DSRC protocol supports both RSU-to-vehicle/vehicle-to-RSU (R2V/V2R) and vehicle-to-vehicle (V2V) communication.

PHY and MAC layers and the communication architecture. The architecture envisaged ad hoc communications among OBUs in vehicles and RSUs. The RSUs would function as data repositories or repeaters. Specifically, through VANETs, safety applications can be obtained based on DSRC to alert drivers about potentially conflicting situations based on information obtained from neighboring vehicles and the roadside units.

Due to the big potentials of VANETs in safety applications, on February 3rd, 2014, the U.S. Department of Transportation's (DOT) National Highway Traffic Safety Administration (NHTSA) announced that it will begin taking steps to enable V2V for vehicles to talk to each other and ultimately avoid crashes altogether by exchanging basic safety data [4]. In addition, motivated by the significant commercial potentials, prominent industrial corporations have also launched multiple projects to promote vehicular communications. For example, "Toyota Friend" builds a private social network for the owners of Toyota cars [5].

1.1 Vehicular Ad Hoc Networks

The vehicular environment creates unique opportunities, challenges, and requirements. For instance, new challenges can be created by high vehicle speeds and highly dynamic operating environments. However, based on the highly mobile environments, an entirely new paradigm for vehicle safety applications can be created, and even other non-safety applications can greatly enhance road and vehicle efficiency.

1.1.1 Applications of VANETs

Generally, VANET applications can be divided into two major categories: 1) safety related applications that increase vehicle safety on the roads ; 2) non-safety related applications that provide value-added services, for example, traffic navigation or path planning in vehicular networks.

At the most basic level, the goal of inter-vehicular wireless communications for safety application is to alert the danger on the move, by sharing current vehicular positions, veloc-

ities, and accelerations. Since most retail vehicles are now outfitted with sensors to measure velocities and accelerations and with transceivers to support the wireless communications among vehicles and infrastructure, this vehicular safety application can come true in reality.

Another kind of application is non-safety related application, e.g., for comfortable driving. In this type of application, information is cooperatively collected and shared within a large area, i.e., in a highway network or the road network of a city. For example, the VANET-based sensing data-sharing systems provide the distributed sensing information about the traffic situation in an entire city, which can be utilized to smooth the vehicle traffic and reduce the individual travel time of vehicles in the whole network.

1.1.2 Characteristics of VANETs

VANETs are the special cases of mobile ad hoc networks (MANETs), where the highly mobile vehicles equipped with OBU communication devices can communicate with other vehicles or the deployed infrastructure (e.g., RSUs) as shown in Fig. 1.1. Then, VANETs have the unique characteristics.

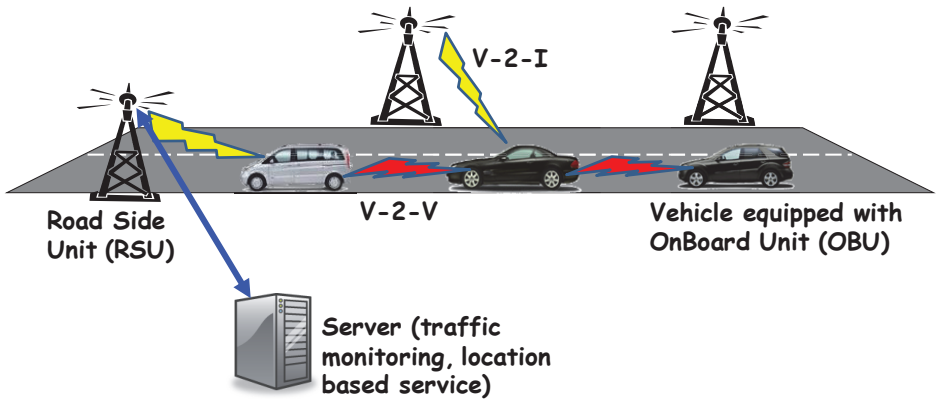

Figure 1.1. Architecture of VANETs

1. *Rapid change in topology:* Since vehicles are moving with high speeds, the topology of VANETs is prone to frequent and rapid changes, and the movements of vehicles usually follows the geometric topology of freeways or streets in real world.

2. *No power constraint:* Since the batteries of the vehicles for the communication are self-charged, vehicular communications in VANETs do not suffer from the conventional power constraints of the hand-held devices in MANETs.

3. *Large scale:* VANETs are composed of a large scale number of vehicles, where the order of the number of vehicles is in the range of 10^7 in reality [6].

4. *Variable network density:* The number of vehicles in one area of the road is both temporally and spatially changing, e.g., roads in the rush hours nearby downtown are more congested than other places at the other times of a day.

5. *High predictable mobility:* The velocity of vehicles in cities ranges from 0 to 60 km/h, and the average velocity can reach up to 100 km/h on a highway. The road geometric topology regulates the mobility of vehicles.

1.1.3 Challenges of VANETs

Most of VANET applications, such as the Internet-based VANET applications (i.e., email, vehicular video conference, and traffic monitoring, etc.), rely on the connections to RSUs to communicate with the remote servers. The communication link relies on the multihop inter-vehicle relays, i.e., the V2V communications, and V2R communications. While having a bright future ahead, enabling efficient vehicular communications faces fundamental challenges.

The first key challenge that VANET applications face is the connectivity of the network, due to the high mobility of vehicles. In general, most VANET applications (e.g., vehicular video conferencing and traffic monitoring) rely on connections to remote Internet servers through RSUs, to extend the limited communication range of V2R communications. Thus, inter-vehicle relaying is typically depending on V2V communications. For example, considering the uplink scenario of VANETs[2], vehicles help each other to relay data towards RSUs,

[2]In VANETs, many basic applications are supported in uplink scenario, such as data uploading, email transmission, road traffic reporting, and environment monitoring.

which then forward received data to the remote server via wired networks [7]. However, due to the fast mobility of vehicles and dynamic topologies, the transient and intermittent connections among vehicles make inter-vehicle transmission performance highly unreliable.

The second challenge comes from the large scale of the vehicular network. As the quality of applications keenly relies on the number of vehicles contending for transmissions and the availability of RSUs, the investigation on how nodal throughput scales with the number of vehicles and the availability of RSUs in VANETs (i.e., asymptotic network throughput capacity) is crucial in adopting the appropriate network mechanisms (e.g., signaling exchanging) and guiding the real-world network planning (e.g., RSU deployment).

As discussed above, VANETs have met technical challenges, due to the specific features of vehicles, for example, mobility and the large scale. However, Grossglauser and Tse have shown in [30] that mobility can *in reverse* improve the achievable throughput capacity as a benefit in MANETs. To this end, we propose the questions: 1) how mobility impacts the capacity of a large scale vehicular network? and 2) how to use the mobility to improve the network performance in a large scale vehicular network? In this thesis, we will discuss these issues in three scenarios, i.e., pure VANETs, VANET-enhanced transportation systems and VANET-enhance smart grid, respectively.

1.2 Mobility in VANETs

Almost since the advent of one prominent symbol of the 20th century, the automobile, scientists and engineers have been trying to understand and reproduce vehicular mobility patterns. This effort has been made more critical with the popularization of the personal automobile and the outbreak of the first traffic congestions. In the middle of the 20th century, a new research domain called traffic theory comes up with the objective of understanding the link between the traffic speed, flow, and density for an efficient dimensioning of the transport infrastructures and to help resolve traffic problems. With the miniaturization of processors and the appearance of mobile sources of energy, mobility quickly attract increasing attention.

Mobility indeed shows to be the source of similar issues, and its modeling and understanding a justification to reach the same objectives, as traffic theory: to improve the dimensioning of data transport infrastructures and solve data traffic problems. With the appearance of VANET, in which vehicles communicate with other vehicles or with road infrastructures, the study of vehicular mobility is motivated for networking research .

In order to produce realistic mobility patterns, in literature, the models are considered in five categories as function of their scopes and characteristics:

1) Random models: Vehicular mobility is considered random and the mobility parameters, such as speed, heading, and destination are sampled from random processes. A very limited interaction between vehicles is considered in this category.

2) Flow models: Following the classification described in flow theory, single and multi-lane mobility models based on flow theory are considered from a microscopic, mesoscopic, or macroscopic point of view.

3) Traffic models: Trip and path models are described in this category,where either each car has an individual trip or a path, or a flow of cars is assigned to trips or paths. Moreover, the impact of time on these models is also described.

4) Behavioral models: They are not based on predefined rules but instead dynamically adapt to a particular situation by mimicking human behaviors, such as social aspects, dynamic learning.

5) Trace-based models: Mobility traces may also be used in order to extract motion patterns and either create or calibrate mobility models. Another source of mobility information also comes from surveys of human behaviors.

1.3 Motivations

From the above lists of applications and economic aspects, VANETs can therefore be seen as a vital part of intelligent transportation systems (ITS) in the future. To our interested in the thesis, we will answer the aforementioned questions (i.e., 1) how mobility impacts the

capacity of a large scale vehicular network? and 2) how to use the mobility to improve the network performance in a large scale vehicular network?) in three scenarios as follows.

1.3.1 Throughput capacity analysis in pure VANETs

As aforesaid, in contrast to the potential benefits, most existing works [1,2], however, fail to offer sufficient insights on the fundamental mobility analysis and the throughput scaling of the multihop vehicular communications. With a large number of mobile vehicles contending for transmissions and the quality of on-top applications keenly relying on the overall performance of multihop inter-vehicle relays, to evaluate the achievable nodal throughput and network-side performance of the VANET communications are crucial in adopting the appropriate network designs, such as the message relay controls, and key to guide the real-world deployment, such as the RSU deployment. To this end in particular, with this motivation, in the first scenario of thesis [8,9], i.e., pure VANETs, we address the following critical issues:

(**Q1**): What is the asymptotic throughput capacity of VANETs for uplink scenario[3], and how to optimally determine the scalability of RSUs to achieve the throughput capacity?

(**Q2**): How to improve the throughput performance by exploiting the mobility of vehicles for approaching the throughput capacity?

To improve the network throughput in the vehicular network, we propose a mobility-aware forwarding scheme, in which we select appropriate relays based on mobility differentiation and the vehicle density around to yield diversity gain. Because this multi-relay diversity is especially based on the mobility differentiation, so we call this diversity as mobility diversity. Further, the mobility differentiation is justified based on the defined mobility characteristics.

[3]In VANETs, the uplink scenario supports the basic applications, i.e., data uploading, email transmissions, road traffic reporting, and environment monitoring.

1.3.2 Path planning for mobile vehicles in the transportation system

Traffic congestion, as an important societal problem, has received considerable attention. The 2007 Urban Mobility Report [10] stated that traffic congestion causes nearly 4.2 billion hours of extra travel every year in US; the extra travel almost accounts for 2.9 billion extra gallons of gasoline. Although many existing advanced Personal Navigation Devices (PNDs) have functionalities of providing an optimal end-to-end path [11] [12], traffic congestion problems in intelligent transportation systems (ITS) have not been fully resolved; on the contrary, conventional approaches still face a number of technical challenges. For example, Google Maps involve existing networks (e.g., Global Position System, Wi-Fi, cellular networks, etc) for individual path planning to avoid the traffic congestion. However, the provided services are very costly, and more importantly, they cannot make quick response to an emergency caused by an accident/incident. The essential reason for this imperfection lies in lack of real-time traffic information. Thus, to enhance the adaptability of path planning, it is indispensable to study how to efficiently collect and further exploit the real-time traffic information for path planning and traffic congestion avoidance.

In the thesis, we propose a real-time global path planning algorithm which exploits VANET communication capabilities to avoid vehicles from congestion in an urban environment [13]. Both the network spatial utilization and vehicle travel cost are considered to optimally balance the overall network smoothness and the drivers' preferences. To this end, in the second scenario of thesis, i.e., VANET-enhanced intelligent transportation systems, three critical issues are addressed:

(**Q1**): How to exploit VANETs in the intelligent transportation system, and how to design the transmission mechanism to collect the real-time vehicle-traffic information?

(**Q2**): How to measure the vehicle-traffic throughput in the transportation system and how to determine the vehicle-traffic capacity in the transportation system?

(**Q3**): How to improve the vehicle-traffic throughput performance approaching the vehicle-traffic capacity by exploiting vehicle mobility?

Specifically, to collect the real-time traffic information, VANETs can provide an ITS system with enhanced communication capabilities for cost-effective and real-time traffic-information delivery. Both V2V and V2R communications are supported in VANETs to efficiently collect/report traffic updates from/to vehicles as well as RSUs. As a result, the collected real-time traffic information can be utilized for traffic-flow managements , individualized vehicle path planning, and vehicle localization.

1.3.3 Mobility-aware coordinated EV charging in VANET-enhanced smart grid

Electric vehicles (EVs), as a promising component of sustainable and eco-friendly transportation systems, have received considerable attention in many countries across the world [14]. Refueled by electricity instead of gasoline, these vehicles have the potential to save thousands of dollars for customers over the vehicle lifetime. For instance, a TESLA Model S (a pioneer retail battery EV produced by TESLA Motors) costs $\$3,492$ per 100 kilo-miles, while a traditional gasoline-fueled premium sedan costs $\$17,727$ [15]. Besides, the adoption of EVs into the transport sector can reduce the consumption of conventional energy sources (e.g., gasoline) and the pollution of environments (e.g., greenhouse gas emissions). As reported in [16], battery EVs, which completely depend on rechargeable batteries and thus produce no emissions, can cut down the overall emissions from the transport sector by 70%. Due to the above advantages, EVs have been accounting for higher market share in the transport sector. According to the report of Electric Power Research Institute (EPRI) [17], the EV penetration level can reach 35%, 51%, and 62% by 2020, 2030, and 2050, respectively.

However, the widespread adoption of EVs in the transportation system will lead to charging problems of mobile EVs that are fully reliant on rechargeable batteries. EV charging, which is very likely to coincide concentratively with the peak demand time of the power system, can incur overloading of a distribution feeder, resulting in the system instability and the reduction in energy utilization [18] [19], especially for fast EV charging as it requires

much higher power than the regular charging. Thus, to avoid power system overload during the peak time and improve energy utilization without additional deployment cost, load management strategies are indispensable to distribute the EV charging load both temporally and spatially in a coordinated fashion. At the same time, for fast EV charging, the assigned charging stations must be within the range of individual mobile EVs given current locations and battery energy levels, due to the tension between the current battery energy levels and the travel cost to reach charging stations, i.e., range anxiety.

There has been abundant literature [20–26] concerning the coordinated EV charging strategy design for EVs. But most of the works so far solve problems only in the power system aspect. That is, the coordinated charging is performed for a group of EVs that are assumed to be ready for charging within an area (e.g., parking lots or residence areas). Little research has considered vehicle-specific features, i.e. the vehicle mobility, into the charging strategy when fast-charging is considered. In fact, as EVs may need charging when moving on the road, the energy consumption on the road to reach the charging station, referred to as the travel cost, should be considered. Otherwise, the charging station assigned by the existing strategies may be too far to reach given the EV's current location and battery energy level. Due to this range anxiety, drivers prefer to charge at locations with less travel cost. Therefore, new charging strategies are required to take the range anxieties and vehicle mobility into consideration to reduce the EV travel cost. In order to track the vehicle mobility, real-time information of EVs (e.g., locations and battery energy levels) should be collected to assist charging strategy design.

To this end, in the third scenario of the thesis, i.e., VANET-enhanced smart grid, we focus on leveraging the real-time mobile vehicle information to help designing an efficient coordinated EV charging strategy [27, 28]. The objective is to improve the overall energy utilization, reduce the average EV travel cost, and prevent the overload of the power system. To properly design the strategy, three underlying key problems should be deliberated:

(**Q1**): How to efficiently and reliably obtain the real-time information of mobile vehicles required by the EV charging strategy?

(**Q2**): How to decide the load capacity of each charging station?

(**Q3**): Based on the collected information, how to perform mobility-aware coordinated EV charging to improve energy utilization and reduce EV travel cost while avoiding power system overload?

Thanks to VANETs, the first problem can have a promising resolution. Exclusively designed for information exchange among highly mobile vehicles and RSUs in a multi-hop fashion. Therefore, VANETs can be integrated into a smart grid to collect the real-time information of mobile EVs and disseminate the charging decisions. To cope with the second and third problems, based on the VANET-enhanced smart grid, we will design a mobility-aware charging strategy for EVs with considering of vehicle mobility to improve the network power utility, approaching the load capacities of charging stations.

1.4 Definitions of Capacity in Different Scenarios

In this thesis, we will consider both throughput and capacity analysis in the aforementioned three scenarios. In each specific scenario, we define the considered capacity, respectively.

1.4.1 Data-traffic capacity of pure VANETs

First, we consider the general data-traffic throughput capacity in VANETs. The fundamental throughput capacity of wireless networks is first investigated by Gupta and Kumar in [29], and they prove that the per-node throughput capacity along multihop relays vanishes to zero as $\Theta(\frac{1}{\sqrt{n}})$ where n is the population of nodes. Grossglauser and Tse extend the results by considering the extreme mobility and report in [30] that constant throughput capacity is achievable. However, the constant per-node throughput capacity is at the cost of enlarged delay. To address this issue, in [31] Neely and Modiano unveil the tradeoff between the throughput capacity and delay for a cell-partitioned ad hoc network. The asymptotic throughput capacity is shown under the different scheduling policies. It is reported that although the scheduling

policies applied with packet redundancy can help to reduce delay, redundancy packets reduce the throughput capacity.

Hence, to define asymptotic throughput capacity in our framework, let $\pi(n)$ denote the scheduling and relaying policy for all vehicles in the network. Time is partitioned into equal intervals, each interval being referred to as a time slot. During T time slots, $M_j^{\pi(n)}(t)$ is denoted as the number of packets received by RSUs from vehicle j at time slot t, $t \in (0, T]$ and $j \in \mathbb{V}$. With the random trajectories of vehicles on the streets, a long-term throughput capacity $\lambda(n)$ (packet/s) under a policy $\pi(n)$ is defined as

$$\lambda(n) = \min_j \{ \lim_{T\to\infty} \inf \frac{1}{T} \sum_{t=1}^{T} M_j^{\pi(n)}(t) \}. \tag{1.1}$$

Specifically, when the vehicles in the network are homogenous, all the vehicles are with the same long-term average throughput performance, and thus the long-term average throughput capacity of $\lambda(n)$ is equal to the average throughput capacity of each vehicle over a long time, i.e.,

$$\begin{aligned} \lambda(n) &= \lim_{T\to\infty, n\to\infty} \inf \tfrac{1}{nT} \sum_{j=1}^{n} \sum_{t=1}^{T} M_j^{\pi(n)}(t) \\ &= \lim_{T\to\infty} \inf \tfrac{1}{T} \sum_{t=1}^{T} M_j^{\pi(n)}(t), \forall j \in \mathbb{V}. \end{aligned} \tag{1.2}$$

1.4.2 Vehicle-traffic capacity in transportation system

To understand a vehicle-traffic flow more clearly, we model vehicle traffic as an "inflow/outflow" system [32]. Each vehicle is expected to follow a planned path from its starting point towards its destination, Here, the planned path can be referred to as a path preset in a Global Position System (GPS) device, according to the driver's preferences and based on the locations of the starting and ending points. The driver will keep following the preset path until the vehicle receives any information on congestion or accident. When an accident or congestion occurs, by running the path planning algorithm, the vehicle-traffic server will be in charge of finding an optimal alternative path or routing for the vehicles of interest. Specifically, we refer to the

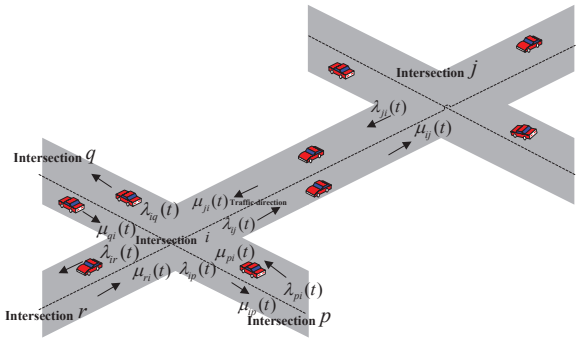

Figure 1.2. Illustration of traffic flow model.

road segments in which one vehicle's starting point and destination are located as s and d, respectively.

Let J_i denote the set of neighboring crossings of intersection i. Define the inflow rate of road segment $(i,\ j)$, $\lambda_{ij}(t)$, as the upstream-vehicle arrival rate from neighboring road segments in time slot t, where $j \in J_i$, as shown in Fig. 4.2. Let $\lambda_{ij}^d(t)$ $(j \in J_i)$ denote the traffic flow rate on road segment $(i,\ j)$ with the same destination d in time slot t, and $\lambda_{ij}(t) = \sum_{d\in\Gamma} \lambda_{ij}^d(t)$. We consider each sample time duration (denoted as Δ and including a series of time slots) as a time unit, which is defined by sampling theorem to avoid information loss in the compressive sensing for traffic estimation. Within the T^{th} sample time duration, based on the traffic flow rates of the involved time slots collected by RSUs, the average inflow rate of road segment $(i,\ j)$ of the T^{th} sample time duration is denoted as $\lambda_{ij}(T)$ and expressed as

$$\lambda_{ij}(T) = \frac{1}{\Delta} \sum_{t=(T-1)\Delta}^{T\Delta} \lambda_{ij}(t). \tag{1.3}$$

Similarly, the outflow rate $\mu_{ij}(T)$ of road segment (i,j) is the average departure rate of vehicles moving to neighboring road segments in the T^{th} sample time. Note that all variables for the opposite directed road segment of (i,j), namely road segment (j,i), can be defined correspondingly, e.g., $\lambda_{ji}(T)$ and $\mu_{ji}(T)$.

Let $c_{ij}(T)$ denote the maximum number of outflow vehicles of road segment $(i,\ j)$ in T^{th}

sample time, i.e., road capacity, which is determined by the road conditions, the number of lanes, the length of the road, and traffic congestion, etc. Due to fluctuating road conditions and traffic flow conditions, the road capacity can fluctuate with time, but is considered to remain constant within one sample time unit.

Basically, there are two kinds of traffic congestion: recurrent congestion and non-recurrent congestion [33]. The recurrent congestion is due to the tension between the current traffic flow situation (e.g., the traffic inflow $\lambda_{ij}(T)$) and the road conditions (e.g., the road capacity $c_{ij}(T)$), which is non-incident related. The non-recurrent congestion is caused by an accident or incident which can reduce the road capacity (to be introduced in Section 4.4). We define a congestion indicator of a warning message, $\delta(I_{ij})(\in [0,1])$, to represent how the congestion type I happening on road segment (i, j) impacts on the road capacity, where $\delta(I_{ij}) = 1$ means recurrent congestion and $\delta(I_{ij}) \in [0,1)$ implies non-recurrent congestion.

1.4.3 Power load capacity of a smart grid

Consider a smart grid in which the power system can be abstracted as a one-line diagram with multiple buses. For further illustration, an example of a 12-bus system is depicted in Fig. 1.3(a). And Fig. 1.3(b) is the equivalent power system model of Fig. 1.3(a). Let N denote the set of buses in the system, with the population of 12 in this example. The *generation buses* are defined as the buses injecting power to the system, i.e., Bus_1 in Fig.1.3(a), while the others which only have load are denoted as the *load buses*, i.e., Bus_3, Bus_6, etc. The power system is supplied through the substation at the generation bus, i.e., Bus_1. EV charging stations are located in the network at load buses, e.g., Bus_3, Bus_6, Bus_9 and Bus_{12}, respectively. Consider that each charging station is connected to the grid via a standard single-phase Alternating-Current (AC) connection.

Based on historic remote terminal unit (RTU) readings of each distribution system bus, the voltage at each charging station in a period can be obtained [34]. Due to the thermal limit of service cable or current rating of fuse, an EV charging station at Bus_j is subject

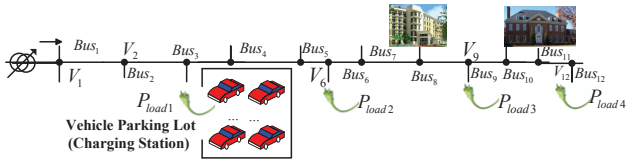

(a) Illustrated power system model.

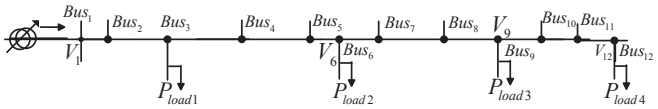

(b) Equivalent power system model.

Figure 1.3. The power system model.

to a load-capacity constraint P_{total}^{j} [35], which is defined as the maximal power that can be supplied by each charging station (i.e., the load-capacity of a charging station).

1.5 Organization and Contributions

The remainder of the proposal is organized as follows: Section 2 presents the preliminaries and related work. In Section 3, we introduce the the asymptotic throughput capacity of VANETs exploiting mobility diversity in pure VANETs. Section 4 presents the mobility-aware vehicle-traffic throughput analysis in VANET-enhanced intelligent transportation system. In Section 5, the mobility-aware coordinated charging for EVs in VANET-enhanced smart grid is shown. Finally, Section 6 concludes the thesis and demonstrate the future work.

Chapter 2

Preliminaries and Related Work

In this chapter, we will discuss the related works, including the mobility models, throughput capacity analysis, vehicle path planning and EV charging strategy design.

2.1 Mobility Description in VANETs

In terms of different vehicle-density, the vehicle-traffic flow conditions are divided into: uncongested, near-capacity, and congested [36]. For the first uncongested case, the vehicle-density is 0-26 vehicle/km; in the near-capacity case, the vehicle density follows 26-42 vehicle/km; while when the vehicle-density is larger than 42 vehicle/km, the vehicle-traffic flow condition is named as congested case. In addition, the uncongested, near-capacity, and congested vehicle-traffic flow conditions corresponds to low, intermediate, and high vehicle densities, respectively.

In the literature, most of the analytical mobility descriptions of vehicles are focusing on the cases of low and intermediate vehicle densities. For these two conditions, based on an average sense to model the vehicle traffic, the vehicle traffic follows a Poisson distribution which is non-dependent and memoryless [37–39]. In these cases, this mobility model is accurate enough for performance analysis. Over a short time of interest, it is reasonable to assume that vehicles move at constant velocities and do not interact with each other. Specif-

ically, as a good approximation, the headway distance between two neighboring vehicles follows the exponential distribution, and vehicles move independently at the speed [37]. For example, the mobility of each vehicle can be characterized by random variables (S, λ), to describe the realistic driving behaviors of people, i.e., a driver drives at a velocity for a period and then changes to a higher/lower velocity based on his/her will, road conditions, or the headway distance between the vehicle and the one in front. The vehicle velocity in this model is represented by S, which takes n possible values. When $n = 2$, S has two states: a lower velocity S_L and a higher velocity S_H and the velocity transition is modeled as a two-state continuous Markov chain with state transition rates, λ_{LH} or λ_{HL}, respectively.

In a high density scenario, e.g., the highway scenario nearby the exit point at peak time, the mobility between vehicles is dependent. In this case, a car following model [40,41] and a Markov Spacing model [36,42] can be used to describe the dependence of vehicle's mobility.

In our thesis, we aim to evaluate the impacts of vehicle mobility on the average network throughput performance in low and medium density cases. In other words, we consider that the headway distance between two neighboring vehicles follows the exponential distribution, and vehicles move independently. And this headway distance distribution will be also evaluated in our simulation results in the following chapters.

2.2 Capacity Analysis for VANETs

The fundamental throughput capacity of wireless networks is first investigated by Gupta and Kumar in [29], and they prove that the per-node throughput capacity along multihop relays vanishes to zero as $\Theta(\frac{1}{\sqrt{n}})$ where n is the population of nodes. Grossglauser and Tse extend the results by considering the extreme mobility and report in [30] that constant throughput capacity is achievable. However, the constant per-node throughput capacity is at the cost of enlarged delay. To address this issue, in [31] Neely and Modiano unveil the tradeoff between the throughput capacity and delay for a cell-partitioned ad hoc network. The asymptotic throughput capacity is shown under the different scheduling policies. It is

reported that although the scheduling policies applied with packet redundancy can help to reduce delay, redundancy packets reduce the throughput capacity. In [43], by employing a more practical restricted random mobility model, Li $et\ al.$ achieve the smooth tradeoff between the throughput capacity and delay by controlling node mobility. In [44], Garetto $et\ al.$ provide a general framework on the analysis of the throughput capacity scaling properties in MANETs with heterogeneous nodes and spatial inhomogeneities. Furthermore, in [45] Garetto and Leonardi show that when the mobile nodes are heterogenous with a restricted random mobility model in the network, the per-node throughput capacity can be a constant and the delay also becomes a constant. In [46] , Ozgur $et\ al.$ consider intelligent node cooperation and distributed multiple-input multiple-output communications to achieve the optimal scaling of throughput capacity. In [47], Wang $et\ al.$ study the achievable rates and the scaling law by proposing relaying scheme corresponding to the power allocation policies. However, most of works above are studied in MANETs.

Although VANETs present to be a special category of MANETs, they distinct features in terms of the network architecture, user mobility patterns, a large number of vehicles, and real-life application scenario. Without taking those features into considerations, the aforementioned research results derived in the general MANETs cannot be accurate enough to represent VANETs. As heterogeneous applications in diverse communication patterns coexist in VANETs, current study on the throughput capacity of VANETs is mainly application (or scenario)-driven [48]; a comprehensive analysis on the general VANETs model is however still unavailable which motivates our work. In [37], Abdrabou and Zhuang derive the effective throughput capacity of the V2R communications to evaluate the end-to-end delay performance between a vehicle and the nearest RSU. In [38, 49, 50], Nik $et\ al.$ study the distance-limited capacity in which a vehicle follows its front vehicle with the same velocity and moving direction. In [51], considering a vehicle restricted mobility network, Lu $et\ al.$ show that it is possible to achieve constant throughput capacity and constant delay based on a variant two-hop forwarding scheme. Most of these works are based on the specific mobility limitations in space. As the demand of a more general mobile scenario, the first topic of

this thesis is devoted to characterizing the achievable throughput capacity in a general hybrid VANET which will be defined as follows and then proposing the relay selection scheme to approach the throughput capacity.

2.3 Path Planning and Route Navigation for Vehicles

Most existing route navigation in conventional ITS usually rely on cellular systems or loop detectors, to collect time-varying traffic-condition information. In [52–55], cellphones or mobile sensors with cellular access have been investigated to collect real-time traffic information for traffic forecast or reconstruction in experimental research. In [56], authors introduce a traffic management system with loop detectors for continuous traffic measurement and monitoring along arterials. However, inevitable drawbacks cast a shadow on the application of cellular systems and loop detectors. For cellular systems, as they are not dedicated for traffic data collection, the collection services can be highly costly; the high volume of traffic data may also cause congestion for other cellular services. For the loop detectors, the deployment expense can also be very high. Besides, the inaccuracy of position measurement becomes a problem for short-distance transmissions especially in dense networks, which will degrade the performance of path planning [57, 58].

Thanks to VANETs, V2V and V2R communications can make real-time message delivery much quicker, cheaper and more efficient than the existing systems even for short-distance transmissions in dense networks [59] [60]. More importantly, RSUs in VANETs can greatly enhance the timeliness of data collection and dissemination [61], which makes it possible to perform coordinated path planning for a group of vehicles. To improve the quality of experience (QoE), a point-to-point based vehicular network can be utilized to support the application of multimedia delivery [62] [63], which however may still experience large transmission delay. A distributed path planning method to avoid congestion is put forward in [64] using real-time traffic data collected from VANETs, with the increased traffic flow. Aiming to save gasoline for individual vehicle, a navigation system is designed in [65] to

avoid congestion. However, the individual-user-optimal schemes may introduce additional traffic congestion due to human uncoordinated selfish behaviors. Thus, the paths of different vehicles should be jointly planned to balance the network traffic. The works [66] and [67] consider multi-vehicle path planning, but the average travel cost or the drivers' preference is not considered. Besides, how communications in VANETs can impact on the path planning algorithm is still not clear.

Therefore, in the second topic of this thesis, a globally optimal path planning algorithm is proposed for vehicles to avoid traffic congestion (including those caused by accidents) in a suburban scenario. With the real-time traffic information collection and decision delivery enabled by a hybrid VANET-enhanced network, the road network resources are fully utilized and the average travel cost of vehicles is significantly reduced. In addition, the impacts of VANETs on the path planning algorithm is further discussed.

2.4 Electric Vehicle Charging Strategy Design

Up to now, many studies have shown that the power system can be significantly affected by high penetration levels of EV charging [23] [24]. To avoid power system overloading during the peak time, load management strategies are indispensable to distribute the EV charging load both temporally and spatially [25]. In [26] [35], to avoid power system overloading, the peak load is shifted to off-peak periods to improve the load factor of the entire grid. In [68] [69], it is shown that global EV charging strategies that coordinate the charging duration and rates of multiple EVs based on global load information have better performance than the local strategy. In [70] [71], the spatial diversity of EV charging is modeled and evaluated to further help regulate the charging profile. However, most of the existing EV charging strategies consider EVs to be stationary when they need to be charged; few works take the vehicle mobility into consideration, which can not be overlooked as it is the most important feature of a vehicle, especially for fast-charging. Due to vehicle mobility, range anxiety, i.e., the tension between the travel cost and the EV battery energy level, is key to

the viability of charging decisions. Therefore, new efficient EV charging strategies must be designed to take care of real-time vehicle information to solve the range anxiety problem.

To obtain the real-time vehicular information, most existing works rely on cellular or Wi-Fi systems [52, 53, 72]. However, inevitable drawbacks of these systems limit their practicability in the collection of vehicle information. First, for dense vehicular networks, the inaccuracy of the location measurement in both systems [57] may considerably degrade the charging performance. Second, as cellular systems are not dedicated for vehicular data collection, the collection services can be highly costly, and the high volume of vehicular data may cause congestion for other cellular services especially when the vehicle density is high; for the Wi-Fi systems, the coverage is very limited which can cause large delay in information delivery, and the high mobility of vehicles may dramatically reduce the delivery ratio.

Thanks to VANETs, the delivery of the real-time message can be much quicker, cheaper and more efficient than the above systems, especially for dense and highly mobile vehicular networks [73]. Exclusively designed for information exchange among highly mobile vehicles and RSUs, the supported short-range V2V and V2R communication effectively expands the transmission range of vehicles in a multi-hop manner with higher data rates. As a result of the RSU sharing and multiple V2V relaying mechanisms, a higher throughput and delivery ratio as well as lower delay can be achieved for the large-volume vehicle information exchange [74] [75], making it possible to perform coordinated charging strategy for a group of vehicles. Hence, we exploit VANETs in a smart grid to support the real-time information exchange among mobile vehicles. Then, the range anxiety which describes the tension between the travel cost and the current energy level can be introduced as a viability of charging decisions for mobile vehicles.

Therefore, with real-time vehicle information collection and decision dissemination via VANETs, our objective in the third scenario of this thesis is to design a mobility-aware coordinated predictive charging strategy for mobile EVs. This strategy improves the energy utilization of the power system and reduces the average EV travel cost while avoiding overload in the power system.

Chapter 3

Throughput Capacity Analysis Exploiting Mobility Diversity in Pure VANETs

In this chapter, we exploit mobility characteristics of vehicle to address the achievable asymptotic throughput capacity in pure VANETs.

3.1 Introduction

VANETs have recently emerged as a promising technology for providing revolutionized broadband services to vehicles. In general, most VANET applications (e.g., vehicular video conferencing and traffic monitoring) rely on connections to remote Internet servers through RSUs. To extend the limited communication range of vehicle-to-RSU communications, thus inter-vehicle relaying is typically used with V2V communications. For example, considering the uplink scenario of VANETs, vehicles help each other to relay data towards RSUs, which then forward received data to the remote server via wired networks [7]. However, due to the fast mobility of vehicles and dynamic topologies, the transient and intermittent connections among vehicles make inter-vehicle transmission performance highly unreliable. As a

result, enabling quality-of-service (QoS) guaranteed transmission from vehicle to an RSU and further to Internet servers for different applications becomes a challenging task.

On the other hand, as the quality of applications keenly relies on the number of vehicles contending for transmissions and the availability of RSUs, the investigation on how nodal throughput scales with the number of vehicles and the availability of RSUs in VANETs (i.e., asymptotic network throughput capacity) is crucial in adopting the appropriate network mechanisms (e.g., signaling exchanging) and guiding the real-world network planning (e.g., RSU deployment). The studies on the capacity scaling law of VANETs can date back to the extensively investigated context of MANETs [29, 30]. However, different from MANETs, VANETs typically involves a great network population and high nodal mobility conformed to street layout, and network connectivity can be enhanced by stationary infrastructure (RSUs). Therefore, the existing works on MANETs cannot be directly applied to evaluate the capacity scaling of VANETs.

The asymptotic throughput capacity of VANETs has been studied in a collections of research works [38, 50, 51], however, with certain spatial limitations on vehicle's mobility. For example, in [38,50], each vehicle moves on a single road section. In [51], vehicles move on multiple roads but within the predefined Manhattan grid with restricted mobility, i.e., vehicles are mobile around their own center spots with power-law distribution. Therefore, by considering a more general scenario, in which vehicles can move across the whole area along roads without above spatial mobility restriction, our work is devoted to characterizing a more generic scaling law of achievable throughput capacity with the RSU deployment in the network. In addition, referred to the recent works on RSU deployment in the urban area, most of the existing works, e.g., [72], focus on selecting the optimal locations for either RSUs or Access Points, based on a given candidate location set. However, the asymptotic bound on the number of RSUs in the network, i.e., the scaling law of RSU deployment, and its performance on the throughput capacity have rarely been studied before.

To address above issues, in this chapter, we develop a generic analytical framework to characterize the capacity scaling law of pure VANET. In particular, we address the following

three issues:

(**Q1**): What is the asymptotic throughput capacity of VANETs in uplink scenario?

(**Q2**): How to optimally determine the scalability of RSUs to achieve the asymptotic throughput capacity?

(**Q3**): How to improve throughput performance in reality to approach the theoretical throughput capacity?

Specifically, considering the unique dynamic features of VANETs, $Q1$ is first addressed to derive the scaling law of throughput capacity in the uplink scenario of VANETs. Our results show that in both free-space propagation and non-free-space propagation environments, the achievable throughput capacity per vehicle can scale as $\Theta(\frac{1}{\log n})$ where n denotes the population of a homogenous set of vehicles in the network[1].

Second, for a large number of vehicles in urban areas, the heavy data traffic makes it necessary to deploy sufficient RSUs in the network to provide guaranteed throughput performance to users. However, overly deployed RSUs will incur high implementation and maintainable cost. Thereby RSU deployment should be carefully designed to effectively solve this tradeoff. By answering $Q2$ we show that, to attain the asymptotic throughput capacity $\Theta(\frac{1}{\log n})$, the number of effective RSUs should scale as $\Theta(\frac{n}{\log n})$. This result can serve as the valuable benchmark for the real-world RSU deployment and service provisioning.

Finally, to address $Q3$, we develop a novel packet forwarding scheme to approach the asymptotic throughput capacity in VANETs. Since the data traffic generated by vehicles can be highly unbalanced in real-world[2], the RSUs cannot be evenly and fully used (i.e., some RSUs are overloaded whereas others are light-loaded without much traffic to deliver), resulting

[1]We consider two functions $f(x) \geq 0$ and $g(x) \geq 0$. The relationship between $f(x)$ and $g(x)$ is defined as $f(x) = O(g(x))$ or $g(x) = \Omega(f(x))$ if $\lim_{x\to\infty} \sup f(x)/g(x) = c < \infty$. $f(x) = \Theta(g(x))$ means $f(x) = O(g(x))$ and $g(x) = O(f(x))$.

[2]For example, the shuttle bus with many passengers on board may generate much more data traffic than sedans; the data generated in the parking lot of a shopping mall are more intensive than that generated in nearby residential areas.

in poor network throughput performance. The proposed scheme makes full use of the mobility diversity of vehicles, to realize load-balanced utilization of RSUs and therefore enhance network throughput. In specific, the source vehicle selects the nearby vehicles whose mobility metrics (in moving direction and velocity) are significantly different from the source's as the relays for inter-vehicle transmissions. The more salient difference that the mobility metrics of two vehicles have, the higher probability that these two vehicles can exploit different RSUs will be. As a result, the data traffic can be balanced throughout the network, and more concurrent uploading opportunities from vehicles to different RSUs can be created, which leads to the improved throughput of uploading sessions in the system-wide.

3.2 Problem Formulation and Definitions

We consider a general urban topology where the streets/roads are arbitrarily distributed across the city with random lengths and directions [76]. The considered topology is normalized to a unit (1×1) square area with the left lower corner denoted as the origin with the coordinate $(0, 0)$ and the right upper corner with the coordinate $(1, 1)$. Let $\mathbb{V}$ denote the homogenous set of vehicles/nodes moving over the network, with the population of vehicles n. The vehicles are uniformly distributed in the network. Thus $\rho(n) = \Theta(n)$ is the density of vehicles. A set of $Q(n)$ RSUs is deployed in a grid pattern on the topology as depicted in Fig. 3.1, where $Q(n) \leq n$. In such VANETs, efficient multihop communications to the RSUs are the basis of many applications, such as data uploading, email transmission and road traffic reporting. Data are generated at some source vehicles and are destined to the Internet through RSUs. Each vehicle can come to be a source vehicle with a predefined probability.

A transmission (either V2V or V2R) is successful if the received signal-to-noise-and-interference ratio (SINR) is no less than a threshold β, i.e.,

$$SINR = \frac{G_{ij}P_i}{N_0 + \sum_{u \neq i} G_{uj}P_u} \geq \beta, \tag{3.1}$$

where $G_{ij} = {d_{ij}}^{-\alpha}$ is the path loss between nodes i and j with d_{ij} denoting the distance between the two nodes and α denoting the path loss exponent. N_0 is the Gaussian noise. P_i is the transmit power of node i. In this proposal, P_i is set to be a unit transmit power for all the vehicles. As the interference power is usually much larger than the noise power in a network of moderate/high density [77], to simplify the analysis, we neglect the noise effect.

3.3 Asymptotic Analysis of Throughput Capacity

In this section, we present an analytical model to evaluate the asymptotic throughput capacity of the VANETs. With the transmission model defined in pervious section, a transmission is successful when the SINR is no less than the threshold. In other words, one receiver receives a packet successfully when it suffers from limited interference. In data uploading scenario, an RSU as a receiver is associated with a guaranteed zone area in which there is no other RSUs deployed and no concurrent V2R transmissions can be scheduled at the same time slot. A vehicle within the guaranteed zone of RSUs can upload data directly to the Internet. Let $R(n)$ denote the maximal available radius of one RSU's guaranteed zone, h the hop number of an end-to-end upload from a source vehicle to the RSU, and $h = \Theta(1)$ as aforesaid, and N the average number of vehicles served by an RSU, which is given by

$$N = \rho(n) \cdot \pi \cdot R^2(n), \tag{3.2}$$

where $\rho(n)$ is the density of vehicles as aforementioned.

The distance between two adjacent RSUs and the average distance between two neighboring vehicles are denoted by D and $2d$, respectively. Since n vehicles are uniformly distributed in a unit area, we have $d = \Theta(\frac{1}{\sqrt{n}})$. Thus, the disjoint region in topology for each vehicle is approximately with the area of πd^2, and the distance between two neighboring RSUs is of the same order as $2R(n)$. With our RSU deployment rule, the number of neighboring guaranteed zones for a central RSU is four (see Fig. 3.1). Connecting the points of

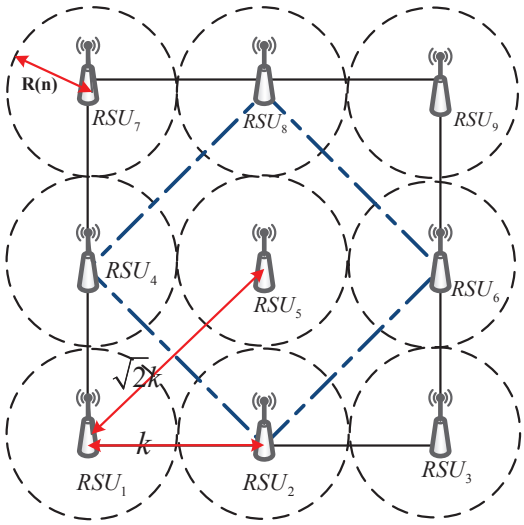

Figure 3.1. Grid RSUs deployment when $k = 2R(n)$.

the RSUs in these neighboring guaranteed zones, we have a square area of $2D^2$. Then, the average number of vehicles in a guaranteed zone can be approximated by

$$N = \frac{2D^2}{\pi d^2} \cdot \frac{1}{2} \cdot \frac{1}{c_1} = \frac{1}{c_2} \cdot \frac{D^2}{d^2} = \frac{k^2}{c_2}, k \in (0, \sqrt{c_2 n}], \tag{3.3}$$

where $k = D/d$ is the distance between two neighboring RSUs normalized by the average distance between two adjacent vehicles, $c_1(> 1)$ is a constant to compensate the area when padding the square area with the guaranteed zones, and c_2 is a constant to simplify the derivation.

The throughput capacity of the network equals to the number of concurrent V2R transmissions in the network. One successful V2R transmission suffers from the interference caused by other V2R and V2V transmissions. If a receiver (i.e., the receiving RSU) is at the boundary of the network, the interference is relatively small, compared to the interference when the receiver is at the center. Further, the receiving RSU in the center of the network faces at most four times the amount of interference that the RSU at the corner is exposed to [78]. Thus the interference of a receiving RSU at the network center has the same order as the interference when the RSU is at the corner. By considering that the receiving RSU

of interest is at the left lower corner (0,0) (e.g., the position of RSU_1 in Fig. 3.1), the upper bound of the interference (I) that the RSU_1 suffers from is given by

$$I = I_{V2R} + I_{V2V}, \tag{3.4}$$

where I_{V2R} is the interference to RSU_1 due to other V2R concurrent transmissions, and let I_{V2V} denote the interference to RSU_1 generated by other V2V concurrent transmissions.

We first study I_{V2R}. In Fig. 3.1, for RSU_1 let the set S_1= $\{\mathrm{RSU}_2, \mathrm{RSU}_4, \mathrm{RSU}_5\}$ be the first tier of its neighboring RSU guaranteed zones, and S_2= $\{\mathrm{RSU}_3, \mathrm{RSU}_6, \mathrm{RSU}_7, \mathrm{RSU}_8, \mathrm{RSU}_9\}$ is for the second tier. Generally, we use S_i, satisfying $|S_i| = 2i+1$, to represent the set of i^{th} tier of its neighboring zone. For a grid RSU deployment, i should be less than $\sqrt{Q(n)}$, thus being less than $\sqrt{n}$ as well. For zone tier i, the normalized distance between RSU_1 and a vehicle that is in transmission with its connected RSU is at least $(k \cdot i - r)$, where r ($< \frac{k}{2}$) is the normalized radius of a vehicle's coverage area. According to (1), $\lambda(n)$ is the throughput capacity achieved by every node, and thus $\lambda(n)$ should be obtained under the interference upper bound. Therefore, accumulating the interference from every zone tier, we have

$$I_{V2R} \leq \sum_{i=1}^{\sqrt{Q(n)}} \frac{2i+1}{(ki-r)^{\alpha}}, \tag{3.5}$$

where α is the path loss exponent. We can further derive the I_{V2R} as follows

$$I_{V2R} \leq \sum_{i=1}^{\sqrt{Q(n)}} \frac{2i+1}{(ki-r)^{\alpha}} \leq \sum_{i=1}^{\sqrt{n}} \frac{2i+1}{(ki-r)^{\alpha}} \leq \frac{3}{k^{\alpha}} \sum_{i=1}^{\sqrt{n}} \frac{1}{(i-\frac{r}{k})^{\alpha-1}}, \tag{3.6}$$

where $\sum_{i=1}^{\sqrt{n}} \frac{1}{(i-\frac{r}{k})^{\alpha-1}} < \frac{1}{(1-\frac{r}{k})^{\alpha-1}} + \sum_{i=1}^{\sqrt{n}-1} \frac{1}{i^{\alpha-1}}$, and $\sum_{i=1}^{\sqrt{n}-1} \frac{1}{i^{\alpha-1}}$ is an $(\alpha-1)$-series. If $\alpha = 2$, the $(\alpha-1)$-series follows the diverging *harmonic series*: $\sum_{i=1}^{\sqrt{n}-1} \frac{1}{i} = \ln(\sqrt{n}-1) + \frac{1}{2(\sqrt{n}-1)} + \Upsilon$, where Υ is the Euler-Mascheroni constant; if $\alpha > 2$, the $(\alpha-1)$-series converge to the

$Riemann\ zeta\ function$: $\xi(\alpha-1)$ [78]. Then, (3.7) can be further simplified as follows

$$I_{V2R} < \begin{cases} \frac{3}{k^2}[\frac{1}{1-\frac{r}{k}} + \ln(\sqrt{n}-1) + \frac{1}{2(\sqrt{n}-1)} + \Upsilon], \text{ if } \alpha = 2 \\ \frac{3}{k^\alpha}[\frac{1}{(1-\frac{r}{k})^{\alpha-1}} + \xi(\alpha-1)], \text{ if } \alpha > 2. \end{cases} \tag{3.7}$$

Note that $(\frac{1}{2(\sqrt{n}-1)} + \Upsilon + \frac{1}{1-\frac{r}{k}})$ has no impact on the scaling law. Then,

$$I_{V2R} < \begin{cases} \frac{3}{2k^2}[\ln n + o(\ln n)], \text{ if } \alpha = 2 \\ \frac{3}{k^\alpha}[\frac{1}{(1-\frac{r}{k})^{\alpha-1}} + \xi(\alpha-1)], \text{ if } \alpha > 2. \end{cases} \tag{3.8}$$

On the other hand, the interference which RSU_1 suffers from is contributed by other V2V concurrent transmissions. Similar to [29], we consider that each receiving vehicle has a guaranteed zone, and the guaranteed zones for the receivers are disjoint. The transmission from vehicle i to vehicle j is successful only when the following condition holds: $d_{uj} \geq (1+\Delta)r$, where d_{uj} is the Euclidean distance between other transmitting vehicle u and the receiver j; $\Delta > 0$ is the guard factor. Let the set X_i be composed of the available V2V-concurrent-transmission guaranteed zones around $V2R_0$ at the i^{th} tier, where $V2V_j(j = 1, 2, 3, ...)$ represents the j^{th} V2V-concurrent-transmission guaranteed zone. As depicted in Fig. 3.2, the network can be divided into n small disjoint guaranteed zones, and there is only one vehicle in each zone. For each guaranteed zone of a receiver, several $V2V$-concurrent-transmission guaranteed zones are around it, as depicted in Fig. 3.2. Let X_i^{max} and X_i^{min} respectively be the largest and the smallest sets of possible V2V-concurrent-transmission guaranteed zones at the i^{th} tier. For instance, considering an interested $V2R$ transmission (e.g., $V2R_0$ in Fig. 3.2), the set X_1^{max} is the largest neighboring V2V-concurrent-transmission guaranteed zone set at the first tier, and obviously there are at most six V2V-concurrent-transmission guaranteed zones around, $X_1^{max} = \{V2V_1, V2V_2, V2V_3, V2V_4, V2V_5, V2V_6\}$. Similarly, the largest set of V2V-concurrent-transmission guaranteed zones at the second tier is $X_2^{max} = \{V2V_7, V2V_8, ..., V2V_{17}, V2V_{18}\}$. Moreover, $|X_i^{max}| = 6i$. The smallest set X_i^{min} is shown as the shadow part in Fig. 3.2. The normalized distance between the V2V

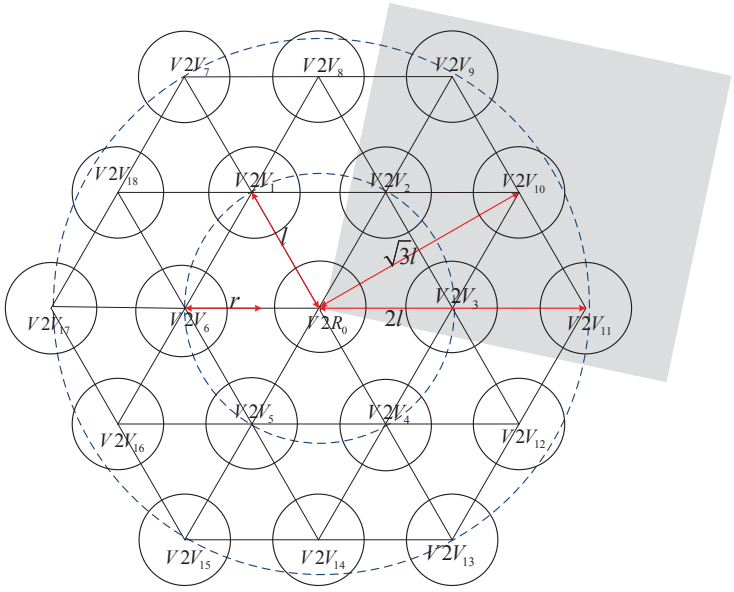

Figure 3.2. A V2R transmission($V2R_0$) with other possible concurrent transmissions.

concurrent transmission in the i^{th} tier and $V2R_0$ is no less than $\frac{\sqrt{3}}{2}li(l \in (0, \sqrt{n}])$, where $l = \frac{c_3 B}{d}$ is the normalized distance between two adjacent V2V-concurrent-transmission guaranteed zones. Here, c_3 is a constant and B is the average distance between the receivers of two concurrent V2V transmissions (the distance between the centers of two vehicle guaranteed zones). Then, we have

$$I_{V2V} \leq \sum_{i=1}^{\sqrt{n}} \frac{6i}{(\frac{\sqrt{3}}{2}li-r)^{\alpha}} < \frac{6}{(\frac{\sqrt{3}}{2}l)^{\alpha}}[\frac{1}{(1-\frac{r}{l})^{\alpha-1}} + \sum_{i=1}^{\sqrt{n}-1} \frac{1}{i^{\alpha-1}}]. \tag{3.9}$$

Similar to (3.7), we can derive

$$I_{V2V} \leq \begin{cases} \frac{4}{l^2}[\ln n + o(\ln n)], \text{ if } \alpha = 2 \\ \frac{6}{(\frac{\sqrt{3}}{2}l)^{\alpha}}[\frac{1}{(1-\frac{r}{l})^{\alpha-1}} + \xi(\alpha-1)], \text{ if } \alpha > 2. \end{cases} \tag{3.10}$$

Therefore, from (3.5), (3.9) and (3.11), we have the following interference upper bound,

$$I < \begin{cases} \frac{3}{2k^2}[\ln n + o(\ln n)] + \frac{4}{l^2}[\ln n + o(\ln n)], \text{ if } \alpha = 2 \\ \frac{3}{k^\alpha}[\frac{1}{(1-\frac{r}{k})^{\alpha-1}} + \xi(\alpha-1)] + \frac{6}{(\frac{\sqrt{3}}{2}l)^\alpha}[\frac{1}{(1-\frac{r}{l})^{\alpha-1}} + \xi(\alpha-1)], \text{ if } \alpha > 2. \end{cases} \tag{3.11}$$

Since a transmission is successful only when the SINR exceeds the threshold β, to guarantee a successful transmission, the upper bound of the interference at a receiver should be bounded. In other words, both $\frac{\ln n}{k^2}$ and $\frac{\ln n}{l^2}$ should be finite, leading to

$$k = \begin{cases} \Omega(\sqrt{\ln n}), \text{ if } \alpha = 2 \\ \Omega((\xi(\alpha-1))^{\frac{1}{\alpha}}), \text{ if } \alpha > 2, \end{cases} \quad l = \begin{cases} \Omega(\sqrt{\ln n}), \text{ if } \alpha = 2 \\ \Omega((\xi(\alpha-1))^{\frac{1}{\alpha}}), \text{ if } \alpha > 2. \end{cases} \tag{3.12}$$

Further, from (3.3), (3.4) and (3.13), we have

$$N = \begin{cases} \Omega(\ln n), \text{ if } \alpha = 2 \\ \Omega((\xi(\alpha-1))^{\frac{2}{\alpha}}), \text{ if } \alpha > 2, \end{cases} \quad R(n) = \begin{cases} \Omega(\sqrt{\frac{\ln n}{n}}), \text{ if } \alpha = 2 \\ \Omega(\frac{(\xi(\alpha-1))^{\frac{1}{\alpha}}}{\sqrt{n}}), \text{ if } \alpha > 2. \end{cases} \tag{3.13}$$

Lemma 1 *Within the network as aforementioned, we have*

i). For a free-space propagation environment (i.e., $\alpha = 2$), when the number of RSUs $Q(n)$ scales as $\Theta(\frac{n}{\log n})$, the throughput capacity $\lambda(n)$ can scale as $O(\frac{1}{\log n})$;

ii). For a non-free-space propagation environment (i.e., $\alpha > 2$), when the number of RSUs $Q(n)$ scales as $\Theta(\frac{n}{(\xi(\alpha-1))^{\frac{2}{\alpha}}})$, the throughput capacity $\lambda(n)$ may scale as $O(\frac{1}{(\xi(\alpha-1))^{\frac{2}{\alpha}}})$ where $\xi(\alpha-1)$ is the Riemann zeta function at point $(\alpha-1)$.

Proof. The throughput capacity, $\lambda(n)$, determined by the total number of concurrent transmissions, should satisfy the inequality as follows,

$$n \cdot \lambda(n) \cdot h \leq \sum_{j=1}^{n} M_j^{\pi(n)} \cdot h \leq \quad Q(n) \leq \frac{n}{N}, \tag{3.14}$$

where h is the hop number for an end-to-end uploading from a source vehicle to an RSU, and it equals to 2 if a two-hop forward scheme is applied. Then,

$$Q(n) = \begin{cases} O(\frac{n}{\ln n}), \text{ if } \alpha = 2 \\ O(\frac{n}{(\xi(\alpha-1))^{\frac{2}{\alpha}}}), \text{ if } \alpha > 2, \end{cases} \quad \lambda(n) = \begin{cases} O(\frac{1}{\ln n}), \text{ if } \alpha = 2 \\ O(\frac{1}{(\xi(\alpha-1))^{\frac{2}{\alpha}}}), \text{ if } \alpha > 2. \end{cases} \tag{3.15}$$

For a free-space propagation environment, when the number of RSUs scales as $Q(n) = \Theta(\frac{n}{\ln n})$, the throughput capacity is $\lambda(n) = O(\frac{1}{\ln n})$. By definition, this throughput capacity should be the lower bound. Furthermore, for uploading applications, the number of concurrent transmissions is at most the number of RSUs. Thus when the number of RSUs scales as $Q(n) = \Theta(\frac{n}{\ln n})$, $\lambda(n) = \Theta(\frac{1}{\ln n})$ is the upper bound of throughput capacity as well. Similarly, for a non-free-space propagation environment, when the number of deployed RSUs $Q(n)$ scales as $\Theta(\frac{n}{(\xi(\alpha-1))^{\frac{2}{\alpha}}})$, the throughput capacity $\lambda(n)$ can scale as $O(\frac{1}{(\xi(\alpha-1))^{\frac{2}{\alpha}}})$. Note that either $(\xi(\alpha-1))^{\frac{2}{\alpha}}$ or $\ln n$ is a small value compared to n. For any environment, $Q(n)$ is a large number. Therefore, with law of large numbers, we can use n instead of $Q(n)$ in (3.7) and (3.10). Note that $\ln n$ and $\log n$ have the same scaling. □

In what follows, we derive the achievable throughput capacity in different fading scenarios characterized by the path loss exponent α.

3.3.1 Free-Space Propagation Environment (for $\alpha = 2$)

Corollary 1 *Within the network as aforementioned, there is* at most *one transmission (both V2R and V2V transmissions) in the guaranteed zone of one RSU.*

Proof. Within a normalized area, when the number of RSUs scales as $\Theta(\frac{n}{\log n})$, it can be deduced from the previous discussion that, the distance between any two neighboring concurrent V2R transmissions D scales as $\Theta(\sqrt{\frac{\log n}{n}})$, and the distance between the receivers of the two concurrent V2V transmissions should satisfy $B = \Theta(\sqrt{\frac{\log n}{n}})$. Therefore, there could be only one V2R or V2V transmission scheduled in one RSU guaranteed zone, due to the constraint of the finite interference. □

Let $f(n)$ denote the possible number of concurrent V2R transmissions in one RSU guaranteed area. We have the following Lemma.

Lemma 2 *Consider that n vehicles are uniformly distributed in a normalized area. If the number of RSUs scales as $\Theta(\frac{n}{\log n})$, with law of large numbers $f(n)$ converges in probability towards a no-less-than-one value for* every *RSU when n goes to infinity, i.e.,*

$$\lim_{n\to\infty} \textit{Pr}\,(\mathrm{f(n)} \geq 1)) = 1, \text{ for } \forall \text{ RSU}.$$

Proof. Let the probability that a vehicle is a source vehicle be ω_0. With the two-hop forwarding scheme, the probability that one vehicle has data to transmit is ω. Here, $\omega_0 \leq \omega$. Because of the nodal uniform distribution in the network, the probability of one vehicle having data to deliver in an RSU guaranteed zone is $w \cdot \frac{\pi \cdot R^2(n)}{1^2}$. The probability (denoted by P) that at least one vehicle with data to transmit in the RSU's guaranteed zone is

$$P = 1 - (1 - w \cdot \frac{\pi \cdot R^2(n)}{1^2})^n. \tag{3.16}$$

Then,

$$\lim_{n\to\infty}[1 - (1 - w \cdot \tfrac{\pi \cdot R^2(n)}{1^2})^n] = 1 - \lim_{n\to\infty} (1 - w \cdot \tfrac{\pi \cdot R^2(n)}{1^2})^n. \tag{3.17}$$

Moreover, with (3.14) we have,

$$\lim_{n\to\infty} (1 - w \cdot \frac{\pi \cdot R^2(n)}{1^2})^n = \lim_{n\to\infty} ((1 - w \cdot \frac{\pi \cdot\ a_1 \cdot \frac{\ln n}{n}}{1^2})^{(-\frac{n\cdot 1^2}{\omega\pi a_1 \ln n})})^{(-\frac{\omega\pi a_1 \ln n}{1^2})}, \tag{3.18}$$

where $a_1 > 0$ is a positive constant, and $\lim_{n\to\infty} (1 - w \cdot \frac{\pi \cdot a_1 \cdot \frac{\ln n}{n}}{1^2})^{(-\frac{n\cdot 1^2}{\omega\pi a_1 \ln n})} = e$. Therefore,

$$\lim_{n\to\infty}[1 - (1 - w \cdot \frac{\pi \cdot R^2(n)}{1^2})^n] = 1. \tag{3.19}$$

Let event A_m denote that there is at least one vehicle with data in the guaranteed zone of RSU_m where $m = 1, 2, ..., Q(n)$. By definition, P is the probability that at least one vehicle

with data is in an RSU guaranteed zone, that is, $P(A_m) = 1 - P(\overline{A_m}) = P$. $P^{Q(n)}$ is the probability that for any RSU at least one vehicle with data is in the RSU's guaranteed zone, and $Q(n)$ scales as $\Theta(\frac{n}{\ln n})$. Therefore, with law of large numbers, based on the union bound we have

$$P^{Q(n)} = P(A_1 \cap A_2 \cap ... \cap A_{Q(n)}) = 1 - P(\overline{A_1} \cup \overline{A_2} \cup ... \cup \overline{A_{Q(n)}}) \geq 1 - \sum_{m=1}^{Q(n)} P(\overline{A_m}) \ . \tag{3.20}$$

Further, for each RSU the probability that at least one vehicle with data to transmit in the RSU's guaranteed zone is denoted by P, namely $P(A_m) = P$. Then,

$$P^{Q(n)} \geq 1 - Q(n) \cdot (1 - P), \tag{3.21}$$

where $\lim_{n\to\infty} Q(n) \cdot (1-P) = \lim_{n\to\infty} a_2 \cdot \frac{n}{\ln n} \cdot (1 - w \cdot \frac{\pi \cdot R^2(n)}{1^2})^n = 0$, with a_2 a positive constant.

Therefore,

$$\lim_{n\to\infty} P^{Q(n)} = 1. \tag{3.22}$$

□

Thus, from $Lemma\ 1$, $Corollary\ 1$ and $Lemma\ 2$, we have $Theorem\ 1$:

Theorem 1 *For a free-space propagation environment with n vehicles uniformly distributed in a normalized area, when the number of RSUs scales as $\Theta(\frac{n}{\log n})$ deployed in a grid pattern, with law of large numbers $f(n)$ converges in probability towards* one *for* every *RSU, i.e.,*

$$\lim_{n\to\infty} \mathrm{Prob}(|\ \mathrm{f(n)} - 1| > \varepsilon) = 0,\ \forall\, \varepsilon > 0,\ \text{for}\ \forall\ \mathrm{RSU}.$$

The achievable *throughput capacity scales as $\Theta(\frac{1}{\log n})$.*

The free-space propagation model can be used to study a sparsely populated network when the vehicle traffic is spare on the road, and not many buildings exist. In what follows, we derive the achievable throughput capacity in a more general fading scenario with the path loss exponent $\alpha > 2$.

3.3.2 Non-Free-Space Propagation Environment (for $\alpha > 2$)

In the non-free-space propagation environment, when the number of RSUs scales as $\Theta(\frac{n}{(\xi(\alpha-1))^{\frac{2}{\alpha}}})$, the throughput capacity should be $\lambda(n) = O(\frac{1}{(\xi(\alpha-1))^{\frac{2}{\alpha}}})$, which however, is not achievable. This is because $(\xi(\alpha-1))^{\frac{2}{\alpha}})$ is smaller than $\ln n$, and thus the number of RSUs for $\alpha > 2$ is larger than the case for $\alpha = 2$. However, constrained by the topologies of vehicles and RSUs, it cannot be guaranteed that there are at least one vehicle with data to transmit in the RSU's guaranteed zone with the number of RSUs increasing. In what follows, we show the necessary condition of RSU deployment to make the throughput capacity achievable.

Theorem 2 *For a non-free-space propagation environment, with the population of vehicles n in a normalized area, when the number of RSUs scales as $O(\frac{n}{(\xi(\alpha-1))^{\frac{2}{\alpha}}})$ and the condition $Q(n) = o(e^{\frac{n\cdot\omega\pi}{Q(n)}})$ holds, the throughput capacity $\Theta(\frac{Q(n)}{n})$ can be achievable. More specifically, when $Q(n) = \Theta(\frac{n}{\log n})$ deployed in a grid pattern, with law of large numbers $f(n)$ converges in probability towards a no-less-than-one value for* every *RSU, i.e.,*

$$\lim_{n\to\infty} \mathrm{Prob}(\ \mathrm{f(n)} \geq 1) = 1,\ \text{for}\ \forall\ \mathrm{RSU}.$$

The achievable throughput capacity scales as $\Theta(\frac{1}{\log n})$.

Proof. We consider P is the probability that at least one vehicle with data is in an RSU guaranteed zone. $P^{Q(n)}$ is the probability that for any RSU at least one vehicle with data is in the RSU's guaranteed zone. When $Q(n) = \Theta(\frac{n}{N})$, combining (3.3) we get $Q(n) = \Theta(\frac{1}{R^2(n)})$. Similarly to (3.22), we have

$$P^{Q(n)} \geq 1 - Q(n)\cdot(1-\omega\cdot\frac{\pi}{Q(n)})^n, \tag{3.23}$$

where $\lim_{n\to\infty} Q(n)\cdot(1-\omega\cdot\frac{\pi}{Q(n)})^n = \lim_{n\to\infty} Q(n)\cdot(1-\omega\cdot\frac{\pi}{Q(n)})^{(-\frac{Q(n)}{\omega\pi})\cdot(-\frac{n\omega\pi}{Q(n)})}$. Therefore, when the condition: $Q(n) = o(e^{\frac{n\cdot\omega\pi}{Q(n)}})$ holds, we can attain $\lim_{n\to\infty} P^{Q(n)} = 1$. In other words, when the number of RSUs scales as $O(\frac{n}{(\xi(\alpha-1))^{\frac{2}{\alpha}}})$ and the condition $Q(n) = o(e^{\frac{n\cdot\omega\pi}{Q(n)}})$ holds,

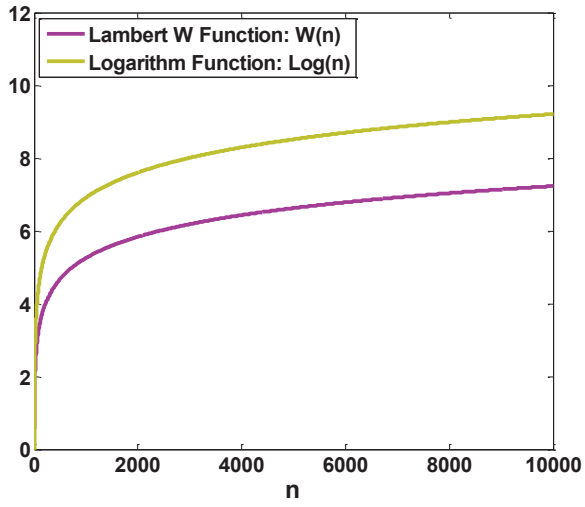

Figure 3.3. Using Log Function to approximate Lambert W Function.

the throughput capacity $\Theta(\frac{Q(n)}{n})$ can be achievable.

Further, the solution of the equation $Q(n) = e^{\frac{n}{Q(n)}}$, is $Q(n) = \frac{n}{W(n)}$, where $W(n)$ is the $Lambert\ W\ Function$ [79], and more specifically $W(n) = \ln n - \ln W(n)$ as depicted in Fig. 3.3. If we use the Logarithm Function to approximate the Lambert W Function, we characterize the condition of RSU deployment: $Q(n) = \Theta(\frac{n}{\ln n})$ for achieving the scaling law accordingly. In other words, for $\alpha > 2$, to obtain one achievable throughput capacity, the number of RSUs $Q(n)$ can be scale as $\Theta(\frac{n}{\ln n})$ and therefore the throughput capacity scales as $\Theta(\frac{Q(n)}{n})$.

This result is the same as the one for the free-space environment. It comes from the limitation of topology that to guarantee at least one vehicle with data in an RSU's guaranteed zone, the scaling of the distance between two adjacent RSUs must be no less than the scaling of $\sqrt{\frac{\ln n}{n}}$.

□

In $Theorem\ 2$ we have used the Logarithm Function to approximate the Lambert W Function. This results in an error $\ln(W(n))$ which is negligible even with very large n as shown in Fig. 3.3. Based on $Theorem\ 1$ and $Theorem\ 2$, we conclude that for either envi-

ronment the achievable throughput capacity scales as $\lambda(n) = \Theta(\frac{1}{\log n})$. First, our throughput capacity $\lambda(n) = \Theta(\frac{1}{\log n})$ is lower than the throughput capacity scaling law $\Theta(1)$ in [30] in which nodes are extremely mobile in the network. Grossglauser and Tse consider that in any time slot, one node is either a source node or a destination node. Thus, there are $\frac{n}{2}$ concurrent transmissions in one time slot. Note that the throughput capacity per node $\lambda(n)$ is as

$$n \times \lambda(n) \times h \leq CT, \tag{3.24}$$

where h is the number of hops in an end-to-end path, CT is the number of possible Concurrent Transmissions. In [30], the number of hops $h = \Theta(1)$, and the number of the concurrent transmissions $CT = \Theta(n)$. Therefore, the throughput capacity can reach $\lambda(n) = \Theta(1)$. On the other hand, when all the nodes are fixed in the network, Gupta and Kumar show the throughput capacity $\lambda(n) = \Theta(\frac{1}{\sqrt{n}})$ in [29]. The transmissions in [29] only happen between the nearest neighboring nodes, and the multihop forwarding scheme is allowed with the number of hops $h = \Theta(\sqrt{n})$. The number of concurrent transmissions scales as $\Theta(n)$, and thus the throughput capacity scales as $\lambda(n) = \Theta(\frac{1}{\sqrt{n}})$. We can conclude that our throughput capacity is higher than $\Theta(\frac{1}{\sqrt{n}})$ in [29] due to the node mobility and the store-carry-forwarding scheme. Nevertheless, the throughput capacity is limited by the RSUs' deployment, and therefore the throughput capacity is lower than the results $\Theta(1)$ in [30]. The throughput capacity bottleneck in our scenario is the number of RSUs when the number of vehicles having data to transmit is huge. Furthermore, when the number of RSUs is $Q(n)$ ($Q(n) = O(\frac{n}{\log n})$), the throughput capacity scales as $\Theta(\frac{Q(n)}{n})$. This can be the benchmark for the RSUs deployment. This leads to the conclusion that for free-space propagation environment in a data uploading scenario the number of RSUs impacts on the throughput capacity as:

$$\lambda(n) = \begin{cases} \Theta(\frac{1}{\log n}), \text{ if } Q(n) = \Theta(\frac{n}{\log n}) \\ \Theta(\frac{Q(n)}{n}), \text{ if } Q(n) = O(\frac{n}{\log n}). \end{cases} \tag{3.25}$$

Therefore, we reach the conclusion that with n vehicles in the network, *at most* $\Theta(\frac{n}{\log n})$ *RSUs are efficiently deployed* as a grid in the network. The optimal available radius of an RSU guaranteed zone(served area in topology) should scale as $\Theta(\sqrt{\frac{\log n}{n}})$.

3.4 Mobility Diversity-Based Data Forwarding Scheme

By exploring node mobility, more concurrent transmissions can be enabled to improve the throughput performance and decrease transmission delay. In this section, we propose a novel mobility diversity based data forwarding scheme to attain this goal.

The path of one vehicle may not be a straight line connecting the starting point and the destination, since the moving direction could be changed at the intersections according to the street pattern. A vehicle j ($j \in \mathbb{V}$) moves away from the starting point S along the path with an initial velocity v_{0j} ($\in [0, v_{max}]$) and a given initial moving direction $\varphi_{0j} = \vartheta_{0j}$, towards its destination D, as depicted in Fig. 3.4. The starting point S and the destination D for each vehicle are known, and thus ψ_{SD} can be determined by the locations of S and D. Let $\mathbb{M}$ denote the set of intersections in the network, where $m(\in \mathbb{M})$ represents the mth intersection ($m = 1, 2, 3, ...$). For vehicle j, if the moving direction deviation at the mth crossroad from its current moving direction ($\varphi_{(m-1)j}$) is represented by ϑ_{mj} ($\in [-\pi, \pi]$) (see Fig. 3.4), the moving direction after the mth crossroad (φ_{mj}) depending on the former turning decisions satisfies $\varphi_{mj} = \varphi_{0j} + \sum_{i=1, i\in\mathbb{M}}^{m} \vartheta_{ij}$, where ϑ_{ij} has a positive (negative) value if the vehicle turns anticlockwise (clockwise). The variable φ_{mj} should depend on the street pattern and be biased to the destination. That is, the smallest difference between φ_{mj} and $\psi_{(m-1)D}$ should be guaranteed, where $\psi_{(m-1)D}$ is the angle between the two lines: the one connecting the $(m-1)th$ intersection and the destination D and the horizontal line.

As aforementioned, define the traveling interval of one vehicle between two crossroads as a *time step*, which depends on the current velocity and the length of street due to street patterns. We use the moving direction and current velocity to represent the mobility characteristic of a vehicle in a time step. Let $\mathbb{B}$ denote the set of mobility characteristics of vehicles

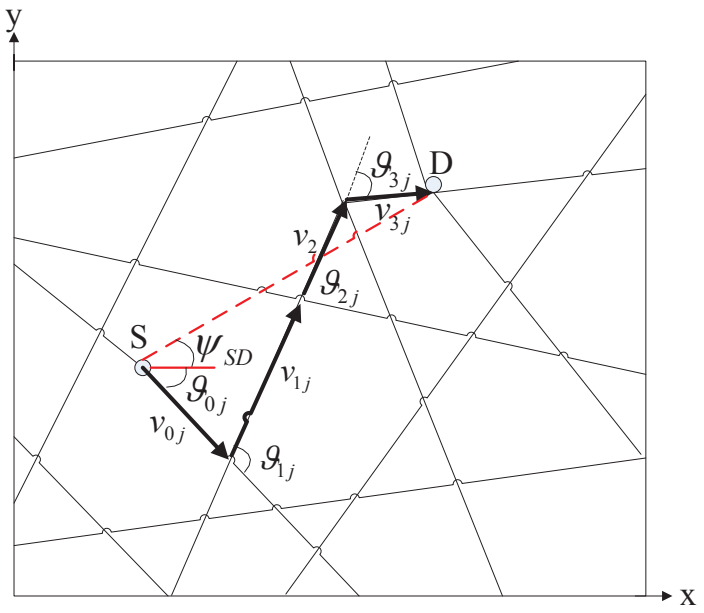

Figure 3.4. The moving path of vehicle j moving from its starting point to the destination.

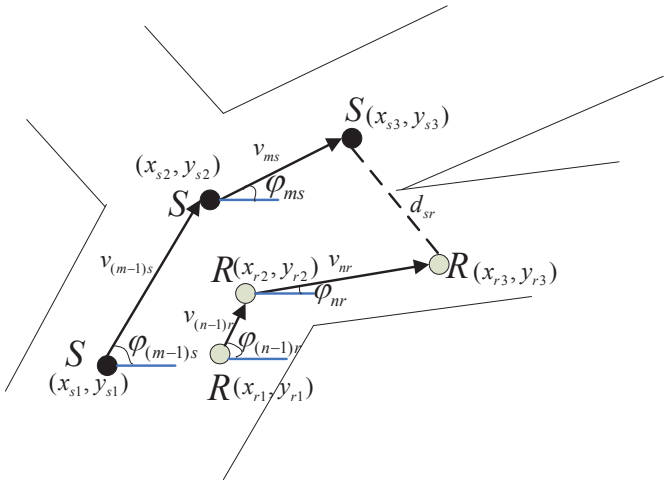

Figure 3.5. To measure the relative distance between S and R.

where each element $\mathbf{b}_{mj}$ ($m \in \mathbb{M}$, $j \in \mathbb{V}$), represents the mobility characteristic of vehicle j in its mth time step along the path. The characteristic $\mathbf{b}_{mj}$ includes the vehicle's moving direction φ_{mj} and current velocity v_{mj}, i.e., $\mathbf{b}_{mj} = (\varphi_{mj}, v_{mj})$. The mobility characteristic has no change for each vehicle within a time step. For the turning options at each intersection, there are at most four scenarios: straight, right, left, and U-turn.

We consider that the city map is known which can be acquired by GPS equipment, then the moving direction deviation at any intersection can be predicted based on the destination. That is, since the vehicle is moving towards the destination, to estimate the vehicle's moving direction deviation at mth intersection (ϑ_{mj}), ϑ_{mj} should lead to the smallest difference between φ_{mj} and $\psi_{(m-1)D}$. Note that the turning decision may be impacted by the human actions and other objective factors. When this vehicle j is moving in its mth time step, the predicted turning decision at its $(m+1)th$ intersection is chosen, and so on. For instance, as depicted in Fig. 3.5, at time t_0 the source vehicle S is in the $(m-1)th$ time step with the position (x_{s1}, y_{s1}), and it can communicate with one neighbor R which is in its $(n-1)th$ time step with the position (x_{r1}, y_{r1}). The source vehicle S is moving with the mobility characteristic $\mathbf{b}_{(m-1)s} = (\varphi_{(m-1)s}, v_{(m-1)s})$, while the neighbor vehicle R moves with $\mathbf{b}_{(n-1)r} = (\varphi_{(n-1)r}, v_{(n-1)r})$. After time t_1, S reaches the mth intersection on the position $(x_{s2},\ y_{s2}) = (x_{s1} + v_{(m-1)s} \cdot t_1 \cdot \cos\varphi_{(m-1)s},\ y_{s1} + v_{(m-1)s} \cdot t_1 \cdot \sin\varphi_{(m-1)s})$, while R reaches its nth intersection after time t_2 on the position of $(x_{r2},\ y_{r2}) = (x_{r1} + v_{(n-1)r} \cdot t_2 \cdot \cos\varphi_{(n-1)r},\ y_{r1} + v_{(n-1)r} \cdot t_2 \cdot \sin\varphi_{(n-1)r})$. Note that t_1 and t_2 can be calculated based on current velocities and the street length. And the turning decisions of both vehicles can be estimated with aforesaid approach. At a certain time $t_0 + \overline{\Delta t}$, the positions for the vehicles along their own paths could be obtained, and therefore the relative distance between the vehicles can be attained. Here, $\overline{\Delta t}$ is denoted as the prediction time. The source node and the neighbors move with their own mobility characteristics, and the positions of vehicle S and vehicle R at the time $t_0 + \overline{\Delta t}$ are (x_{s3}, y_{s3}) and (x_{r3}, y_{r3}). The relative distance d_{sr} at the time $t_0 + \overline{\Delta t}$ between this pair of vehicles is as

$$d_{sr} = \sqrt{(x_{s3} - x_{r3})^2 + (y_{s3} - y_{r3})^2}. \tag{3.26}$$

During the prediction time, if the vehicle encounters several intersections, the most possible route should be chosen based on a series of turning options at the intersections being passed by. With this relative distance after a certain prediction time, we can describe the spatial

differentiation among the vehicles. When the source vehicle receives the neighbor vehicles' predicted locations, it only transmits the data to the neighbors whose relative distance after a certain prediction time is far enough from its own, by more than the threshold (e.g., $2R(n)$), to achieve mobility differentiation. Note that there are a number of neighbors, and we can select appropriate relays whose mobility characteristics are different from the source vehicle's to yield diversity gain. Because this multi-relay diversity is based on the mobility differentiation, so we call this diversity as mobility diversity. The central philosophy behind this forwarding scheme is that by exploring the mobility diversity, multiple cooperative vehicles are used to reallocate the unbalanced data traffic and further allowed to concurrently transmit data packets which are generated by the same source vehicle to different RSUs. Therefore, concurrent transmissions can be scheduled to balance the RSUs' load, improving the throughput performance. Note that if the number of vehicles with data is huge, the efficiency of this forwarding scheme is not obvious any more.

In the scheme, we track the vehicles' mobility differentiation with two parameters: the velocity and the moving direction. In the urban area, the velocity of one vehicle is around the limited speed with little deviation from other vehicles, while the moving directions vary much from other vehicles. Thus the mobility differentiation can be reflected on the nodal variation of the moving directions. On the other hand, in the highway scenario, the moving direction deviation is limited by the highway pattern, while the velocity of a vehicle changes frequently and may vary much from others. That is, the mobility differentiation in a highway scenario is mainly caused by the velocity difference.

3.5 Performance Evaluation

3.5.1 Simulation Settings

We evaluate the efficiency of proposed forwarding scheme with a discrete-event simulator developed by C++ language. The simulation is performed based on the real-world trace

collected from the trajectory information of 4000 taxis in Shanghai on Feb. 20, 2010 [39]. In each experiment, we select the densely populated downtown area (with 20×10 km^2) in Shanghai where RSUs are deployed in a grid pattern as in Fig. 3.1. The transmission range of a vehicle is set to be 350 meters.

To investigate the impacts of vehicle mobility on the throughput performance of VANETs, we deploy two different kinds of mobility patterns as follows. In the first mobility pattern, all vehicles in the network move all the time without stopping throughout the simulation run. In the second mobility pattern, vehicles may stay still on the road without any movements for a long period, e.g., a taxi may be waiting for customers outside the hotels or shopping malls. Comparing the two patterns, the mobility diversity is greater in the first pattern. In addition, different values of prediction time T_P in Fig. 3.6 are tested to find its impact on the performance of the proposed mobility diversity based scheme.

3.5.2 Simulation Results

Fig. 3.6 shows the throughput performance of the proposed scheme with two different mobility patterns. ω_0 is set to be 0.1 such that a vehicle may transmit as a data source with probability 0.1. As we can see in Fig. 3.6, with different mobility patterns applied and other network configurations kept same, the throughput achieved in the first mobility pattern is greater than that achieved in the second mobility pattern. This indicates that with greater mobility diversity, more throughput can be achieved. In addition, it can be seen that the proposed mobility diversity based data forwarding scheme can outperform the legacy two-hop forwarding scheme. This also unveils that impacts of the mobility diversity on the throughput performance and validates the effectiveness of our proposed scheme. Moreover, Fig. 3.6 shows that the achieved throughput performance of the proposed scheme is closely related to the prediction time T_P. As can be seen in Fig. 3.6, the throughput achieved when T_P is 300 is greater than that when T_P is 30 and 700, respectively. This is because that when T_P is small, the mobility pattern of vehicles will not change much in the interval of mobility

prediction. As such, it is difficult for the source to explore good relays with the satisfactory mobility diversity. An overly long prediction time, however, decreases the throughput capacity as enabling many non-necessary competing. In Fig. 3.6, it can be seen that all the curves increase when the network size increases. This is because that with ω_0 remaining the same, the the number of source vehicles increases with the network size and therefore more data traffic is generated for transmissions in the network.

Fig. 3.7 shows the throughput performance of the proposed scheme and the legacy two-hop relay scheme when the network size increases and $\omega_0 = 0.8$. Different from Fig. 3.6, the throughput of both schemes in this scenario reduce when the network size increases. This is because that with a large value of ω_0, the traffic volume generated in the network increases dramatically when increasing the network size. As such, RSUs are likely to be heavily loaded or overloaded. In this case, exploring the mobility diversity to balance the traffic transmissions can no longer increase the concurrent transmissions of data uploading, and is therefore not helpful to increase the throughput capacity. However, in the real-world deployment, the overloaded use of RSUs should be avoided and RSUs should be over provisioned to guarantee the quality of service to users.

Fig. 3.8 shows the impacts of source vehicles on the throughput performance when the number of RSUs is fixed (e.g., 90 RSUs). In this experiment, vehicles follow the second mobility pattern and the prediction time is set to be 300s. The throughput capacity is plotted as well for comparison. With more source vehicles, more relay vehicles can help forwarding data and thus the throughput is enhanced. From Fig. 3.8, it can be observed that the curve of simulated throughput first increases due to the increasing number of efficient relays in the network which can enable more concurrent transmissions. More concurrent transmissions however also result in more interference, and then the large density of vehicles will reduce the throughput performance in the network. Thus, to obtain better throughput performance, there exists a tradeoff between the number of concurrent transmissions and the accumulated interference resulting from the concurrent transmissions.

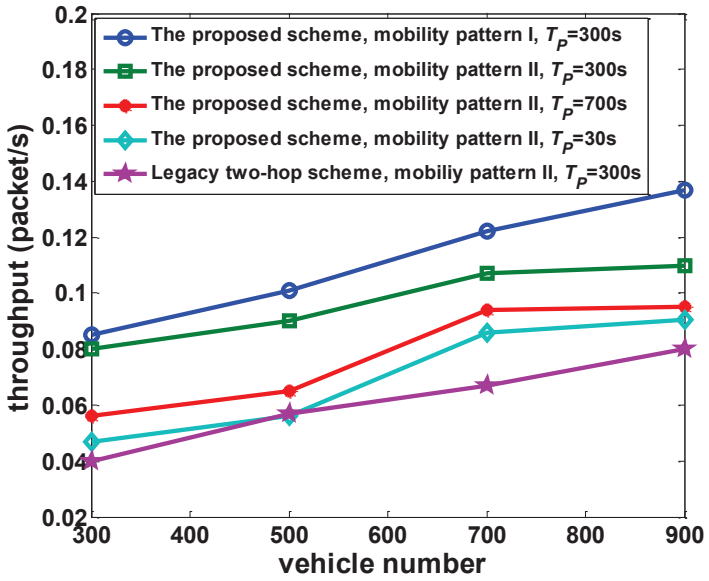

Figure 3.6. Throughput performance comparison with different schemes.

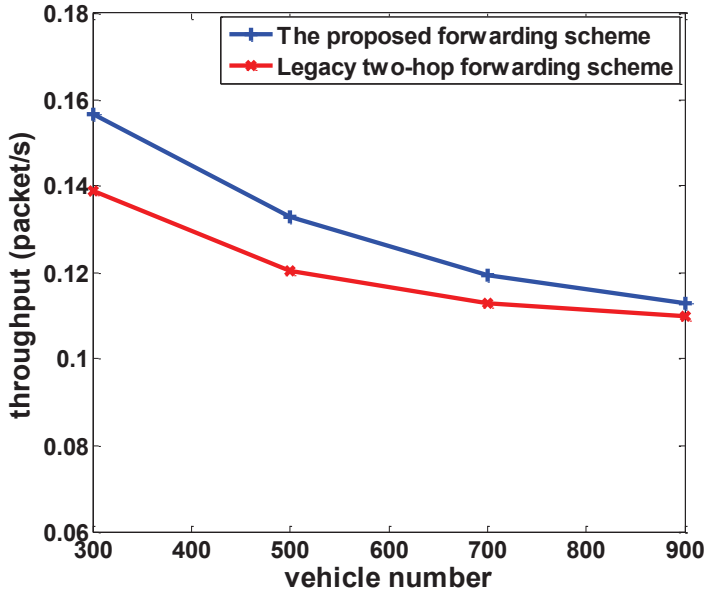

Figure 3.7. Efficiency of the proposed scheme when $\omega_0 = 0.8$.

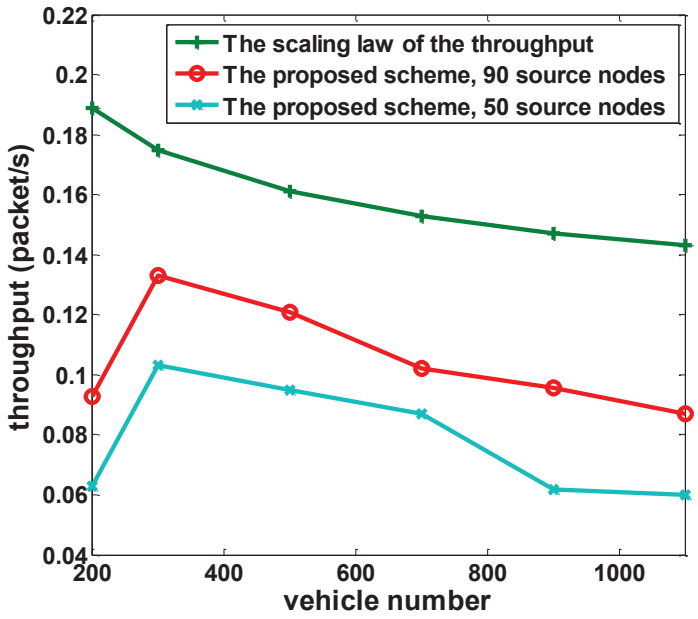

Figure 3.8. Simulated results vs. analytical results when $Q(n) = 90$.

3.6 Summary

We have analyzed the throughput capacity of VANETs for the content uploading applications in the urban area. In both the free-space propagation and non-free-space propagation environments, the achievable throughput capacity of VANETs scales as $\Theta(\frac{1}{\log n})$ decreasing with the population of vehicles n, with the number of RSUs scaling as $\Theta(\frac{n}{\log n})$. This result can be used as the benchmark of the RSU deployment for telecommunication company in realistic. Furthermore, a mobility-diversity based forwarding scheme is designed to improve the network throughput approaching the network capacity. The central philosophy of our proposed forwarding scheme is that by exploring the mobility differentiation among vehicles, data-traffic can be balanced to increase the concurrent transmissions leading to the increased network throughput.

Chapter 4

Path Planning for Mobile Vehicle in Hybrid-VANET Transportation System

In this chapter, we establish a hybrid intelligent transportation system (ITS), i.e., a hybrid-VANET-enhanced ITS, which utilizes both VANETs and cellular systems of the public transportation system to enable real-time communications among vehicles, RSUs, and a vehicle-traffic server in an efficient way. Then, we propose a real-time path planning algorithm, which not only improves the overall spatial utilization of a road network but also reduces average vehicle travel cost for avoiding vehicles from getting stuck in congestion.

4.1 Introduction

Traffic congestion, as an important societal problem, has received considerable attention. The 2007 Urban Mobility Report [10] stated that traffic congestion causes nearly 4.2 billion hours of extra travel every year in US; the extra travel almost accounts for 2.9 billion extra gallons of gasoline. Although many existing advanced Personal Navigation Devices (PNDs) have functionalities of providing an optimal end-to-end path [11] [12], traffic congestion problems in an ITS have not been fully resolved; on the contrary, conventional approaches still face a number of technical challenges. For example, Google Maps involve existing

networks (e.g., Global Position System, Wi-Fi, cellular networks, etc) for individual path planning to avoid the traffic congestion. However, the provided services are very costly, and more importantly, they cannot make quick response to an emergency caused by an accident/incident. The essential reason for this imperfection lies in lack of real-time traffic information. Thus, to enhance the adaptability of path planning, it is indispensable to study how to efficiently collect and further exploit the real-time traffic information for path planning and traffic congestion avoidance.

First, to collect the real-time traffic information, the emerging VANETs can provide an ITS system with enhanced communication capabilities for cost-effective and real-time traffic-information delivery. Both V2V and V2R communications are supported in VANETs to efficiently collect/report traffic updates from/to vehicles as well as RSUs. As a result, the collected real-time traffic information can be utilized for freeway-traffic-flow managements, individualized vehicle path planning, and vehicle localization [56]. However, most of the related works assume that the incorporated VANETs have sufficiently small delivery delay for real-time information collection. Actually, as VANETs rely on short-range multi-hop communications, the end-to-end transmission delay can be non-neglectable in some scenarios. Therefore, evaluations should be conducted to study how the end-to-end transmission performance of vehicular communications impacts on the performance of path planning in different scenarios and how to design the transmission mechanisms to reduce the delay when delay is not neglectable.

Second, to exploit the obtained real-time traffic information, many algorithms are designed to discover optimal paths for individual vehicles [64] [65]. But individual path planning may lead to new congestion if performed uncoordinatedly. To smooth the overall network flow, many works plan optimal paths from a global perspective for a group of vehicles simultaneously [67] [66]. However, most existing globally optimal path planning algorithms focus on the network-side performance improvement and neglect the drivers' preferences (e.g., shorter travel length or time). Since the replanning decisions are made to avoid congestion and balance the traffic rather than discover optimal paths for individuals, some vehicles

may pay additional cost (e.g., a longer traveling length). Therefore, algorithms should be designed to jointly consider the balance of the network traffic and the reduction of average vehicle travel cost.

To this end, we propose a real-time global path planning algorithm which exploits VANET communication capabilities to avoid vehicles from congestion in an urban environment. Both the network spatial utilization and vehicle travel cost are considered to optimally balance the overall network smoothness and the drivers' preferences. Specifically, the contributions of this chapter are threefold:

- First, to facilitate the application of real-time path planning, we propose a hybrid-VANET-enhanced ITS framework, exploiting both the VANETs and the public transportation system. Based on the proposed hybrid ITS framework, a multi-hop message forwarding mechanism is designed to collect the real-time traffic information or the emergent warning messages, which usually have strict delay bounds. A theoretical analysis on the end-to-end transmission delay performance of the mechanism is presented as well;

- Second, we design a real-time global path planning algorithm to not only improve network spatial utilization but also reduce average vehicle travel cost per trip. A low-complexity algorithm is developed based on Lyapunov optimization to make real-time path planning decisions. With the proposed path planning algorithm, the tradeoff between the overall network spatial utilization and drivers' preferences can be well balanced; and

- Finally, the transmission performance of the hybrid-VANETs is first evaluated under different vehicle densities via VISSIM, and then extensive simulations validate the effectiveness and efficiency of the proposed path planning algorithm. The results confirm that our proposed path planning algorithm is able to find alternative paths for vehicles to bypass congestion areas while reducing the average travel cost in an efficient, timely and coordinated way.

4.2 Definitions and System Models

Aiming at providing real-time planned paths for vehicles from a global perspective, we first introduce the following network architecture. The traffic flow model is then elaborated, followed by the vehicle categorization and mobility model.

4.2.1 Hybrid-VANET-Enhanced Transportation System

Fig. 4.1 shows the architecture of the considered hybrid-VANET-enhanced transportation system, consisting of vehicles, RSUs, cellular base stations (BSs) and a vehicle-traffic server.

Vehicles are equipped with OBUs which enable multi-hop V2V communication used in delivering the periodic vehicle information (e.g., vehicle velocity, density and location). When vehicles sense accident-related congestion, the warning message can be generated to alert the emergent accident information, and then be shared not only among vehicles but also with the nearest RSU via V2R communications. Besides pure VANETs, cellular communications, e.g., a global system for mobile communications (GSM) system which is set up for the functions such as mobile telemonitoring and management systems for inter-city public transportation [80], are also involved. Hence, the taxis or buses can directly upload the received warning message to the nearest cellular BS and the BS will deliver the message to the vehicle-traffic server.

RSUs deployed along the roads are assumed to be able to obtain vehicle-traffic statistical information (e.g., the vehicle arrival/departure rate on each road). We consider that taxis and buses are perfectly connected to the cellular system, and RSUs are well connected with each other through wireline. If RSUs are deployed at intersections, the traffic information can be detected by the equipped cameras or traffic flowmeters connected to RSUs directly [81]. Otherwise, the traffic flow can be predicted by the nearest RSUs based on the obtained vehicle information (e.g, periodically obtained vehicle density and velocity) from the VANETs [82]. An RSU can share its own collected information with other RSUs and the vehicle-traffic server. When an accident happens, based on all the collected information, the

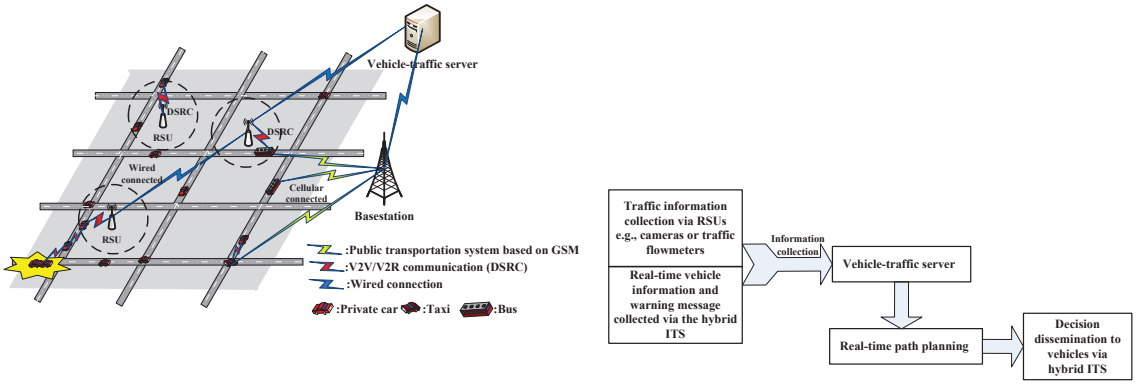

(a) Hybrid VANET-enhanced network architecture. (b) Path planning in a VANET-enhanced ITS.

Figure 4.1. Real-time path planning in VANET-enhanced hybrid networks.

vehicle-traffic server is capable of performing real-time path planning to provide globally optimized travel paths for vehicles of interest.

We further define a road network into four main components (i.e., intersections, roads, vehicles, and RSUs) as $\varsigma = (\mathbb{I}, \Gamma, \mathbb{V}, \mathbb{R})$. The set of all intersections is denoted as $\mathbb{I}$. Let Γ be the set of all the roads in the network. Each road between two adjacent intersections is assumed bi-directional, possibly with multiple lanes in one direction. We refer to each of those lanes with the same direction in a road as a road segment, i.e., one normal bi-direction road between two adjacent intersections i and j has two different road segments with opposite directions, i.e., road segment (i, j) and road segment (j, i). The set of vehicles and that of RSUs are defined as $\mathbb{V}$ and $\mathbb{R}$, respectively.

4.2.2 Traffic Flow Model

To understand a vehicle-traffic flow more clearly, we model vehicle traffic as an "inflow/outflow" system [32]. Each vehicle is expected to follow a planned path from its starting point towards its destination, Here, the planned path can be referred to as a path preset in a GPS, according to the driver's preferences and based on the locations of the starting and ending points. The driver will keep following the preset path until the vehicle receives any information on congestion or accident. When an accident or congestion occurs, by running the path planning

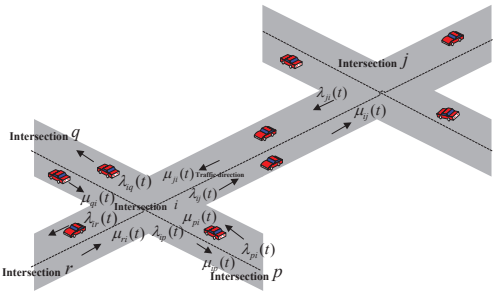

Figure 4.2. Illustration of traffic flow model.

algorithm, the vehicle-traffic server will be in charge of finding an optimal alternative path or routing for the vehicles of interest. Specifically, we refer to the road segments in which one vehicle's starting point and destination are located as s ($\in \Gamma$) and d ($\in \Gamma$), respectively.

Let J_i denote the set of neighboring crossings of intersection i. Define the inflow rate of road segment $(i,\ j)$, $\lambda_{ij}(t)$, as the upstream-vehicle arrival rate from neighboring road segments in time slot t, where $j \in J_i$, as shown in Fig. 4.2. Let $\lambda_{ij}^d(t)$ ($j \in J_i$) denote the traffic flow rate on road segment $(i,\ j)$ with the same destination d in time slot t, and $\lambda_{ij}(t) = \sum_{d\in\Gamma} \lambda_{ij}^d(t)$. We consider each sample time duration (denoted as Δ and including a series of time slots) as a time unit, which is defined by sampling theorem to avoid information loss in the compressive sensing for traffic estimation in [39]. Within the T^{th} sample time duration, based on the traffic flow rates of the involved time slots collected by RSUs, the average inflow rate of road segment $(i,\ j)$ of the T^{th} sample time duration is denoted as $\lambda_{ij}(T)$ and expressed as

$$\lambda_{ij}(T) = \frac{1}{\Delta} \sum_{t=(T-1)\Delta}^{T\Delta} \lambda_{ij}(t). \tag{4.1}$$

Similarly, the outflow rate $\mu_{ij}(T)$ of road segment (i,j) is the average departure rate of vehicles moving to neighboring road segments in the T^{th} sample time. Note that all variables for the opposite directed road segment of (i,j), namely road segment (j,i), can be defined correspondingly, e.g., $\lambda_{ji}(T)$ and $\mu_{ji}(T)$.

Let $c_{ij}(T)$ denote the maximum number of outflow vehicles of road segment $(i,\ j)$ in T^{th}

sample time, i.e., road capacity, which is determined by the road conditions, the number of lanes, the length of the road, and traffic congestion, etc. Due to fluctuating road conditions and traffic flow conditions, the road capacity can fluctuate with time, but is considered to remain constant within one sample time unit.

Basically, there are two kinds of traffic congestion: recurrent congestion and non-recurrent congestion [33]. The recurrent congestion is due to the tension between the current traffic flow situation (e.g., the traffic inflow $\lambda_{ij}(T)$) and the road conditions (e.g., the road capacity $c_{ij}(T)$), which is non-incident related. The non-recurrent congestion is caused by an accident or incident which can reduce the road capacity (to be introduced in Section 4.4). We define a congestion indicator of a warning message, $\delta(I_{ij})(\in [0,1])$, to represent how the congestion type I happening on road segment (i, j) impacts on the road capacity, where $\delta(I_{ij}) = 1$ means recurrent congestion and $\delta(I_{ij}) \in [0,1)$ implies non-recurrent congestion.

Each vehicle traveling from one intersection to the next is called routing. For each intersection (say intersection i), consider that the RSU nearest to the intersection maintains a virtual queue of length $Q_i^d(T)$, representing the number of the buffered vehicles at this intersection specifically destined to destination d ($\in \Gamma$) in sample time T. Then, the total length of all virtual queues of intersection i for all destinations is $Q_i(T) = \sum_{d\in\Gamma} Q_i^d(T)$, where

$$Q_i^d(T) = \max\{Q_i^d(T-1) - \textstyle\sum_{j\in J_i}\mu_{ij}^d(T-1), 0\} + \sum_{u\in J_i}\lambda_{ui}^d(T-1) \tag{4.2}$$

with $\mu_{ij}^d(T-1)$ being the outflow rate of road segment (i, j) with destination d in the $(T-1)^{th}$ sample time, satisfying $\mu_{ij}(T-1) = \sum_{d\in\Gamma}\mu_{ij}^d(T-1)$. Similarly, for road segment (i, j), we define the leftover number of vehicles in sample time T as $Q_{ij}(T) = \max\{Q_{ij}(T-1) - \mu_{ij}(T-1), 0\} + \lambda_{ij}(T-1)$.

4.2.3 Vehicle Categorization and Mobility Model

Three types of vehicles are considered in this work, namely private cars, taxis, and buses. GPS devices are supposed to be deployed on all vehicles, and GPS devices have ordered the

service of providing shortest paths. Compared with changeable paths of taxis or private cars, scheduled paths of buses are usually fixed. Let $w_m \in \{0, 1\}(m \in \mathbb{V})$ denote the capability of flexible turning for the vehicle m when the vehicle receives any information about congestion or accident, and take the value 1 if vehicle m is a taxi or a private car and 0 otherwise, since taxis or private cars can change their paths while buses have to wait until the traffic trap is cleaned up.

Furthermore, we refer to taxis and buses as super-nodes, connected to a control center through GSM systems. With a specially designed message transmission mechanism (to be introduced in Section 4.3), warning messages can be delivered to the vehicle-traffic server as efficiently as possible to facilitate real-time path planning.

The mobility of each vehicle can be characterized by two random variables (V, D) [83]. Here, V represents the vehicle velocity which takes two possible values (i.e., a lower velocity v_L and a higher velocity v_H). The velocity transition is modeled as a two-state continuous time Markov chain (TCMC) with state transition rate $\frac{1}{D}$. Under this model, a vehicle initially chooses v_L (or v_H), and after an exponentially distributed time interval with the mean of D, the velocity changes to v_H (or v_L). The model can be exploited to describe the realistic driving behaviors, i.e., a driver usually drives at a constant velocity for a period and then changes to a higher/lower velocity based on his/her will and/or road conditions. Besides, when the vehicle density is low or medium (e.g, no larger than 30 vehicle/km/lane), vehicles can be considered to move independently [84] and the headway distance[1] follows the exponential distribution with rate ζ [85].

4.3 Transmission Mechanism and Performance Analysis

Since the incident-related warning message is pivotal to the viability of a real-time path planning algorithm, we propose the following rapid message transmission mechanism and give corresponding analytical results on the end-to-end transmission performance.

[1]The headway distance is defined as the distance between two neighboring vehicles in the same lane.

4.3.1 Outline of Transmission Mechanism

After sensing the congestion, vehicles in the vicinity of the congestion will generate and forward the warning message to other vehicles via multi-hop V2V relaying. If a super-node receives a warning message, it will upload the message to the nearest cellular BS through cellular communication of the public transportation system; otherwise, the message will be transmitted all the way to one RSU via V2V and V2R transmissions. To reduce the redundancy of multi-hop relaying, the following relay node selection is adopted. If there is one bus/taxi within the transmission range of a vehicle, the bus/taxi will be the next-hop receiver; otherwise, the farthest vehicle ahead in the same lane within the transmission range will be selected as the next relay [83]. Besides, we assume that a vehicle deletes the warning message once it has been transmitted. On the other hand, a global message lifetime T_L is preset for each warning message, at the end of which all the transmissions of the corresponding message will be terminated, thus to further control the redundancy in message delivery. Once an RSU or cellular BS receives a warning message, it forwards the message to the vehicle-traffic server via wireline. Upon receiving the warning message, the traffic server will operate the path planning algorithm based on the collected timely road-traffic information. By leveraging this transmission mechanism, emergent messages (e.g., congestion indicators) are promising to be disseminated more efficiently as compared with only utilizing VANETs or the cellular communication capabilities of the public transportation system. Finally, after the vehicle-traffic server finishing path planning, replanned paths are fed back to vehicles demanding path planning via a downlink transmission (i.e., the traffic server - an RSU/vehicle relay - the vehicle in need of path planning).

As shown in Fig. 4.1, the overall communications in the proposed VANET-enhanced ITS can be divided into three layers: V2V and V2R communications in VANETs, wireless communication between super-nodes and BSs via a cellular system, and wired communication between RSUs (or BSs) and the vehicle-traffic server. Thus, the main issues affecting the efficiency of the end-to-end message transmission comes to transmission delay in VANET-

s. By considering the following ideal medium access control (MAC) for V2V and V2R communications, we will analyze the transmission delay in VANETs in the next subsection. Specifically, for analytical simplicity, we assume that once a vehicle moves into the coverage range of an RSU or another vehicle, time slots can be scheduled with neglectable delay for the corresponding V2R or V2V transmissions. Besides, the link rate of a V2V or V2R transmission is assumed to be constant, and the contact duration between each transmission pair is considered long enough to accomplish at least one packet delivery, which can be achieved by appropriately setting the packet size [74].

In general, the transmission delay in VANETs can be discussed under two cases: 1) when the vehicle density is very high (e.g., more than 56 vehicles/mile), the connections among vehicles can be found with high probability, considering that the transmission range of a vehicle (e.g., more than 100m as shown in DSRC) is way more than the average headway distance. In this case, for a given connection path for example from a vehicle to an RSU, we consider neglectable transmission delay because of the assumption of the ideal MAC and small-size packet delivery; 2) for the medium or sparse vehicle density case, due to the intermittency of vehicle communications caused by high-speed mobility and/or node sparsity, the inter-contact time, namely, the waiting time of each hop for the receiver (vehicle or RSU) to fall into the transmission range of the transmitter dominates the end-to-end transmission delay. Notice that congestion may cause an unbalanced vehicle distribution on neighboring roads, and the traffic information report on a road of low node density can be the bottleneck of the VANET-assisted information collection. As such, in the following we analyze the impact of vehicle density on the inter-contact time of one-hop V2V or V2R transmission and further on the end-to-end transmission delay along the transmission path.

4.3.2 End-to-End Delay Analysis

In the following, we analyze the inter-contact time for the aforementioned transmission mechanism. The end-to-end delay analysis begins from the transmissions in pure VANETs,

and then involves the public transportation system.

End-to-End Delay in Pure VANETs

First, consider an uplink with no taxis or buses, i.e., all the hops are based on V2V and V2R communications. We evaluate the transmission delay for the last hop of the V2R transmission. The transmission delay here is mainly due to the inter-contact time between a vehicle and an RSU. Similar to [83], we define the last hop as an "on-off" model, where a vehicle either directly connects to an RSU (i.e., during the "on" state) or is the only vehicle approaching the RSU and there is no other vehicle in the transmission range of the RSU (i.e., during the "off" state). According to the transmission model, the transmission delay of a packet during the "on" state should be way smaller than that during the "off" state. Therefore, the transmission delay of the last V2R hop is mainly due to the "off" period.

Denote the "on" period and the "off" period of a vehicle as T_{on} and T_{off}, respectively. Accordingly, the travel distances within the two periods are defined as U_{on} and U_{off}, respectively, with $T_{on} = \frac{U_{on}}{\overline{V}}$ and $T_{off} = \frac{U_{off}}{\overline{V}}$, where $\overline{V}$ is the average velocity for a vehicle based on the "on-off" mobility model (see Section 5.2.4). Similar to [83], the event that a vehicle moves a distance of at least u during T_{on} before being scheduled to communicate with an RSU should satisfy: 1) there is no other vehicle within the distance u from the end of the RSU coverage ahead of the vehicle, and 2) there is at least one vehicle within the distance $2R - u$, which results in this vehicle moving at least u distance to avoid the collision, with R representing the transmission range of an RSU or a vehicle. Then, we have

$$P_r(U_{on} > u) = \frac{(e^{-\zeta \cdot u})^{b\gamma - 1}[1-(e^{-\zeta \cdot (2R-u)})^{b\gamma - 1}]}{1-(e^{-\zeta \cdot 2R})^{b\gamma}} \tag{4.3}$$

where b is the summation of all road lengths, and γ is the average vehicle density on the roads. Since the vehicle headway distance follows an exponential distribution as mentioned in Section 5.2.4, the probability that a headway distance is larger than u is $e^{-\zeta \cdot u}$. Based on

(4.3), we can obtain

$$E[U_{on}] = \int_0^{2R} P_r(U_{on} > u)du. \tag{4.4}$$

Similarly, the event that a vehicle moves a distance of at least u during T_{off} should satisfy: 1) there is no vehicle within a distance of $2R + u$ from the end of the coverage range of the nearest RSU ahead of the vehicle, and 2) there is at least one vehicle within the distance $L - (u + 2R)$, where L is the distance between the adjacent RSUs. Then, we have

$$P_r(U_{off} > u) = \frac{(e^{-\zeta\cdot(2R+u)})^{b\gamma-1}[1-(e^{-\zeta\cdot(L-(2R+u))})^{b\gamma-1}]}{(e^{-\zeta\cdot 2R})^{b\gamma}[1-(e^{-\zeta\cdot(L-2R)})^{b\gamma}]} \tag{4.5}$$

$$E[U_{off}] = \int_0^{L-2R} P_r(U_{off} > u)du. \tag{4.6}$$

In addition, the previous hops between vehicles within a transmission path except the last hop can be characterized with the vehicle mobility model. The process of the relative velocity between two vehicles can be represented by a CTMC with a state space $\mathbb{H} = \{h_0, h_1, h_2\}$. Here, h_0 represents a negative relative velocity when the vehicle in front moves with v_L while the vehicle behind moves with v_H; h_1 models a zero relative velocity (i.e., both vehicles move with the same velocity); h_2 represents a positive relative velocity. If each vehicle keeps the same velocity for an exponential time with an average of D, the transition rate between any two states of the Markov process is equal to $2/D$. Thus, from [83], the average number of hops M of an end-to-end transmission path from a message source to an RSU in pure VANETs can be approximated as

$$M = \frac{6(L-E[U_{on}]-E[U_{off}])}{D(v_L+v_H)}. \tag{4.7}$$

Then, based on the average number of hops, the transmission delay of such a transmission path can be shown as

$$\psi = (M-1)E[T_{V2V}] + E[T_{off}] \tag{4.8}$$

where $E[T_{V2V}] = \frac{1}{1-e^{-\zeta R}}$ is the average transmission delay for a V2V hop, since the head-

way distance follows an exponential distribution. $E[T_{off}]$ is the average duration of the "off" period as defined before. If we consider the downloading as a similar process with uploading, the total transmission delay can be approximated by 2ψ [2]. Note that this transmission delay is related to the parameters including vehicle mobility parameters (V and D), vehicle density (γ), and RSU related parameters (the transmission range R and the average distance between RSUs L). Then, the probability of a M-hop transmission path with all V2V and V2R communications equals the probability that there is neither taxi nor bus in any hop within the M-hop transmission path, i.e., $(1 - P_T - P_B)^M$, where P_T (P_B) is the percentage of taxis (buses) in the traffic stream.

End-to-End Delay in Hybrid-VANET-enhanced Network

If the public transportation system is involved in delivering messages as aforementioned, the probability of a given number of hops from a private car to the nearest bus/taxi follows a geometric distribution. The average number of hops in the hybrid VANET-enhanced ITS, M', is as

$$M' = M \cdot (1 - P_B - P_T)^M + \sum_{i=1}^{M} (i-1) \cdot (1 - P_B - P_T)^{i-1} \cdot (P_B + P_T). \tag{4.9}$$

Then, if we consider that the public transportation system are perfectly connected with no delay, the average transmission delay is dominated by the transmission delay in VANETs. Based on the probability of a given number of hops from a private car to the nearest bus/taxi, the transmission delay in a multihop message transmission path is rewritten as

$$\psi' = \psi \cdot (1 - P_B - P_T)^M + \sum_{i=1}^{M} (i-1) \cdot (1 - P_B - P_T)^{i-1} \cdot (P_B + P_T) \cdot E[T_{V2V}]. \tag{4.10}$$

From (4.10), the end-to-end transmission delay in hybrid ITS is related to 1) vehicle mobility parameters (i.e., V and D), 2) vehicle density and super-node percentage (i.e., γ, P_B, and

[2]The approximation is valid if the end-to-end transmission delay can be well controlled to a small value in which the network topology changes little or the source vehicle only moves a relatively small distance.

P_T), and 3) RSU deployment in the network (e.g., the transmission range R and the average distance between RSUs L).

4.4 Problem Formulation

In this section, based on the traffic flow model defined in Section 4.2.2, the traffic flow balance constraint of each intersection is first identified. The road capacity and congestion indicator are then discussed under different traffic conditions. Subsequently, considering the drivers' travel-cost preferences in the path planning, the cost metric of path planning for individual vehicle is defined. In addition, the network stability constraint is shown. Finally, the real-time path planning problem is formulated to not only avoid the congestion but also reduce the average travel cost caused by path planning.

4.4.1 Intersection Flow Balance Constraint

For an intersection i ($\in \mathbb{I}$), the following flow balance equation should be satisfied to guarantee that the aggregate vehicle arrival rate is equal to the aggregate vehicle departure rate

$$\sum_{j \in J_i} \mu_{ji}(T) = \sum_{u \in J_i} \lambda_{iu}(T), \ \forall i \in \mathbb{I}, \tag{4.11}$$

where the left and right side of the equation are respectively referred to as the aggregate vehicle arrival and departure rates.

4.4.2 Road Capacity and Congestion Indicator

For road segment (i, j), the vehicle inflow rate for sample time T is $\lambda_{ij}(T)$. The average outflow rate changes with the inflow rate, but with some time delay (denoted as Λ seconds which is the travel time for a vehicle moving from intersection i to intersection j), i.e., $\mu_{ij}(T) = \lambda_{ij}(T - \Lambda)$, until reaching the outflow rate limit, i.e., road capacity $c_{ij}(T)$. Here,

Λ is decided by the tension between the traffic inflow and road capacity. Once an incident/accident occurs, the outflow rate drops dramatically on one road segment. To illustrate the road capacity under different traffic conditions, we discuss the road capacity in two cases: 1) no incident-related congestion (i.e., recurrent congestion), and 2) the incident-related congestion (i.e., non-recurrent congestion). The road capacities under two cases will be illustrated respectively as follows.

1) When there is no incident-related congestion on (i, j), according to [33], we have

$$c_{ij}(T) = c_{ij}^N = N_{ij} \cdot c_{ij}^p \cdot F_{PH} \cdot \frac{1}{(1 + E_B \cdot P_B) \cdot A} \tag{4.12}$$

where c_{ij}^N is the road capacity under no incident-related congestion case. N_{ij} is denoted as the number of lanes in road segment (i, j). The ideal capacity per lane is c_{ij}^p. F_{PH} is the peak-hour factor, i.e., the ratio of the peak 15-min flow rate in vehicles per hour (vph) to the average hourly flow rate (vph). E_B is the bus equivalent[3] to private cars or taxis. P_B is the percentage of buses in the traffic stream. A is an adjustment factor to account for other factors with impact on road capacity. Under this case,

$$\mu_{ij}(T) = \min\{\lambda_{ij}(T - \Lambda^r), c_{ij}(T)\} \tag{4.13}$$

with Λ^r called recurrent delay [33] and satisfying

$$\begin{aligned} \Lambda^r = T_{ij}^0 + D_{ij}^q + 0.25T[(\tfrac{\lambda_{ij}(T)}{c_{ij}(T)} - 1) + \\ \sqrt{(\tfrac{\lambda_{ij}(T)}{c_{ij}(T)} - 1)^2 + \tfrac{16 J_{ij} \cdot L_{ij}^2 \cdot \lambda_{ij}(T)}{N_{ij}^2 \cdot T^2 \cdot c_{ij}(T)}}]. \end{aligned} \tag{4.14}$$

Here, $T_{ij}^0 = L_{ij}/V_0$ is the segment travel time measured at free flow speed V_0, with L_{ij} being the length of road segment (i, j). $J_{ij} = \frac{(T_{ij}^c - T_{ij}^0)^2}{L_{ij}^2}$ is a calibration parameter, with T_{ij}^c being the segment travel time measured when the traffic demand equals road capacity. D_{ij}^q is the

[3]The bus equivalent is the number of buses displaced by a single taxi or private car in a suburban area [86].

delay due to leftover queue from the prior sample time, i.e.,

$$D_{ij}^{q} = \frac{Q_{ij}(T)}{2 \cdot c_{ij}(T) \cdot T} \cdot \min\{T, \frac{Q_{ij}(T)}{c_{ij}(T) \cdot [1 - \min(1, \frac{\lambda_{ij}(T)}{c_{ij}(T)})]}\}.$$

2) When there is an incident I_{ij} on road segment (i, j), we still hold

$$\mu_{ij}(T) = \min\{\lambda_{ij}(T - \Lambda^{nr}), c_{ij}(T)\} \tag{4.15}$$

where Λ^{nr} is called non-recurrent delay and can also be calculated based on (4.14). However, in this case,

$$c_{ij}(T) = c_{ij}^{I} = c_{ij}^{N} \cdot \delta(I_{ij}), \forall \delta(I_{ij}) \in [0, 1) \tag{4.16}$$

where $\delta(I_{ij})$ is the percentage of remaining road capacity during incident type I on road segment (i, j), i.e., congestion indicator. The value of $\delta(I_{ij})$ depends on the incident type I and is considered to be sensed by witness/victim vehicles and delivered to the nearest RSU or BS. c_{ij}^{I} is thus the road capacity under the incident I. Take the case that a road segment has one lane in each direction as an example. When an accident I happens, we may consider that $\delta(I_{ij}) = 0$ and $\mu_{ij}(T) = c_{ij}^{I} = 0$, since no vehicle-traffic flow will pass. On the other hand, in a case that a road segment has multiple lanes in each direction, the traffic flow will not be zero, but might still drop dramatically.

Furthermore, if there is no incident-related congestion on road (i, j), $\delta(I_{ij}) = 1$. Then, we can extend the following relationship between the indicator and road capacity:

$$c_{ij}(T) = c_{ij}^{N} \cdot \delta(I_{ij}), \forall \delta(I_{ij}) \in [0, 1] \tag{4.17}$$

which implies that the road capacity drops once an accident happens on a certain segment until the accident is cleaned up. The outflow rate should be always no more than the according road capacity, i.e.,

$$\mu_{ij}(T) \leq c_{ij}(T). \tag{4.18}$$

4.4.3 Path Planning Cost Metric

The path planning algorithm is to avoid the congestion on the road, with considering the preference of drivers, e.g., the shortest path or the most familiar path. Here, we consider the path length as the driver's first-order preference. Let $L_{r_{ij}}^{m_d}$ denote the changed path for vehicle m (with destination d) at intersection i, where r_{ij} means that, according to the newly planned path, vehicle m changes its path by going through road segment $(i,\ j)$ towards destination d, satisfying $j \in J_i$. Compared to current path length $L_{S_i}^{m_d}$, the increased path length is $|L_{r_{ij}}^{m_d}| - |L_{S_i}^{m_d}|$, where S_i is the path choice before being replanned. Obviously, it is possible that the changed path leads to more travel time and more consumed fuel energy. Let $p_{r_{ij}}^{m_d}$ denote the cost of vehicle m for a certain turning decision r_{ij} towards destination d, given $S_i \neq r_{ij}$. If intersection i is not in the current path of m_d, $p_{r_{ij}}^{m_d}$ is zero; otherwise, it is modeled with respect to the increased path length as follows

$$p_{r_{ij}}^{m_d} = \rho(|L_{r_{ij}}^{m_d}| - |L_{S_i}^{m_d}|) \tag{4.19}$$

where $\rho(.)$ is a non-negative increasing function to measure impacts of the increase of path length $(|L_{r_{ij}}^{m_d}| - |L_{S_i}^{m_d}|)$ [87]. Then, the average cost of vehicles taking turning r_{ij} on road segment (i, j) can be calculated as

$$p_{ij}(T) = \begin{cases} \frac{1}{\sum\limits_{m\in\mathbb{V}} w_m} \sum\limits_{m\in\mathbb{V}, d\in D} w_m \cdot p_{r_{ij}}^{m_d},\ \text{if} \sum\limits_{m\in\mathbb{V}} w_m \neq 0; \\ \infty, \quad \text{otherwise.} \end{cases} \tag{4.20}$$

For an intersection (say intersection i), since there may be several neighboring intersections as the candidates of the coming intersections, the average cost of vehicles belonging to intersection i is defined as

$$p_{iJ_i}(T) = \begin{cases} \frac{1}{\sum\limits_{j\in J_i} \alpha_{ij}(T)} \sum\limits_{j\in J_i} \alpha_{ij}(T) p_{ij}(T),\ \text{if} \sum\limits_{j\in J_i} \alpha_{ij}(T) \neq 0; \\ 0,\ \text{otherwise} \end{cases} \tag{4.21}$$

where $\alpha_{ij}(T)$ is set as 1 in the first case of Eq. (4.20) (i.e., when $\sum_{m \in \mathbb{V}} w_m \neq 0$); otherwise 0.

4.4.4 Network Stability

The definition of *Queue and Network Stability* [88] is used to represent traffic congestion avoidance in our path planning optimization problem[4]. For intersection i, $Q_i(T)$ is strongly stable if and only if

$$\lim_{T_0 \to \infty} \sup \frac{1}{T_0} \sum_{T=0}^{T_0} E[Q_i(T)] < \infty. \tag{4.22}$$

The information on $Q_i(T)$ is required to identify whether an intersection is stable or not. If the traffic inflow and outflow information is detected by the cameras or traffic flowmeters connected to RSUs, $Q_i(T)$ is expected to be calculated directly. If the traffic information is relayed in VANETs as there is no RSU at the intersection, the relayed information is utilized in the vehicle-traffic server to predict the traffic flow information with a certain transmission delay. According to (4.10), this uploading transmission delay can be estimated as $\frac{\psi'}{\Delta}$, which here is mainly caused by the intermittent connections in VANETs. With this transmission delay, the proposed algorithm can utilize a more accurate virtual queue information for path planning in each sample time, i.e., $Q_i(T - \left\lceil \frac{\psi'}{\Delta} \right\rceil)$. Note that if and only if all queues in the network are strongly stable, vehicle traffic in the whole road network is strongly stable.

4.4.5 Utilization-Minus-Cost Maximization Problem

Taking account of both the traffic flows of the network and the path planning cost of vehicles, the objective of the path planning algorithm is considered to maximize the overall spatial-utilization-minus-planning-cost at the same time with the network congestion avoidance. This objective indicates that the total traffic flow improvement and the path planning cost reduction should be jointly considered and carefully balanced. Specifically, once the traffic

[4]The definition of *Queue and Network Stability* is also used for example in [89] and [90] for the stability and utility optimization to make online control decisions.

server receives the traffic flow and accident warning messages collected from both RSUs and vehicles via VANETs (or cellular netowrks), a path planning algorithm is calculated to update and determine $\lambda_{ij}(T)$ according to the optimization problem, i.e., the number of vehicles dispatched over road segment (i, j) in the T^{th} sample time.

$$\begin{aligned} &\max \textstyle\sum_{i\in\mathbb{I}}\sum_{j\in J_i}\lambda_{ij}(T) - \sum_{i\in\mathbb{I}}p_{iJ_i}(T) \\ &\text{s.t. } (4.11), (4.18), (4.22) \end{aligned} \tag{4.23}$$

This objective is to maximize the spatial utility while minimizing travel cost, under the constraints: 1) the flow balance of each intersection; 2) the limitation of outflow rate on each road segment; and 3) the congestion avoidance of each intersection. We exploit Lyapunov optimization process [91] to solve this problem (to be introduced in Section 4.5). Then, in the sample time T, based on the path planning algorithm, a vehicle with destination d can be dispatched from one intersection to another (say from intersection i to intersection j with contribution $\lambda_{ij}(T)$), in order to improve the spatial utility as well as to reduce travel cost. And this updated path will deliver to the GPS device to navigate the required vehicle. In other words, a turning decision, r_{ij}, for a taxi or a private car at intersection i, can be decided based on the corresponding $\lambda_{ij}(T)$ and $p_{iJ_i}(T)$, and furthermore the replanned path can be calculated based on this turning decision. Note that if the traffic flow information is collected by VANETs (or cellular networks), the transmission delay in VANETs, i.e., $\frac{\psi'}{\Delta}$, should be considered in the third constraint as discussed in Section 4.4.4.

4.5 Mobility-aware Real-time Optimal Path Planning in the Vehicular Networks

In this section, the path panning algorithm is first proposed to help vehicles to bypass congestion and balance traffic evenly in the whole network. Then, the convergence and the computation complexity of the proposed algorithm are discussed.

4.5.1 Path Planning Algorithm Design

The optimization problem (4.23) can be solved by applying the drift-plus-penalty framework in Lyapunov optimization process [91]. By following dynamic algorithm at each sample time, we derive vehicles' turning decisions for maximizing the lower bound of network throughput. According to the Lyapunov optimization process, let $W_{iJ_i}(T)$ denote the weight of intersection i in sample time T,

$$\begin{aligned} W_{iJ_i}(T) = \textstyle\sum_{j\in J_i}\alpha_{ij}(T)\min\{c_{ij}(T), \sum_{d\in D}\{Q_i^d(T)-Q_j^d(T)\}\} \\ -Kp_{iJ_i}(T) \end{aligned} \tag{4.24}$$

where K is a non-negative constant defined by vehicle traffic server used for all vehicles, with the same order of the reciprocal of travel cost (i.e., $p_{iJ_i}(T)$) [91]. Equation (4.24) implies that the weight of an intersection (say intersection i) is realted to i) the differential queue backlog between intersection i and its neighboring intersections; ii) average intersection travel cost. Vehicles at intersection with the largest weight are replanned first. Vehicles with destination d stored at intersection i, should be dispatched to queue $Q_{j_d^*}^d(T)$ of intersection j_d^*, where $j_d^* = \underset{j\in J_i}{\operatorname{argmax}}\{Q_i^d(T) - Q_j^d(T)\}$, according to the largest differential queue backlog. The number of the vehicles with destination d replanned to intersection j_d^* is $\min\{Q_i^d(T) - Q_{j_d^*}^d(T), c_{ij_d^*}(T)\}$. Then queues at all the remaining intersections are updated correspondingly. The same process continues until all intersections related are processed. The implication of path planning is to prioritize those vehicles in such an intersection with larger differential queue backlogs and shorter increased path lengths under new turning decisions (i.e., lower average travel cost).

4.5.2 Analysis of Algorithm Performance

For the network stability of the proposed path planning algorithm, we have the following Lemma 1.

Lemma 3 *With the proposed path planning algorithm, network stability can be guaranteed.*

Proof. To prove network stability, according to [91], we need to show that the summation of the average square of queue sizes of those intersections' virtual queues does not increase with time. Consider the inter-flow exchange between any two intersections (say i and j). Let $Q_i(T)$ ($Q_i(T+1)$) and $Q_j(T)$ ($Q_j(T+1)$) respectively denote the queue lengths of intersections i and j in sample time T ($T+1$). In specific, based on our path planning algorithm, between two neighboring intersections, vehicles are always dispatched from a long queue to a short queue. Assume that the change of the queue length of the two intersection is because $q_j^d(T)$ vehicles, where $d \in \Gamma$, are dispatched from intersection i to intersection j, i.e., $Q_i^d(T+1) = Q_i^d(T) - q_j^d(T)$ and $Q_j^d(T+1) = Q_j^d(T) + q_j^d(T)$. Then, the consequence of $q_j^d(T)$ dispatched vehicles is,

$$\begin{aligned} &E\{([Q_i(T+1)]^2 + [Q_j(T+1)]^2) - ([Q_i(T)]^2 + [Q_j(T)]^2)\} \\ &= 2E\{(\sum_d q_j^d(T) - Q_i(T) + Q_j(T)) \cdot \sum_d q_j^d(T)\}, \end{aligned} \tag{4.25}$$

where $\sum_d q_j^d(T)$ is the total number of vehicles, which are dispatched from intersection i to intersection j at time T. As we have $q_j^d(T) = \min\{Q_i^d(T) - Q_j^d(T), c_{ij}(T)\}$, $Q_i(T) = \sum_d Q_i^d(T)$ and $Q_j(T) = \sum_d Q_j^d(T)$, the following inequality holds

$$\sum_d q_j^d(T) + Q_j(T) - Q_i(T) \leq 0. \tag{4.26}$$

Thus, the right side of (4.25) is no more than zero. Then, the summation of average squares of queue size is satisfied as,

$$E\{[Q_i(T+1)]^2\} + E\{[Q_j(T+1)]^2\} \leq E\{[Q_i(T)]^2\} + E\{[Q_j(T)]^2\}. \tag{4.27}$$

That is, the summation of average square of queue size of those intersections' virtual queues does not increase with time. Under the cases with all destinations and multiple intersections, the similar results still hold, which implies the stability of network and the avoidance of

traffic congestion in a network as discussed in [91]. □

Furthermore, the computational complexity of the proposed algorithm is given as following Lemma 2.

Lemma 4 *The total computational complexity is proportional to the square of the number of intersections in the map times the upper bound of the number of neighboring intersections.*

Proof. We first calculate the weight of each intersection, thus the complexity of this step is $O(|\mathbb{I}|)$. Second, we schedule each intersection in I_c. For each intersection to be scheduled, we need to find the right neighboring intersection j_d^* for each destination d. Therefore, the complexity of the second step is $O(|I_c|((1+|I_c|)/2+|\Gamma|U))$, where U is the upper bound of the number of neighboring intersections of one intersection. As the $|I_c|$ and $|\mathbb{I}|$ are in the same order, the overall complexity is given by

$$O(|\mathbb{I}|)+O(\frac{|\mathbb{I}|+|\mathbb{I}|^2}{2}+|\mathbb{I}||\Gamma|U). \tag{4.28}$$

Furthermore, as the number of roads $|\Gamma|$ and that of intersections $|\mathbb{I}|$ have the relationship $2\Gamma/U \leq |\mathbb{I}|$, the complexity can be further simplified as

$$O(|\mathbb{I}|)+O(\frac{|\mathbb{I}|+|\mathbb{I}|^2}{2}+\frac{|\mathbb{I}|^2U^2}{2})=O(|\mathbb{I}|^2U^2). \tag{4.29}$$

Thus, the total computational complexity is proportional to the square of the number of intersections in the map times the upper bound of the number of neighboring intersections. □

The proposed path planning algorithm can perform better than the conventional path planning, because (1) the proposed path planning algorithm is updated based on real-time and accurate messages received from V2V/V2R communication, by which, for instance, a warning message of traffic jam can be delivered and impact timely on decisions of path planning; (2) furthermore, in hybrid VANET-enhanced networks, public transportation system can help to deliver the messages, leading to the reduced transmission delay for delay-sensitive real-

Figure 4.3. The simulation scenario of University of Waterloo region in VISSIM.

time path planning; (3) the proposed path planning is designed to reduce traveling cost in a coordinated manner to avoid particular parts of the road network overloaded; and 4) the relatively low computational complexity of the proposed algorithm makes the path planning algorithm achieve better performance in a reasonable and realistic way.

4.6 Performance Evaluation

In this section, we consider a realistic suburban scenario as shown in Fig. 5.4(a), which is the region around the campus of University of Waterloo (Waterloo, ON, Canada). To emulate the timeliness of the proposed communication framework, a highly realistic microscopic vehicle traffic simulator, VISSIM [92], is employed to generate vehicle trace files for recording the vehicle mobility characteristics, based on which the effectiveness of the hybrid communication in supporting real-time path planning is studied. However, since the pathes of vehicles cannot be changed or controlled by the external algorithm in VISSIM, we further develop a Java-based platform to investigate the performance of the proposed path planning algorithm. Specifically, average moving delay (AMD), defined as the average travel time per trip, is used as a metric in the evaluation.

4.6.1 Simulation Setup

Simulation settings in VISSIM

To simulate a VANET with VISSIM in Kitchener-Waterloo (K-W) downtown region, vehicles are pushed into the region of 6000m $* 2800$m, as shown in Fig. 5.4(a). At the beginning of the simulation, vehicles are set to enter the region from the preset entries (e.g., 9 entries at the ends of main roads), following a Poisson process at a rate 2500 vehicle/hour/entry. The proportion of a bus or a taxi in the traffic flow is set as 5%. After the duration of the first 240s, the vehicle pushing-in stops to reach an equivalent average density 30 vehicle/km/lane which represents a medium density scenario. Similarly, if the first duration is set to be 480s, the scenario becomes a high density one. In the VISSIM, vehicle information (e.g., location and velocity, etc) is recorded every 0.2s. The total simulation time lasts for 3600s. In addition, the velocity distribution for all vehicles follows the velocity model described in Subsection 5.2.4 with parameters $v_L = 30$km/hour, $v_H = 60$km/hour, and $D = 600$s. The reduced speed areas can be set at any time during the simulation in VISSIM, to simulate different kind of incidents/accidents in the suburban scenarios.

Simulation settings in Java

To evaluate the performance of the path planning algorithm in Java, with the same region, 500 vehicular nodes with transmission radius of 150 meters are first randomly deployed to cover K-W downtown region, as shown in Fig. 5.4(a). In addition, 12 intersections are chosen as candidates for RSU deployment in the region. Further, each vehicle moves to its destination with a velocity of 60 km/h (or 30 km/h). The path planning can be performed at the beginning of a sample time, e.g., 10s. The lifetime of a warning message, T_L, is set as 300s. The duration for each simulation is set to be three hours, and the results are averaged over 100 runs. To illustrate the effect of different kinds of accidents on path planning, big accidents are set to last for 20 mins, while small accidents are set to last for only 10mins.

4.6.2 Evaluation of Transmissions in VISSIM

We first evaluate the transmission performance of VANETs in a high density scenario. The evaluated metrics are the connection probability of a vehicle to an RSU and the end-to-end transmission delay. As shown in Fig. 4.4(a), in a high density scenario, the connection probability is high even without the support of cellular network. For instance, when the vehicle transmission range is 120m (which is very easy to be reached as discussed in [1] and way larger than the average headway distance), the connection probability can be 80%. As the transmission range of vehicle increases, the connection probability increases, since the increased the transmission range supplies more chances to connect with other vehicles or RSUs. Furthermore, as shown in Fig. 4.4(a), in the high density case, the transmission delay is only around 5.5s, which is less than a sample time 10s. Notice that a short end-to-end transmission delay facilitates the implementation of real-time path planning, which needs traffic information update as timely and accurate as possible.

The inter-contact time is evaluated through the vehicle headway distance (i.e., V2V distance) and the last-hop V2R distance. Based on the trace files from VISSIM, Fig. 5.5(a) shows the probability density function (PDF) of vehicle headway distance. It is shown that the PDF of the headway distance matches well with an exponential distribution as shown in Fig. 5.5(a), which validates the premise in Subsection 5.2.4. Based on the resultant headway-distance distribution, the average V2V inter-contact time, $E[T_{v2v}]$, can be obtained, as shown in Section 4.3.2.

Besides, the PDF of the distance from the last-hop vehicle to the nearest RSU for one delivery is given in Fig. 5.5(b). The simulated PDF matches well with the theoretical PDF, which is calculated with the parameters in the simulation setup based on Eq. (5.18). According to Fig. 5.5(b), the average distance from a last-hop vehicle to its neatest RSU can be further calculated to be around 180m. Then the transmission delay incurred by the inter-contact time of the last-hop V2R transmission can be calculated as discussed in Section 4.3.2, i.e., $E[T_{off}] = E[U_{off}]/\overline{V} = E[Last-hop\,V2R\,distance - R]/\overline{V}$.

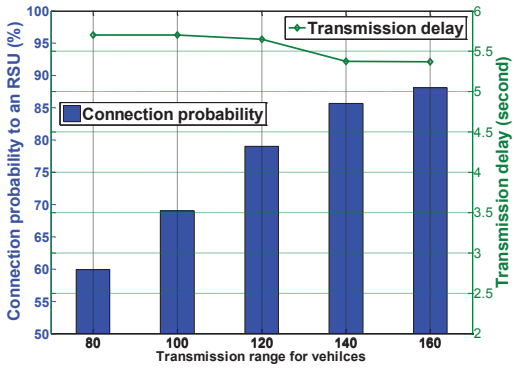

(a) Transmission performances in a high vehicle-density scenario.

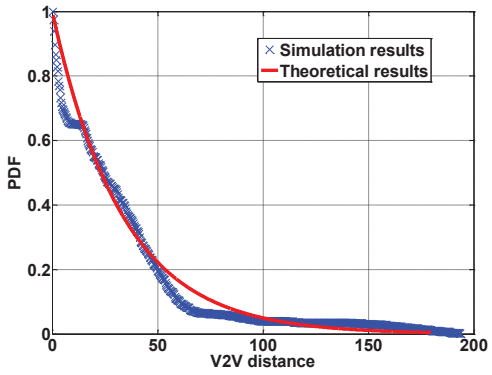

(b) The PDF of V2V distance.

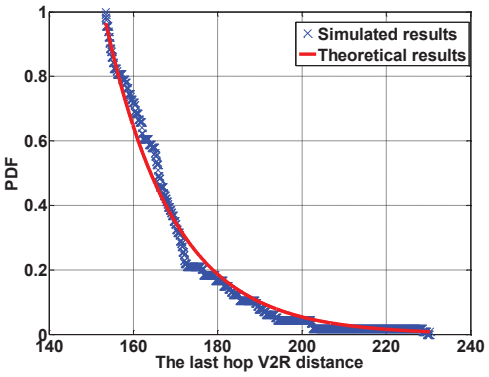

(c) The PDF of the last hop V2R distance.

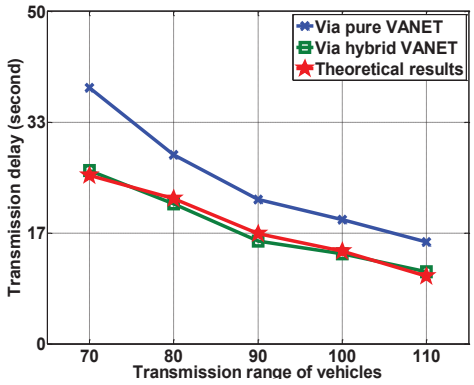

(d) The transmission delay of a vehicle to an RSU given transmission range.

Figure 4.4. The performance of the proposed transmission mechanism.

We then investigate the end-to-end transmission performance in terms of the connection probability and transmission delay in the medium density scenario. Based on the proposed transmission mechanism, a hybrid VANET is utilized to reduce the transmission delay, making the path planning more efficient and timely. As shown in Fig. 4.4(d), via pure VANETs, the average end-to-end transmission delay decreases as the transmission range increases, since the increased transmission range gives higher possibilities for a transmitting vehicle to find an end-to-end path to an RSU (given neglectable transmission delay when two vehicles are within the transmission range of each other). Moreover, in hybrid VANETs, when the public transportation system is utilized, the increased transmission range can significantly

create more chances to meet a bus or a taxi, thus leading to a smaller transmission delay. Notice that once any bus or taxi nodes receive the messages, they can help deliver the messages to the vehicle-traffic server directly via the cellular network, and the intermittent connections of the multi-hop VANET can be efficiently reduced. Especially, as the transmission range of vehicles becomes smaller (i.e., the problem of intermittent connections in VANETs is severer), the delay reduction comes to be bigger if the hybrid VANET-enhanced transportation system is involved. The reason is that with a smaller transmission range, an end-to-end transmission path is more difficult to be guaranteed by pure VANETs, leading to a larger delay gap compared to the one that utilizes the hybrid VANET-enhanced transportation system. In addition, the simulated results of transmission delay match well to the theoretical ones shown in Eq. (4.10). Hence, based on the proposed transmission mechanism, an efficient and timely message transmission for path planning can be achieved, which makes it possible to perform global real-time path planning.

4.6.3 Simulation of the Proposed Path Planning in Java

Fig. 4.5(a) shows the average moving delay with and without implementing the proposed path planning algorithm. We can observe that the AMD with the proposed path planning is much lower than that without path planning. For example, when accident number is two, AMD is reduced by 35%. Furthermore, with more accidents, AMD becomes longer; however, the ones utilizing the proposed path planning algorithm increase more slowly. The cost of path planning in terms of the increased path length is also shown in Fig. 4.5(a). When a vehicle wants to change its previous shortest path due to a sensed accident ahead, a novel smooth path is generated with less AMD at the cost of the increased path length. It shows that the average cost for users is still admissible when traffic environments are in terrible conditions.

In addition, Fig. 4.5(b) shows the AMD comparison between our proposed path planning algorithm and a distributed path planning algorithm proposed in [93]. In the distributed path

planning, each individual vehicle re-searches a new path based on the known information of accidents when it receives any information on congestion or accidents, but neither with coordination among vehicles nor considering the individual cost of path planning. As shown in Fig. 4.5(b), AMD under our proposed path planning is reduced on average by 27% as compared with that of the distributed algorithm. Because each individual vehicle plans path only on its own interest, it is very possible that a number of vehicles swarm into the same road segment based on the same warning message information. Then new traffic jam can happen with high probability and result in the increased AMD. Fig. 4.5(b) shows a good adaptability of the proposed path planning algorithm to avoid introducing other traffic jam.

Fig. 4.6(a) illustrates the effect of different kinds of accidents on AMD. It is shown that when a big accident continues for a long duration (i.e., 20 minutes), AMD increases, compared to a small accident (i.e., lasting 10 minutes only). This is because that some vehicles have no capabilities to change their current paths (e.g., buses), AMD increases due to their longer trapped time in congestion. Similarly, when the number of accidents increases, AMD becomes longer, but not much. Thus, it implies that our proposed path planning algorithm is with a good adaptability to different accident durations. Besides, if the number of slow-speed vehicles increases, more vehicles slowed down to 30 km/h will introduce larger AMD as shown in Fig. 4.6(b). Since more slow vehicles on one road can result in a high vehicle density, Fig. 4.6(b) shows a good adaptability to vehicle densities. Furthermore, comparing this performance with the one in Fig. 4.5(a), AMD is a little longer than the case under few slow vehicles, since network vehicle-traffic throughput is diminished due to more vehicles with slow speed stranded on one road.

The sensitivity analyses in terms of both the vehicle number and the number of accidents on average moving delay (AMD) are discussed in Fig. 4.7. Here, we considerer that the accidents are big ones, lasting for 20 mins. First, we can see that the AMD increases with the increased number of vehicles under our algorithm in Fig. 4.7. The reason for this AMD increment is that more vehicles may result in a higher probability of introducing another traffic jam at crossings. However, taking the case with three accidents as an example, even

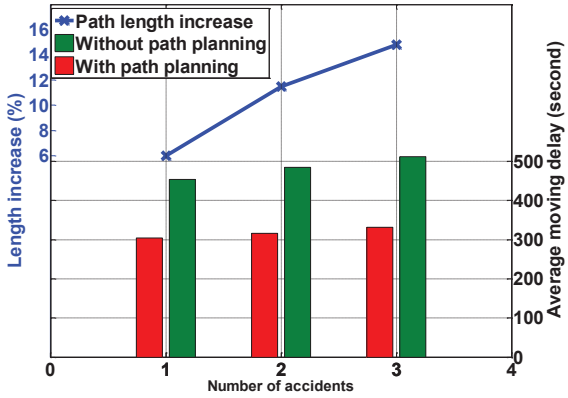

(a) Comparison of AMD between the proposed path planning and the traditional one.

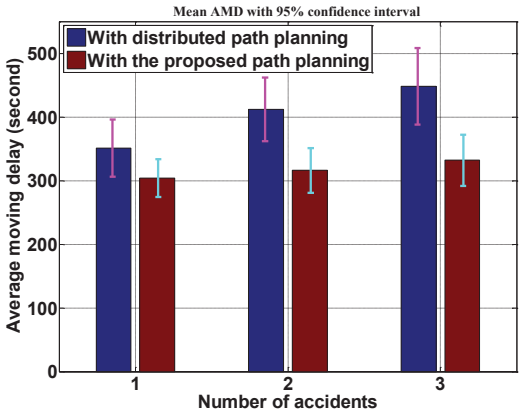

(b) Comparison of AMD between the proposed path planning and one distributed algorithm.

Figure 4.5. AMD reduction by path planning.

when the number of vehicles increases to 800, AMD is relatively small, around 375s as shown in Fig. 4.7. This result shows a good adaptability of the proposed path planning algorithm to the total vehicle number. In addition, Fig. 4.7 shows that the AMD increases with the increased number of accidents with the similar trend as aforementioned.

4.7 Summary

In this chapter, considering the mobility of vehicles, with the help of vehicular communications, real-time path planning has been designed to smooth the vehicle traffic in an ITS, to

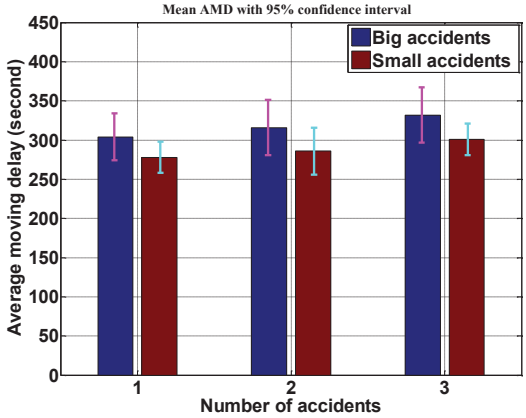

(a) AMD comparison between different accident time duration.

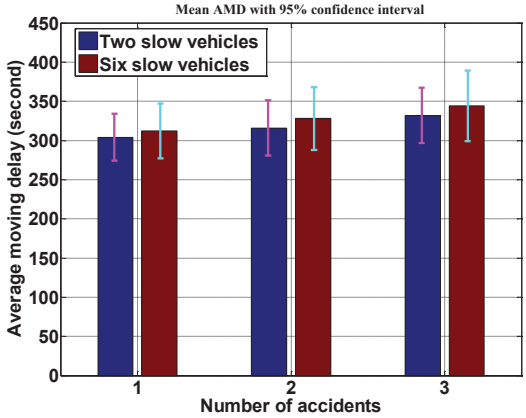

(b) AMD comparison between different numbers of slow vehicles.

Figure 4.6. AMD versus specified accidents.

efficiently relieve traffic congestion in urban scenarios. This strategy can be used to smooth the vehicle traffic of an urban scenario in realistic, to avoid the vehicle-traffic congestion. The central philosophy of our proposed path planning is that based on the real-time collected vehicular information, the traffic-server can balance the vehicle traffic of the whole network by utilizing the mobility of vehicles, to increase vehicle-traffic throughput with approaching the vehicle-traffic capacity.

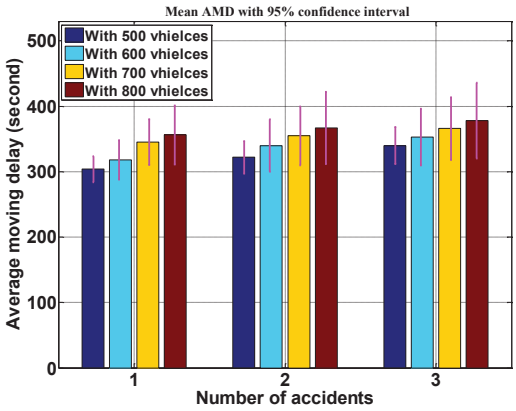

Figure 4.7. AMD versus both the number of vehicles and specified accidents.

Chapter 5

Mobility-Aware Coordinated EV Charging in VANET-Enhanced Smart Grid

In this chapter, we investigate a special smart grid with enhanced communication capabilities, i.e., a VANET-enhanced smart grid. It exploits VANETs to support real-time communications among RSUs and highly mobile EVs for collecting real-time vehicle mobility information or dispatching charging decisions. Then, we propose a mobility-aware coordinated charging strategy for EVs, which not only improves the overall energy utilization while avoiding power system overloading, but also addresses the range anxieties of individual EVs by reducing the average travel cost.

5.1 Introduction

EVs, as a promising component of sustainable and eco-friendly transportation systems, have received considerable attention in many countries across the world [27] [14]. Refueled by electricity instead of gasoline, these vehicles have the potential to save thousands of dollars for customers over the vehicle lifetime. Besides, the adoption of EVs into the transport sector

can reduce the consumption of conventional energy sources (e.g., gasoline) and the pollution of environments (e.g., greenhouse gas emissions). As reported in [16], battery EVs, which completely depend on rechargeable batteries and thus produce no emissions, can cut down the overall emissions from the transport sector by 70%. Due to the above advantages, EVs have been accounting for higher market share in the transport sector. According to the report of Electric Power Research Institute (EPRI) [17], the EV penetration level can reach 35%, 51%, and 62% by 2020, 2030, and 2050, respectively.

However, the widespread adoption of EVs in the transportation system will lead to charging problems of mobile EVs that are fully reliant on rechargeable batteries. EV charging, which is very likely to coincide concentratively with the peak demand time of the power system, can incur overloading of a distribution feeder, resulting in the system instability and the reduction in energy utilization [18] [19], especially for fast EV charging as it requires much higher power than the regular charging. Some works use energy storage systems to mitigate the impact of fast EV charging on the power system, but at an additional cost of deploying the energy storage devices [14]. Thus, to avoid power system overload during the peak time and improve energy utilization without additional deployment cost, load management strategies are indispensable to distribute the EV charging load both temporally and spatially in a coordinated fashion. At the same time, for fast EV charging, the assigned charging stations must be within the range of individual mobile EVs given current locations and battery energy levels, due to the tension between the current battery energy levels and the travel cost to reach charging stations, i.e., range anxiety.

There has been abundant literature [20–26, 35, 68–71] concerning the coordinated EV charging strategy design for EVs. But most of the works so far solve problems only in the power system aspect. That is, the coordinated charging is performed for a group of EVs that are assumed to be ready for charging within an area (e.g., parking lots or residence areas). Little research has considered vehicle-specific features, i.e. the vehicle mobility, into the charging strategy when fast-charging is considered. In fact, as EVs may need charging when moving on the road, the energy consumption on the road to reach the charging station,

referred to as the travel cost in this chapter, should be considered. Otherwise, the charging station assigned by the existing strategies may be too far to reach given the EV's current location and battery energy level. Due to this range anxiety, drivers prefer to charge at locations with less travel cost. Therefore, new charging strategies are required to take the range anxieties and vehicle mobility into consideration to reduce the EV travel cost. In order to track the vehicle mobility, real-time information of EVs (e.g., locations and battery energy levels) should be collected to assist charging strategy design.

To this end, in this chapter, we focus on leveraging the real-time mobile vehicle information to help designing an efficient coordinated EV charging strategy. The objective is to improve the overall energy utilization, reduce the average EV travel cost, and prevent the overload of the power system. To properly design the strategy, two underlying key problems should be deliberated: 1) how to efficiently and reliably obtain the real-time information of mobile vehicles required by the EV charging strategy; and 2) based on the collected information, how to perform mobility-aware coordinated EV charging to improve energy utilization and reduce EV travel cost while avoiding power system overload.

Thanks to VANETs, the first problem can have a promising resolution. Exclusively designed for information exchange among highly mobile vehicles and road-side units (i.e., RSUs) in a multi-hop fashion, VANETs can deliver the required real-time information efficiently via short-range V2V and V2R communication, making large-volume vehicle information collection cheaper and faster compared to the other networks (e.g., cellular networks and Wi-Fis) [59]. More importantly, RSUs in VANETs can greatly enhance the timeliness of data collection and dissemination, which makes it possible to perform coordinated charging strategies for a group of moving vehicles [61]. Therefore, in this work, VANETs are integrated into a smart grid to collect the real-time information of mobile EVs and disseminate the charging decisions. Moreover, as the running EVs still consume energy when waiting for the charging decision, the transmission delay for information exchange in VANETs may cause additional travel cost for EVs. Thus in this chapter, the transmission delay is analyzed based on the RSU deployment and vehicle densities.

To cope with the second problem, in this work, based on the VANET-enhanced smart grid, the range anxieties are considered based on vehicle mobility in the charging strategy design. Specifically, we propose a mobility-aware coordinated EV charging strategy to make charging decisions based on the collected real-time vehicle information and the historic remote terminal unit (RTU) readings of the power grid. With all the collected information, the following questions are answered in a coordinated fashion: 1) should a vehicle be charged in the next period based on current battery energy level; 2) which charging station should this vehicle go to with the consideration of the range anxiety based on its current location; and 3) how much energy should be charged for this vehicle to improve the energy utilization and guarantee the power system stability. The optimal charging problem is formulated as a time-coupled mixed-integer linear programming (MILP) problem, which is difficult to be solved. However, by unveiling the linear relationship among EV charging loads of feeders, we decouple the MILP problem into a series of sub-MILPs through Lagrange duality [91]. Each sub-MILP can be further solved by the branch-and-cut-based outer approximation algorithm [101].

In summary, to deal with the range anxieties of EVs, we incorporate VANETs into the smart grid to collect real-time vehicle information for tracking the vehicle mobility (e.g., locations) and battery energy levels. A predictive mobility-aware coordinated EV charging strategy is proposed to improve the power utilization and reduce average EV travel cost while preventing overload of the power system for the following charging period. The main contributions of the chapter are listed as fourfold.

- First, we propose the system architecture of the VANET-enhanced smart grid, in which VANETs enable efficient communication among mobile vehicles and RSUs to collect useful information and dispatch the decisions of the EV charging strategy in a real-time manner; a traffic server is in charge of processing the collected information and performing the predictive coordinated EV charging strategy for EVs;
- Second, considering the range anxieties of EVs, we design a mobility-aware coor-

dinated EV charging strategy to improve the overall energy utilization of the power system and reduce the average EV travel cost while avoiding the overload of the power system. Particularly, we discover that the EV charging loads of charging stations present a linear relation, which is critical for the load assignment; furthermore, the travel cost is defined and formulated to reveal the impact of vehicle mobility on the charging strategy design;

- Third, the globally optimal charging problem is formulated as a time-coupled MILP problem which is decoupled into a series of sub-MILPs through Lagrange duality. Each sub-MILP is further solved by the branch-and-cut-based outer approximation algorithm; and

- Finally, we carry out extensive simulations to validate the effectiveness and efficiency of our proposed EV charging strategy. The simulation traces are extracted from VISSIM [92], by which a highly realistic suburban scenario is built. And the transmission delay induced by VANETs is fully evaluated. Then, the proposed strategy is demonstrated to considerably outperform the traditional autonomous charging strategy (without VANETs) on the metrics of the energy utilization and the average EV travel cost.

5.2 System Model

Aiming at providing a predictive coordinated mobility-aware charging strategy for EVs based on the real-time vehicle information, we first introduce a VANET-enhanced smart grid architecture to efficiently operate the coordinated EV-charging strategy. Then, the power flow equations are elaborated in the corresponding power system. Furthermore, the mobility model, charging model and transmission model of EVs are discussed.

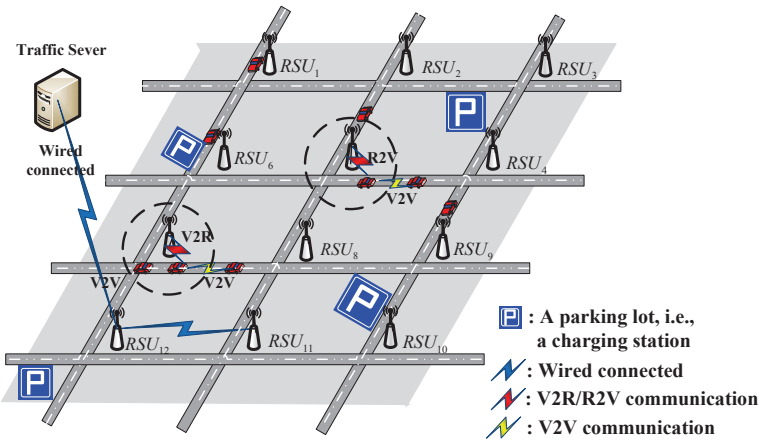

Figure 5.1. The VANET-enhanced smart grid architecture.

5.2.1 VANET-Enhanced Smart Grid

Fig. 5.1 shows the components of the proposed VANET-enhanced smart grid architecture, consisting of a power distribution system, charging stations (e.g., at parking lots), a traffic server, EVs and access points (i.e., RSUs) along road sides. The power distribution system supplies energy to the whole network through power feeders (i.e., buses). Besides, the charging stations provide fast-charging for all the EVs.

Based on historic RTU readings of each distribution system bus, the voltage at each charging station in the following period can be obtained [34]. The maximal power that can be supplied by each charging station (i.e., the load-capacity of each charging station) is preknown. In the following context, we denote the load-capacity of Bus_j as P^j_{total}. The historic readings are delivered to the traffic server via wireline. A traffic server is capable of performing predictive charging strategy to provide globally optimized charging decisions for EVs, according to the real-time EV information collected through VANETs and the historic RTU readings. The operation is conducted period by period. Specifically, the charging decisions include the charging load/rate of EV v at Bus_j in period k (denoted as $Pch_{v,j,k}$) and the charging indicator of vehicle v indicating whether EV v will be charged at station j in period k, which is denoted as $x_{v,j,k}$. And $x_{v,j,k}$ is set to 1 when EV v is charged at Bus_j in period k, and 0 otherwise.

In VANETs, consider a set of EVs, denoted as $\mathbb{V}$, moving around in the network region following map-based paths. EVs may need to be charged while moving on their ways. The real-time EV information can be exchanged among the OBUs installed in vehicles, through multi-hop V2V relaying, based on DSRC protocol [1], with a transmission range R. Besides, GPS devices, which offer the service of shortest-path navigation, are also equipped in EVs and keep wired connection with the OBU. Furthermore, a set of RSUs, denoted as $\mathbb{R}$, are uniformly deployed along roads and capable to collect the vehicle information (e.g., locations and battery energy levels) of EVs through V2R transmissions, based on DSRC protocol, with the transmission range R. Wiredly connected to the traffic server, RSUs can relay the collected vehicle information to the traffic server for calculating the globally optimized charging strategies for EVs. Thereafter, if RSUs obtain the EV charging decisions from the traffic server, they can relay the charging decisions to the EVs through R2V and V2V transmissions.

In summary, the VANET-enhanced smart grid system operates as follows.

- Information collection and delivery to the traffic server: The requested information are two-fold, i.e., the historic RTU readings of each bus in the power system and the real-time vehicle information. The former is delivered to the traffic server through wireline, based on which the charging load constraints of charging stations can be predicted; the latter is collected through multi-hop V2V relaying and V2R transmission;

- Decision making of the predictive coordinated EV charging: The traffic server then fuses all the collected information and calculates the optimal EV charging strategy to improve the power utilization of the grid and reduce the average EV travel cost while avoiding power system overloading;

- Decision dissemination: As soon as the OBU of an EV receives its own charging decision from either the neighboring EVs or an RSU, it will deliver the decision to the GPS, and the GPS will navigate that EV to the designated charging station.

5.2.2 Power System Model

In order to implement charging control for EVs in the VANET-enhanced smart grid, the power flow on the feeders should be considered. In the following, a power system model is described, where the relationship between bus voltages and loads are given to help derive the relation among EV charging loads of feeders.

Consider a smart grid based on the system model as shown in Fig. 5.1. The power system can be abstracted as a one-line diagram with multiple buses. For further illustration, an example of a 12-bus system is depicted in Fig. 5.2(a). And Fig. 5.2(b) is the equivalent power system model of Fig. 5.2(a). Let N denote the set of buses in the system, with the population of 12 in this example. The *generation buses* are defined as the buses injecting power to the system, i.e., Bus_1 in Fig.5.2(a), while the others which only have load are denoted as the *load buses*, i.e., Bus_3, Bus_6, etc. The power system is supplied through the substation at the generation bus, i.e., Bus_1. EV charging stations are located in the network at load buses, e.g., Bus_3, Bus_6, Bus_9 and Bus_{12}, respectively. Consider that each charging station is connected to the grid via a standard single-phase Alternating-Current (AC) connection. Due to the thermal limit of service cable or current rating of fuse, an EV charging station at Bus_j is subject to a load-capacity constraint P^j_{total} [35]. Although the concept of vehicle-to-grid for a local system exists [20], bi-directional flow of electricity or the directional flow from an EV battery is not considered in this work.

The voltages of two neighboring buses in period k, e.g., $V_{i,k}$ and $V_{j,k}$ as depicted in Fig. 5.3, can be approximated as [34]

$$V_{i,k} - V_{j,k} = \frac{P_{ij,k} \cdot r_{ij} + Q_{ij,k} \cdot x_{ij}}{V_{j,k}} \tag{5.1}$$

where $P_{ij,k}$ and $Q_{ij,k}$ are the active and reactive power flow from Bus_i to Bus_j in period k, respectively, while $r_{ij} + jx_{ij}$ is the impedance of the feeder line i-j. In per unit, (5.1) is

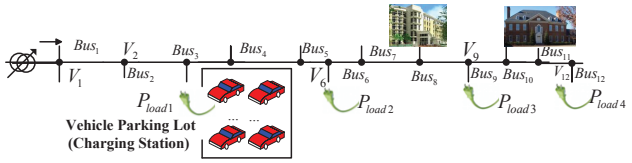

(a) Illustrated power system model.

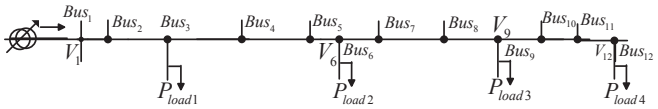

(b) Equivalent power system model.

Figure 5.2. The power system model.

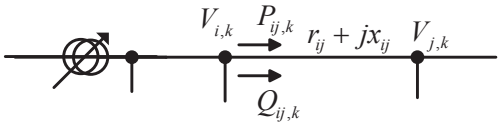

Figure 5.3. The power flow illustration.

usually approximated as

$$V_{i,k} - V_{j,k} = P_{ij,k} \cdot r_{ij} + Q_{ij,k} \cdot x_{ij}. \tag{5.2}$$

Note that all the voltages of buses should be within a certain range which is the main constraint of distribution system operation [34]. Specifically, the voltage magnitude at Bus_j in period k is bounded by the upper and lower limits $V_{j,k}^{\min}$ and $V_{j,k}^{\max}$, respectively, i.e., $V_{j,k}^{\min} \leq V_{j,k} \leq V_{j,k}^{\max}$. As proved in [34], the minimum voltage point can occur only at the end of the feeder, since only one generation bus is located at the beginning of the distribution system[1]. The minimum voltage $V_{N,k}$ can be calculated as

$$V_{N,k} = V_{1,k} - \sum_{i=1}^{N-1} [P_{i(i+1),k} \cdot r_{i(i+1)} + Q_{i(i+1),k} \cdot x_{i(i+1)}]. \tag{5.3}$$

[1]Note that if the distributed generation is adopted in the distribution system, the overloading problem should also be considered.

5.2.3 EV Mobility and Charging Model

Consider that EVs move along the roads in the studied area. The mobility of each EV can be characterized by two random variables (V, D) [83]. Here, V represents the vehicle velocity which takes two possible values (i.e., a lower velocity v_L and a higher velocity v_H). The velocity transition is modeled as a two-state continuous Markov chain with state transition rate $\frac{1}{D}$. Under this model, a vehicle initially chooses v_L (or v_H), and after a time interval which is exponentially distributed with the mean of D, the velocity changes to v_H (or v_L). The model can be exploited to describe the realistic driving behaviors of people, i.e., a driver usually drives at a constant velocity for a period and then changes to a higher/lower velocity based on his/her will or road conditions. Besides, when the vehicle density is low or medium (e.g, when the vehicle density is no larger than 30 vehicle/km/lane), vehicles can be considered to move independently [84] and the headway distance[2] follows the exponential distribution with rate ζ [85].

When a mobile EV needs to be charged, the charging load of EV v ($\in \mathbb{V}$) at Bus_j in period k, i.e., $Pch_{v,j,k}$, should be within a certain range, i.e.,

$$0 \leq Pch_{v,j,k} \leq Pch_{v,j,k}^{\max} \tag{5.4}$$

where $Pch_{v,j,k}^{\max}$ is the predefined charging load bound of $Pch_{v,j,k}$ [94]. If EV v is not planned to be charged in period k, i.e., $x_{v,j,k} = 0$, the charging load of EV v in period k should be 0, i.e.,

$$\frac{Pch_{v,j,k}}{Pch_{v,j,k}^{\max}} \leq x_{v,j,k} \tag{5.5}$$

Also, $x_{v,j,k}$ should satisfy

$$\begin{aligned} &\sum_{j \in H} x_{v,j,k} \leq 1 \; and \; x_{v,j,k} \in X = [0,1] \cap \mathbb{Z} \\ &\sum_{k} \sum_{j \in H} x_{v,j,k} \leq X_{max} \end{aligned} \tag{5.6}$$

[2]The headway distance is defined as the distance between two neighboring vehicles in the same lane.

where X_{max} is the upper bound of the total charging times for an EV within all the considered periods, since the frequently charging is not necessary for EVs and may result in battery damages [95]. For example, if each EV has at most three chances to be charged within all the considered periods, $X_{max} = 3$. During a charging period, the charging energy of each EV should be limited by its battery-capacity $C^{\max}_{battery}$, and the battery should not be depleted on the way and failed to be charged, i.e.,

$$0 \leq P^{init}_{v,k} + (\sum_{j \in H} a \cdot Pch_{v,j,k} - P^{v,k}_{cost} - P^{k}_{cons} \cdot (1 - \sum_{j \in H} x_{v,j,k})) \leq C^{\max}_{battery} \tag{5.7}$$

where $P^{init}_{v,k}$ is the initial energy stored in EV v in period k obtained via VANETs, and $P^{v,k}_{cost}$ is the travel cost for charging in period k for EV v. Let P^{k}_{cons} be the average non-charging energy cost of each EV for moving on the road if the EV is not charged in period k. The duration of each period is a hours. For instance, if we consider a 30-minutes duration for each period, we have $a = 0.5$. Then, for an EV charging station at Bus_j, the total EV load $Pch_{j,k}$ in period k is

$$Pch_{j,k} = \sum_{v \in \mathbb{V}} Pch_{v,j,k}. \tag{5.8}$$

5.2.4 Transmission Model in VANETs

To support the V2V and V2R communication in VANETs, the draft standard IEEE 802.11p [96] (DSRC) is adopted, which is designed particularly for short-range and intermittent vehicle-based communications among vehicles and RSUs. For analytical simplicity, in the link layer, we consider ideal medium access control (MAC) protocol. Under ideal MAC, the interference among V2V transmissions can be avoided, and once one vehicle moves into the coverage range of an RSU, the RSU is capable to schedule time slots of V2R transmission for the vehicle with no collisions. Besides, the link data rate of a V2V or V2R transmission is considered to be constant, and the contact duration between each transmission pair (e.g., V2V or V2R) is considered long enough to accomplish one packet delivery, which can be achieved by appropriately setting the packet size [73–75]. Moreover, due to the intermitten-

cy of vehicle communications caused by high-speed mobility, the waiting time for obtaining a transmission opportunity is dominant in the transmission delay compared to the queueing delay and the random backoff time due to the channel contention. Therefore, only the former is considered.

5.3 Problem Formulation

In this section, charging load constraints are first calculated for the buses with EV charging stations. And the relationship among the EV charging loads of buses are discovered. Then, considering the mobility of EVs, the EV's travel cost is formulated to represent the range anxieties of EVs, which particularly involves the cost induced by the transmission delay in VANETs. Finally, the mobility-aware coordinated EV charging problem is formulated to maximize the overall charging-energy-minus-travel-cost with power system overloading avoidance. This objective indicates that the total charging energy improvement and the charging travel cost reduction should be jointly considered and carefully balanced.

5.3.1 Charging Load Constraints

The charging station at Bus_j is subject to a load-capacity constraint P^j_{total}. Combining the load-capacity constraint with the total EV load at Bus_j in period k of (5.8), we have

$$Pch_{j,k} \leq P^j_{total}. \tag{5.9}$$

Moreover, subject to the additional load of EVs, the voltage of one bus will decrease with the increased load [34]. If a voltage sags out of the threshold at a bus, the reactive power cannot be correctly and efficiently injected. To keep the voltage within the certain range, it is indispensible to reduce the load. Therefore, there should exist a tradeoff between voltages and loads. In the following, we give the inherent relationship among the EV charging loads of buses in *Theorem 1*, and the proof is given based on power flow analysis in the power

system.

Theorem 3 *(***Linear relation among EV charging loads of buses***) Given the total supplied power of the feeder and the power demand of non-EV charging load, the total power supply to all EV charging stations can be calculated; and the power supplied to an individual charging station has a* linear relation *with those to the other charging stations.*

Proof. For all the buses, the voltages should be no less than the minimal required voltage, for example, 0.9 per unit voltage [35]. From (5.3), the lowest voltage is $V_{N,k}$ of Bus_N. Then,

$$\begin{aligned} V_{N,k} &= V_{1,k} - \sum_{i=1}^{N-1} [P_{i(i+1),k} \cdot r_{i(i+1)} + Q_{i(i+1),k} \cdot x_{i(i+1)}] \\ &\geq V_{min} \end{aligned} \tag{5.10}$$

where V_{min} is the minimal required voltage. Rearranging equation (5.10), we have

$$\sum_{i=1}^{N-1} [P_{i(i+1),k} \cdot r_{i(i+1)} + Q_{i(i+1),k} \cdot x_{i(i+1)}] \leq V_{1,k} - V_{min}. \tag{5.11}$$

Let w be the sorted index of the bus without EV charging load and W be the set of these buses $w \in W(\subset N)$; let j be the sorted index of the bus with EV charging load and H be the set of these buses $j \in H(\subset N)$. Then, (5.11) can be represented by

$$\begin{aligned} &\sum_{w \in W} (P_{w(w+1),k} \cdot r_{w(w+1)} + Q_{w(w+1),k} \cdot x_{w(w+1)}) \\ &+ \sum_{j \in H} j \cdot (P_{j,k} \cdot r_j + Q_{j,k} \cdot x_j) \leq V_{1,k} - V_{min} \end{aligned} \tag{5.12}$$

where $P_{j,k}$ and $Q_{j,k}$ are the active and reactive power load on Bus_j in period k, and $r_j = \frac{1}{j} \sum_{h=1}^{j-1} r_{h(h+1)}$ and $x_j = \frac{1}{j} \sum_{h=1}^{j-1} x_{h(h+1)}$ represent the average impedance of the feeder line among Bus_1 and Bus_j. Since the loads of the buses without EV loading are constant based

on the forecast [97] [98], we have

$$\begin{aligned}\sum_{j\in H} j(P_{j,k}\cdot r_j + Q_{j,k}\cdot x_j) \leq V_{1,k} - V_{min} \\ - \sum_{w\in W}(P_{w(w+1),k}\cdot r_{w(w+1)} + Q_{w(w+1),k}\cdot x_{w(w+1)}).\end{aligned} \tag{5.13}$$

Since each charging station is connected to the grid via a single-phase AC connection and EV charging only draws active power, we have $P_{j,k} = Pch_{j,k}$ and $Q_{j,k} = 0$. Therefore, (5.13) can be rewritten as

$$\sum_{j\in H} jPch_{j,k}\cdot r_j \leq \Xi \tag{5.14}$$

where Ξ is a constant representing the RHS of inequality (5.13). The inequality (5.14) implies that the total power supply to EV charging stations is related to the locations of charging stations and the total number of the charging stations. If the total power supply to EV charging stations, i.e., Ξ, is given, the total EV load of the charging station at Bus_j, $Pch_{j,k}$, in period k, presents a *linear relation* with the others. □

5.3.2 Travel Cost for EV Charging

With the mobility model defined in Subsection 5.2.3, the travel cost $P_{cost}^{v,k}$ for EV v to be charged in period k should consist of two parts. On one hand, moving EVs may have different locations and battery energy levels at different periods. Due to the range anxiety, drivers prefer closer charging stations with less travel distance. Thus the travel distance from EV v's current position to a charging station in period k, denoted as $p_{v,k}$, should be considered. On the other hand, the vehicle mobility will result in intermittent V2V and R2V connections, which can introduce a transmission delay and thus involve an additional travel distance until EV v receives the charging decision from the RSUs. Thus the travel cost caused by the transmission delay for EV v to receive a charging decision via VANETs, denoted as $c_{v,k}$, should also be considered.

1) *Travel cost due to the EV travel distance to a charging station*: If the charging strategy

guides EV v to be charged in the next period k, then $\sum_{j \in H} x_{v,j,k} = 1$. The traveling path for EV v to the charging station j in period k is calculated by the deployed GPS based on the shortest path algorithm [99], whose path length is denoted as $S(x_{v,j,k})$. Thus, the travel distance of EV v in period k for charging is defined as

$$p_{v,k} = \sum_{j \in H} S(x_{v,j,k}) \cdot x_{v,j,k}. \tag{5.15}$$

Based on $p_{v,k}$, the travel cost for EV v in period k in terms of energy is denoted as $PC(p_{v,k})$, where $PC(\cdot)$ is a linear non-decreasing function to measure the impacts of travel distance on the travel cost [20].

2) *Travel cost due to the transmission delay in VANETs*: The other part of the travel cost comes from the transmission delay for an EV to send (receive) the charging request (decision) to (from) the nearest RSU, due to the vehicle intermittent connections in the vehicular network.

First, we evaluate the transmission delay for the last hop of an uplink (i.e., the last V2R hop); the transmission delay is mainly due to the inter-contact time between a vehicle and an RSU. Define the last hop as an "on-off" model [83] where the vehicle either directly connects to an RSU (i.e., during the "on" state) or is the only vehicle approaching the RSU and there is no other vehicles in the transmission range of the RSU (i.e., during the "off" state). Since during the "on" state, the transmission delay for a message-packet is way smaller than the delay in the "off" state, the transmission delay is mainly due to the "off" period. Note that the period here is a random variable and is different from the charging period.

Denote the "on" period and the "off" period of a vehicle as T_{on} and T_{off}, respectively. Accordingly, the travel distances within the periods are defined as U_{on} and U_{off} respectively, with $T_{on} = \frac{U_{on}}{\overline{V}}$ and $T_{off} = \frac{U_{off}}{\overline{V}}$. Here, $\overline{V}$ is the average velocity for a vehicle based on the "on-off" mobility model as defined in Section 5.2.3. Similar to [83], the event that a vehicle moves a distance of at least u during T_{on} before being scheduled to communicate with RSU should satisfy that 1) there are no other vehicles within the distance u, and 2) there is at

least one vehicle within the distance $2R - u$ which results in this vehicle moving at least u distance to avoid the collision, where R is the transmission range of both an RSU and a vehicle. Then, we have

$$P_r(U_{on} > u) = \frac{(e^{-\zeta \cdot u})^{b\Gamma - 1}[1-(e^{-\zeta \cdot (2R-u)})^{b\Gamma - 1}]}{1-(e^{-\zeta \cdot 2R})^{b\Gamma}} \tag{5.16}$$

where b is the total length of roads, while Γ is the vehicle density on the roads. Since the vehicle headway distance follows an exponential distribution as mentioned in Section 5.2.3, the probability that a headway distance is larger than u is $e^{-\zeta \cdot u}$. And

$$E(U_{on}) = \int_0^{2R} P_r(U_{on} > u)du. \tag{5.17}$$

Similarly, the event that a vehicle moves a distance of at least u during T_{off} should satisfy that 1) there are no vehicles within a distance of $2R + u$ from the end of the coverage range of the nearest RSU ahead the vehicle, and 2) there is at least one vehicle within the distance $L - (u + 2R)$, where L is the distance between the adjacent RSUs. Then, we have

$$P_r(U_{off} > u) = \frac{(e^{-\zeta \cdot (2R+u)})^{b\Gamma - 1}[1-(e^{-\zeta \cdot (L-(2R+u))})^{b\Gamma - 1}]}{(e^{-\zeta \cdot 2R})^{b\Gamma}[1-(e^{-\zeta \cdot (L-2R)})^{b\Gamma}]} \tag{5.18}$$

$$E(U_{off}) = \int_0^{L-2R} P_r(U_{off} > u)du. \tag{5.19}$$

In addition, the previous hops within a communication link except the last hop are based on V2V communications which can be characterized with the mobility model of vehicles. The process of the relative velocity between two vehicles can be represented by a continuous time Markov chain (CTMC) with a state space $\mathbb{H} = \{h_0, h_1, h_2\}$. Here, h_0 represents a negative relative velocity when the vehicle in front moves with v_L while the vehicle behind moves with v_H; h_1 models a zero relative velocity (i.e., both vehicles move with the same velocity); h_2 represents a positive relative velocity. If each vehicle keeps the same velocity for an exponential time with an average time of D, the transition rate between any two states

of the Markov process equals to $2/D$. Thus, from [83], the average number of hops M within a communication link can be approximated as

$$M = \frac{6(L-E[U_{on}]-E[U_{off}])}{D(v_L+v_H)}. \tag{5.20}$$

Then, based on the average number of hops, the transmission delay of a uplink can be shown as

$$\psi = (M-1)E[T_{V2V}] + E[T_{off}] \tag{5.21}$$

where $E[T_{V2V}]$ is the average transmission delay for a V2V hop. And $E[T_{V2V}] = \frac{1}{1-e^{\zeta R}}$ with the vehicle transmission range R, since the headway distance follows exponential distribution. If we consider the downloading as a similar process with uploading, the total transmission delay should be 2ψ. Note that this transmission delay is related to the parameters in the network, e.g., vehicle mobility parameters (i.e., v_L, v_H, ζ and D), the vehicle density (i.e., Γ), and the RSU deployment in the network (i.e., the transmission range R and the average distance between RSUs L).

Therefore, the average travel distance, $c_{v,k}$, during which EV v is moving and waiting for the charging decision in period k, can be calculated as

$$c_{v,k} = E[O_v] \cdot \sum_{j \in H} x_{v,j,k} \tag{5.22}$$

where $O_v = \overline{V} \cdot 2\psi(v_L, v_H, D, \zeta, \Gamma, R, L)$ is defined as the travel distance for EV v due to the transmission delay. Similarly, the travel cost due to the transmission delay is denoted as a linear non-decreasing function $PC(c_{v,k})$ to measure the energy cost for EV v to wait for receiving the decision in period k. With the defined $PC(p_{v,k})$ and $PC(c_{v,k})$, the current stored energy, $P_{v,k}^{init}$, should be no less than the summation of $PC(p_{v,k})$ and $PC(c_{v,k})$; otherwise, the battery will be depleted before the EV reaching the destination,

$$P_{cost}^{v,k} = PC(p_{v,k}) + PC(c_{v,k}) \leq P_{v,k}^{init}. \tag{5.23}$$

Note that $P_{v,k}^{init}$ can be real-time collected by RSUs based on V2V and V2R communications.

5.3.3 Mobility-Aware EV Charging Optimization Problem

Taking account of both the EV charging load relationship among charging stations and the travel cost for EVs, the objective of the charging strategy is to maximize the overall charging-energy-minus-travel-cost with power system overloading avoidance [91]. This objective indicates that the total charging energy improvement and the charging travel cost reduction should be jointly considered and carefully balanced. Specifically, once the traffic server receives 1) the historic information from the RTUs located at the buses, and 2) the vehicle information via VANETs, a charging strategy is calculated to determine $Pch_{v,j,k}$ and $x_{v,j,k}$, according to the optimization problem shown as follows.

$$
\begin{aligned}
&\max \ \sum_{k}\sum_{v\in\mathbb{V}}\sum_{j\in H} a\cdot Pch_{v,j,k} \ - \sum_{k}\sum_{v\in\mathbb{V}}(PC(p_{v,k})+PC(c_{v,k}))\\
&s.t.\\
&0\le Pch_{v,j,k}\le Pch_{v,j,k}^{\max}, \forall v\in\mathbb{V}, \forall j\in H, \ and \ \forall k\\
&Pch_{j,k}=\textstyle\sum_{v\in\mathbb{V}} Pch_{v,j,k}\le P_{total}^{j}, \forall k, \forall j\in H\\
&\sum_{j\in H} jPch_{j,k}\cdot r_j\le \Xi, \ \forall k\\
&0\le P_{v,k}^{init}+(\sum_{j\in H} a\cdot Pch_{v,j,k}-PC(p_{v,k})-PC(c_{v,k})\\
&\quad -P_{cons}^{k}\cdot(1-\sum_{j\in H} x_{v,j,k}))\le C_{battery}^{\max}, \forall v\in\mathbb{V}, \forall k\\
&\tfrac{Pch_{v,j,k}}{Pch_{v,j,k}^{\max}}\le x_{v,j,k}, \forall v\in\mathbb{V}, \forall j\in H, \ and \ \forall k\\
&\sum_{j\in H} x_{v,j,k}\le 1 \ and \ x_{v,j,k}\in X=[0,1]\cap\mathbb{Z}, \forall v\in\mathbb{V}, \forall j\in H, and \forall k\\
&PC(p_{v,k})+PC(c_{v,k})\le P_{v,k}^{init}, \forall v\in\mathbb{V}, \forall k\\
&\sum_{k}\sum_{j\in H} x_{v,j,k}\le X_{max}, \forall v\in\mathbb{V}
\end{aligned}
\tag{5.24}
$$

The constraints are according to (5.4)-(5.9), (5.14) and (5.23), respectively. And the transmission delay in VANETs is integrated in the constraint of (5.23).

5.4 The Coordinated Predictive EV Charging Strategy

In this section, we derive the solution of problem (5.24) to obtain the coordinated predictive EV charging strategy. The original problem (5.24) is a time-coupled mixed-integer linear programming (MILP) problem and thus very complicated to solve, however, having observed that the last constraint of (5.24) is the only time-coupled constraint, the original time-coupled MILP problem can be first time-decoupled into a series of sub-MILPs through Lagrange duality [91]. The optimal solutions of all the sub-MILPs can form a ϵ-optimal solution to the original problem [100]. In other words, with Lagrange duality, only solving the decoupled sub-MILP problem in each period can lead to an ϵ-optimal solution for the whole periods. Each sub-MILP can be further solved by the branch-and-cut-based outer approximation (BCBOA) algorithm [101]. The optimality of BCBOA is also proved.

5.4.1 Optimization Decoupling Based on Lagrange Duality

First, we decouple the original optimization problem (5.24) into a series of sub-problems with respect to period k by applying the Lagrange duality [91]. The basic idea is to add the time-coupled constraints of (5.24) into the objective function by augmenting the objective function with a weighted sum of the time-coupled constraint functions. In this way, the original problem can be time-decoupled into a series of sub-problems, each corresponding to a period k with only parameters and decision variables of that period. The intrinsic philosophy behind the ϵ-optimal solution to the original MILP after decoupling, is that the objective function is linear; and all the inequality constrains are linear [100]. We define the Lagrangian $L(.)$ associated with the problem (5.24) as

$$\begin{aligned} L(Pch_{v,j,k}, x_{v,j,k}) = \sum_{k} \{ \sum_{v\in\mathbb{V}} \sum_{j\in H} a \cdot Pch_{v,j,k} \; - \sum_{v\in\mathbb{V}} (PC(p_{v,k}) \\ + PC(c_{v,k}))\} - \sum_{v\in\mathbb{V}} \iota_v [\sum_{k} \sum_{j\in H} x_{v,j,k} - X_{max}] \end{aligned} \tag{5.25}$$

where ι_v is the Lagrange multipliers associated with the v^{th} inequality constraint

$$\sum_{k} \sum_{j \in H} x_{v,j,k} \leq X_{max}. \tag{5.26}$$

The vector set $\{\iota_v\}$ is called the dual variables or Lagrange multiplier vector. Rearranging Eq. (5.25), we can obtain

$$\begin{aligned} L(Pch_{v,j,k}, x_{v,j,k}) = \sum_{k} \{ (\sum_{v \in \mathbb{V}} \sum_{j \in H} a \cdot Pch_{v,j,k}\ ) - \sum_{v \in \mathbb{V}} (PC(p_{v,k}) \\ + PC(c_{v,k})) - \sum_{v \in \mathbb{V}} \iota_v [\sum_{j \in H} x_{v,j,k}] \} + \sum_{v \in \mathbb{V}} \iota_v X_{max}. \end{aligned} \tag{5.27}$$

We further decouple the problem into a series of uncoupled sub-problems corresponding to each period k by means of dual decomposition [91], and let $D^k(\iota_v)$ denote the maximum value of Lagrangian $L(.)$ over $Pch_{v,j,k}$ and $x_{v,j,k}$ in period k, i.e.,

$$\begin{aligned} D^k(\iota_v) = \max_{Pch_{v,j,k}, x_{v,j,k}} \{ (\sum_{v \in \mathbb{V}} \sum_{j \in H} a \cdot Pch_{v,j,k}\ ) \\ - \sum_{v \in \mathbb{V}} (PC(p_{v,k}) + PC(c_{v,k})) - \sum_{v \in \mathbb{V}} \iota_v [\sum_{j \in H} x_{v,j,k}] \}. \end{aligned} \tag{5.28}$$

Then, let Lagrangian dual function $D(\iota_v)$ be the maximum value of Lagrangian $L(.)$ over $Pch_{v,j,k}$ and $x_{v,j,k}$, then

$$D(\iota_v) = \sum_{k} D^k(\iota_v) + \sum_{v \in \mathbb{V}} \iota_v X_{max}. \tag{5.29}$$

By minimizing the Lagrangian dual function over dual variable, ι_v, we can get the ϵ-optimal solution of (5.24).

$$\begin{aligned} &\min_{\iota_v} D(\iota_v) \\ &\text{s.t.} \iota_{\text{v}} \geq 0. \end{aligned} \tag{5.30}$$

As shown in [100], for a given ι_v, if the solution $Pch_{v,j,k}$ and $x_{v,j,k}$ is optimal in Eq. (5.28) and satisfies the time-coupled constraint of Eq. (5.26), the solution are the ϵ-optimal solution to the original problem, with $\epsilon = -\sum_{v \in \mathbb{V}} \iota_v [\sum_{k} \sum_{j \in H} x_{v,j,k} - X_{max}]$.

5.4.2 Solving the Sub-MILP Problem Based on BCBOA Algorithm

From the observation of (5.28), the sub-optimization problem, P, is

$$
P\begin{cases}
\max\limits_{Pch_{v,j,k},x_{v,j,k}} \{(\sum\limits_{v\in\mathbb{V}}\sum\limits_{j\in H} a\cdot Pch_{v,j,k}\,) - \sum\limits_{v\in\mathbb{V}}(PC(p_{v,k}) \\
\qquad +PC(c_{v,k})) - \sum\limits_{v\in\mathbb{V}} \iota_v[\sum\limits_{j\in H} x_{v,j,k}]\} \\
s.t. \\
f_{j,1}(x,Pch) = Pch_{j,k} = \sum_{v\in\mathbb{V}} Pch_{v,j,k} - P^j_{total} \le 0, \\
\qquad \forall j\in H \\
f_2(x,Pch) = \sum\limits_{j\in H} Pch_{j,k}\cdot jr_j - \Xi \le 0 \\
f_{v,3}(x,Pch) = P^{init}_{v,k} + (\sum\limits_{j\in H} a\cdot Pch_{v,j,k} - PC(p_{v,k}) \\
-PC(c_{v,k}) - P^k_{cons}(1-\sum\limits_j x_{v,j,k})) - C^{\max}_{battery} \le 0, \forall v\in\mathbb{V} \\
f_{v,4}(x,Pch) = -[P^{init}_{v,k} + (\sum\limits_{j\in H} a\cdot Pch_{v,j,k} - PC(p_{v,k}) \\
-PC(c_{v,k}) - P^k_{cons}(1-\sum\limits_j x_{v,j,k}))] \le 0, \forall v\in\mathbb{V} \\
f_{v,j,5}(x,Pch) = \frac{Pch_{v,j,k}}{Pch^{\max}_{v,j,k}} - x_{v,j,k} \le 0, \forall v\in\mathbb{V}, \forall j\in H \\
f_{v,6}(x,Pch) = \sum\limits_{j\in H} x_{v,j,k} - 1 \le 0, \forall v\in\mathbb{V} \\
f_{v,7}(x,Pch) = PC(p_{v,k}) + PC(c_{v,k}) - P^{init}_{v,k} \le 0, \forall v\in\mathbb{V} \\
0 \le Pch_{v,j,k} \le Pch^{\max}_{v,j,k},\ \ x_{v,j,k}\in\{0,1\},\ \ \forall v\in\mathbb{V}, \forall j\in H
\end{cases}
\tag{5.31}
$$

where x and Pch are the set of all $x_{v,j,k}$ and $Pch_{v,j,k}$, respectively.

Since the sub-optimization problem (5.31) is an MILP, it can be solved by the BCBOA Algorithm [101]. The BCBOA algorithm is an iterative procedure that solves the original MILP by solving an alternating sequence of relaxed MILPs and linear programs (LPs). The relaxed MILP is obtained from the original problem P by replacing the original constraints with linear functions by polyhedral outer approximations (OAs). The OA is to provide polyhedral representation of the feasible space of P. Such a representation will render linearly in the continuous variable, and enable to reduce the complexity of the original problem. Given any set of possible solutions $\mathbb{T} = \{(x^1, Pch^1), ..., (x^t, Pch^t), ...\}$, the MILP is given as

follows,

$$P^{OA}(T)\begin{cases} \max \varpi \\ s.t. \\ \nabla G(x,Pch)^T_{|(x^t,Pch^t)} \begin{pmatrix} x-x^t \\ Pch-Pch^t \end{pmatrix} \\ +G(x^t,Pch^t) \geq \varpi \\ \nabla F(x,Pch)^T_{|(x^t,Pch^t)} \begin{pmatrix} x-x^t \\ Pch-Pch^t \end{pmatrix} \\ +F(x^t,Pch^t) \leq 0 \\ \forall (x^t,Pch^t) \in \mathbb{T},\ x \in X \cap Z^n, \\ 0 \leq Pch_{v,j,k} \leq Pch^{\max}_{v,j,k}, \varpi \in R \end{cases} \tag{5.32}$$

where

$$G(x,Pch) = \{(\sum_{v\in\mathbb{V}} \sum_{j\in H} a \cdot Pch_{v,j,k}\ ) - \sum_{v\in\mathbb{V}} (PC(p_{v,k}) + PC(c_{v,k})) \qquad - \sum_{v\in\mathbb{V}} \iota_v[\sum_{j\in H} x_{v,j,k}]\},$$
$$F = \{f_{j,1}, f_2, f_{v,3}, f_{v,4}, f_{v,j,5}, f_{v,6}, f_{v,7}\},\ \forall v \in \mathbb{V},\ \forall j \in H$$

and ϖ is an auxiliary variable. Here, $\nabla G(\cdot)^T$ denotes the transpose of the gradient of G.

The LP is obtained from the original problem P with x fixed to $\bar{x}$, where $\bar{x}$ is the optimal solution of x in MILP (5.32). In summary, the OA algorithm utilizes the gradients of the objective and constraint functions at different points to build a MILP relaxation of the problem. It should be noted that since all the functions in problem P were linear, the relaxed MILP at the first iteration would be identical to the original problem, and hence the BCBOA would terminate in at most two iterations. The following theorem shows that if 1) the solution set, $\mathbb{T}$, contains suitable points; 2) KKT conditions are satisfied at these points, the problems $P^{OA}(T)$ and P are equivalent.

Theorem 4 *Consider that P has a finite set of optimal solutions. For all $\bar{x} \in X \cap Z^n$, if the*

problem

$$P_{\bar{x}}\begin{cases}\max G(\overline{x}, Pch)\\ s.t.\\ f_{j,1}=\sum_{v\in\mathbb{V}} Pch_{v,j,k}-P^{j}_{total}\le 0,\ \forall j\in H\\ f_2=\sum\limits_{j\in H}(Pch_{j,k}\cdot jr_j)=\sum\limits_{j\in H}(\sum\limits_{v\in\mathbb{V}} Pch_{v,j,k}\cdot jr_j)-\Xi\le 0\\ f_{v,3}=P^{init}_{v,k}+(\sum\limits_{j\in H} a\cdot Pch_{v,j,k}-\overline{PC(p_{v,k})}-\overline{PC(c_{v,k})}\\ \qquad -P^{k}_{cons}(1-\sum\limits_{j}\overline{x_{v,j,k}}))-C^{\max}_{battery}\le 0,\forall v\in\mathbb{V}\\ f_{v,4}=-[P^{init}_{v,k}+(\sum\limits_{j\in H} a\cdot Pch_{v,j,k}-\overline{PC(p_{v,k})}-\overline{PC(c_{v,k})}\\ \qquad -P^{k}_{cons}(1-\sum\limits_{j}\overline{x_{v,j,k}}))]\le 0,\forall v\in\mathbb{V}\\ f_{v,j,5}=\frac{Pch_{v,j,k}}{Pch^{max}_{v,j,k}}-\overline{x_{v,j,k}}\le 0,\ \forall j\in H,\ \forall v\in\mathbb{V}\\ 0\le Pch_{v,j,k}\le Pch^{\max}_{v,j,k}\end{cases}\tag{5.33}$$

is feasible, there exists $\overline{Pch}$ *to be its optimal solution. Otherwise, if* $P_{\bar{x}}$ *is not feasible,* $\overline{Pch}$ *is as the optimal solution to the following problem*

$$P^{F}_{\bar{x}}\begin{cases}\min\limits\sum\limits_{jj=1}^{|H|+1+2|\mathbb{V}|+|H||\mathbb{V}|} u_{jj}\\ s.t.\ \ f_{j,1}-u_{jj}\le 0,\ jj=\{1,\cdots,|H|\},\ j\in H\\ f_2-u_{|H|+1}\le 0\\ f_{v,3}-u_{jj}\le 0, jj=\{|H|+2,\cdots,|H|+1+|\mathbb{V}|\}, v\in\mathbb{V}\\ f_{v,4}-u_{jj}\le 0,\\ \qquad jj=\{|H|+2+|\mathbb{V}|,\cdots,|H|+1+2|\mathbb{V}|\},\ v\in\mathbb{V}\\ f_{v,j,5}-u_{jj}\le 0,\ jj=\{|H|+2+2|\mathbb{V}|,\cdots,\\ \qquad\qquad |H|+1+2|V|+|\mathbb{V}||H|\},\ v\in\mathbb{V},\ j\in H\\ 0\le Pch_{v,j,k}\le Pch^{\max}_{v,j,k}\end{cases}\tag{5.34}$$

where each u_{jj} *has one-to-one match with each linear constraint (i.e.,* $f_{j,1}$,f_2,$f_{v,3}$,$f_{v,4}$, *and* $f_{v,j,5}$*) and there are totally* $|H|+1+2|\mathbb{V}|+|H||\mathbb{V}|$ *constraints except the constraint* $0\le Pch_{v,j,k}\le Pch^{\max}_{v,j,k}$. *Let* $\bar{\mathbb{T}}$ *be the set of all such solutions* $(\bar{x},\overline{Pch})$. *If the KKT conditions are satisfied at every point of* $P_{\bar{x}}$, *then* P *and* $P^{OA}(\bar{\mathbb{T}})$ *have the same optimal value.*

Proof. Similar to [102], we denote X^F be the set of feasible $x \in X \cap Z^n$ in the problem $P_{\bar{x}}$ and X^I be the complement of X^F in $X \cap Z^n$. And $X^F \neq \emptyset$.

When $\bar{x} \in X^I$, the problem $P_{\bar{x}}$ is infeasible and therefore $\bar{\mathbb{T}}$ should contain the point ($\bar{x}$, $\overline{Pch}$) with an optimal solution of $P^F_{\bar{x}}$. Therefore, $P^{OA}(\bar{\mathbb{T}})$ contains the constraint

$$\begin{aligned} &\nabla F(x, Pch)^T_{|(\overline{x},\overline{Pch})} \begin{pmatrix} x - \bar{x} \\ Pch - \overline{Pch} \end{pmatrix} + F(\overline{x}, \overline{Pch}) \leq 0 \\ &where\ F = \{f_{j,1}, f_2, f_{v,3}, f_{v,4}, f_{v,j,5}, f_{v,6}, f_{v,7}\},\ \forall v \in \mathbb{V},\ \forall j \in H \end{aligned} \tag{5.35}$$

In addition since $\overline{Pch}$ is an optimal solution of $P^F_{\bar{x}}$ and the KKT conditions are satisfied, there exists $\mu \in R_+^{2*[|H|+1+2|\mathbb{V}|+|H||\mathbb{V}|]}$ such that the first $|H| + 1 + 2|\mathbb{V}| + |\mathbb{V}| \cdot |H|$ elements in μ has one-to-one match with each constraint in F and

$$\begin{aligned} &\sum_{jj=1}^{|H|+1+2|\mathbb{V}|+|H||\mathbb{V}|} \mu_{jj} \nabla_{Pch}[f_{jj}(\overline{x}, \overline{Pch})] = 0, \\ &\forall f_{jj} \in F = \{f_{j,1}, f_2, f_{v,3}, f_{v,4}, f_{v,j,5}\},\ \forall v \in \mathbb{V},\ \forall j \in H. \end{aligned} \tag{5.36}$$

$$\begin{aligned} 1 - \mu_{jj} - \mu_{|H|+1+2|\mathbb{V}|+|\mathbb{V}|\cdot|H|+jj} = 0, \\ jj = 1, ..., |H| + 1 + 2|\mathbb{V}| + |\mathbb{V}| \cdot |H| \end{aligned} \tag{5.37}$$

$$\begin{aligned} \mu_{jj}[f_{jj}(\overline{x}, \overline{Pch}) - \bar{u}_{jj}] = 0, \\ jj = 1, ..., |H| + 1 + 2|\mathbb{V}| + |\mathbb{V}||H| \end{aligned} \tag{5.38}$$

$$\begin{aligned} \mu_{|H|+1+2|\mathbb{V}|+|\mathbb{V}||H|+jj} \overline{u}_{jj} = 0, \\ jj = 1, ..., |H| + 1 + 2|\mathbb{V}| + |\mathbb{V}||H|. \end{aligned} \tag{5.39}$$

Based on (5.35), we further have

$$\begin{aligned} \nabla_{Pch}[f_{jj}(\overline{x}, \overline{Pch})]^T \left(Pch - \overline{Pch}\right) + f_{jj}(\overline{x}, \overline{Pch}) \leq 0, \\ jj = 1, \cdots, |H| + 1 + 2|\mathbb{V}| + |H||\mathbb{V}|,\ \forall f_{jj} \in F. \end{aligned} \tag{5.40}$$

Adding $|H| + 1 + 2|\mathbb{V}| + |H||\mathbb{V}|$ inequalities in (5.40) with the nonnegative multipliers

μ_1,...,$\mu_{|H|+1+2|\mathbb{V}|+|H|\cdot|\mathbb{V}|}$, after rearranging, we obtain

$$\begin{aligned}&\sum_{j=1}^{|H|+1+2|\mathbb{V}|+|H||\mathbb{V}|} \mu_{jj}\nabla_{Pch}[f_{jj}(\overline{x},\overline{Pch})]^T(Pch-\overline{Pch})\\ &\leq -\sum_{j=1}^{|H|+1+2|\mathbb{V}|+|H||\mathbb{V}|} \mu_{jj}f_{jj}(\overline{x},\overline{Pch}),\ \forall f_{jj}\in F.\end{aligned} \tag{5.41}$$

Based on (5.36), the left hand side of (5.41) equals to zero. While based on (5.38), the right hand side of (5.41) equals to $-\sum_{jj=1}^{|H|+1+2|\mathbb{V}|+|H||\mathbb{V}|} \mu_{jj}\bar{u}_{jj}$. From (5.39), $\mu_{jj+|H|+1+2|\mathbb{V}|+|\mathbb{V}||H|}=0$ if $\overline{u_{jj}}>0,\ \forall jj\in\{1,...,|H|+1+2|\mathbb{V}|+|\mathbb{V}||H|\}$. Then, combining (5.37), we get $\mu_{jj}=1$ for $\forall jj\in\{1,...,|H|+1+2|\mathbb{V}|+|\mathbb{V}||H|\}$ that satisfies $\overline{u_{jj}}>0$. This implies that the RHS of (5.41), i.e., $-\sum_{jj=1}^{|H|+1+2|\mathbb{V}|+|\mathbb{V}||H|} \bar{u}_{jj}$, is strictly negative otherwise $P_{\bar{x}}$ would be feasible. Therefore, the inequality (5.41) has no solution. This implies that the maximum value of $P^{OA}(\bar{\mathbb{T}})$ is to be found as the maximum value over all $x\in X^F$.

Furthermore, let $\overline{Pch}$ be an optimal solution to $P_{\bar{x}}$. $(G(\bar{x},\overline{Pch}),\ \bar{x},\ \overline{Pch})$ is a feasible solution of $P^{OA}_{\bar{x}}(\bar{\mathbb{T}})$. Therefore, $G(\bar{x},\overline{Pch})$ is a lower bound on the optimal value ϖ of $P^{OA}_{\bar{x}}(\bar{\mathbb{T}})$. Next this value $G(\bar{x},\overline{Pch})$ will be proved to be also an upper bound, i.e., $\varpi\leq G(\bar{x},\overline{Pch})$. When $\overline{Pch}$ is an optimal solution of $P_{\bar{x}}$ and satisfies the KKT conditions. There exists $\mu\in\mathbb{R}_+^{|H|+1+2|\mathbb{V}|+|\mathbb{V}||H|}$ such that

$$-\nabla_{Pch}G(\bar{x},\overline{Pch})+\sum_{jj=1}^{|H|+1+2|\mathbb{V}|+|\mathbb{V}||H|}\mu_{jj}\nabla_{Pch}[f_{jj}(\overline{x},\overline{Pch})]=0,\ \forall f_{jj}\in F \tag{5.42}$$

$$\mu_{jj}f_{jj}(\overline{x},\overline{Pch})=0,\ jj=1,...,|H|+1+2|\mathbb{V}|+|\mathbb{V}||H|. \tag{5.43}$$

By outer-approximation programming, any solution of $P^{OA}_{\bar{x}}(\bar{\mathbb{T}})$ should satisfy

$$\begin{aligned}&-\nabla_{Pch}G(\bar{x},\overline{Pch})^T\left(Pch-\overline{Pch}\right)-G(\bar{x},\overline{Pch})\leq-\varpi\\ &\nabla_{Pch}[f_{jj}(\overline{x},\overline{Pch})]^T(Pch-\overline{Pch})+f_{jj}(\overline{x},\overline{Pch})\leq 0,\\ &\quad jj=1,\cdots,|H|+1+2|\mathbb{V}|+|\mathbb{V}||H|\end{aligned} \tag{5.44}$$

Multiplying the second inequality set in (5.44) by the Lagrange multipliers (i.e., $\mu_{jj}\geq 0$)

and then adding to the first inequality in (5.44), we rearrange the left hand side and obtain

$$\begin{aligned}&\{-\nabla_{Pch}G(\bar{x},\overline{Pch})+\sum_{j=1}^{|H|+1+2|\mathbb{V}|+|\mathbb{V}||H|}\mu_{jj}\nabla_{Pch}f_{jj}(\overline{x},\overline{Pch})\}^T\\&\cdot\left(Pch-\overline{Pch}\right)+\sum_{j=1}^{|H|+1+2|\mathbb{V}|+|\mathbb{V}||H|}\mu_{jj}f_{jj}(\overline{x},\overline{Pch})-G(\bar{x},\overline{Pch})\\&=-G(\bar{x},\overline{Pch})\leq-\varpi.\end{aligned}\tag{5.45}$$

From (5.42) and (5.43), the left hand side of (5.45) is equivalent to $-G(\overline{x},\overline{Pch})$. Therefore, we get $G(\overline{x},\overline{Pch})\geq\varpi$. In other words, for any $\bar{x}\in X^F$, the problem $P_{\bar{x}}^{OA}(\bar{\mathbb{T}})$ and $P_{\bar{x}}$ have the same objective value. □

Therefore, the optimality of BCBOA is proved. In summary, the proposed charging strategy can be obtained by first time-decoupling the original problem into a series of sub-MILPs through Lagrange duality, and then solving the sub-MILPs based on the branch-and-cut-based outer approximation (BCBOA) algorithm. The charging decisions in terms of $Pch_{v,j,k}$ and $x_{v,j,k}$ are dispatched to each EV via VANETs.

5.5 Performance Evaluation

We consider a realistic suburban scenario as shown in Fig. 5.4, which is the region around the campus of University of Waterloo (Waterloo, ON, Canada). RSUs are uniformly deployed along roads, and two charging stations are deployed as marked in Fig. 5.4(a). The parameters of the 12-bus distribution system (only load buses) in [34] are considered, with the load enlarged to MW level. Two charging stations are connected to Bus_2 and Bus_{11}, respectively. Loads connected at each bus at 21:00 is given in Table 5.1. The input voltage is set to 1.0pu, and the minimum allowable voltage is 0.9pu, with the impedance of any line section being $0.005+j0.0046$. The normalized power over the power at 21:00 for all the buses without EV charging load is shown in Table II, according to the trend in [103]. Vehicles move in this region following the aforementioned mobility model in Section 5.2.3. To model the vehicle traffic, a highly-realistic microscopic vehicle traffic simulator, VISSIM [92], is employed

(a) A snap shot of the simulation region with signing the simulated roads in blue.

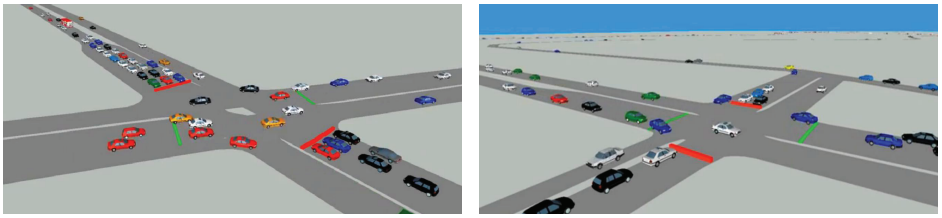

(b) The 3D vehicle traffic illustrations of two intersections highlighted in red on the upside.

Figure 5.4. The simulation scenario of University of Waterloo region in VISSIM.

Table 5.1 An example of active and reactive power value at each bus of the system

Hour	Bus Number	2	3	4	5	6	7	8	9	10	11	12
21:00	P(MW)	TBD	4.0	5.5	-	6.0	5.5	4.5	-	3.5	TBD	3.0
	Q(MVar)	-	3.0	5.5	-	1.5	5.5	4.5	-	3.0	-	1.5

to generate vehicle trace files for recording the vehicle mobility characteristics. Based on the trace files, we first evaluate the average transmission delay incurred by VANETs for an EV to receive a charging decision. Then, combining the power system data, we investigate the performance of our proposed EV charging strategy, using a custom simulator built in Matlab. The proposed strategy is compared to an existing coordinated charging strategy without considering the EV mobility and the travel cost [35]. The compared performance metrics include the total EV charging energy (TECE), the average EV travel cost (AETC), and the percentage of EVs that succeed or fail in charging.

Table 5.2 Normalized power over the power at 21:00 without EV charging load during a day

Hour	1:00	2:00	3:00	4:00	5:00	6:00
Normalized Power	0.5	0.5	0.5	0.5	0.7	0.9
Hour	7:00	8:00	9:00	10:00	11:00	12:00
Normalized Power	1.3	1.5	2.1	2.3	2.5	2.5
Hour	13:00	14:00	15:00	16:00	17:00	18:00
Normalized Power	2.5	2.3	2.1	1.8	1.5	1.4
Hour	19:00	20:00	21:00	22:00	23:00	24:00
Normalized Power	1.3	1.2	1.0	0.7	0.7	0.7

5.5.1 Simulation Setup

To simulate a VANET with VISSIM, vehicles are pushed into the region of $6000\text{m} * 2800\text{m}$, as shown in Fig. 5.4(a). At the beginning of the simulation, vehicles enter the region from the preseted entries (e.g., 9 entries at the ends of main roads), following a Poisson process at a rate ζ (e.g., ζ = 2500 vehicle/hour/entry). After a certain duration t_ζ (e.g., 240s), the vehicle pushing-in stops to reach the density 30 vehicle/km/lane. The information (e.g., locations, velocities, etc) of vehicles can be recorded at the end of every simulation step (e.g., 0.2s) in the recorded trace files. In addition, a set of RSUs (e.g., 25 RSUs) is deployed uniformly along roads in the region, with the transmission range of R (e.g., 150m). And the total simulation time is 3000s.

The car following model, Wiedemann 74 model [104], is utilized for modeling the traffic; the vehicle acceleration is a function of the vehicle velocity, the characteristics of the driver (or the vehicle), and the difference in distance and velocity between the subject vehicle and the vehicle in front [104]. At an intersection, the vehicle traffic is controlled either by a traffic light or a stop sign based on the reality, as shown in Fig. 5.4(b). The velocity distribution for all vehicles follows the velocity model described in Subsection 5.2.3 with parameters $V = \{v_L, v_H\}$ and D (e.g., taking $v_L = 30$km/hour, $v_H = 60$km/hour, $D = 60\text{s}$ as a case study).

Besides, in the EV charging simulations, we set the EV battery capacity to 85KWh according to the TESLA Model S [15]. The charging period is set as 30min as a case study, with the maximum charging energy of 30KWh. If an EV is not scheduled for charging in a

period, the energy cost for running on the road in that period is set to be uniformly distributed within [0,10]KWh. And the maximal charging times for EVs i.e., X_{max}, is set as 3. To better illustrate the performance of the proposed charging strategy, the centralized charging strategy in [35] is compared where the optimization objective is to only maximize the total amount of EV charging energy.

5.5.2 Simulation Results of VANETs

Based on the trace files obtained from VISSIM, Fig. 5.5(a) shows the probability density function (PDF) of vehicle headway distance under the above simulation settings when $\zeta = 2500$ vehicles/hour/entry. It is shown that the PDF of the headway distance matches well with an exponential distribution, which validates the premise in Subsection 5.2.3 that the headway distance follows an exponential distribution when the vehicle density is low or medium. Besides, from the exponential distribution in Fig. 5.5(a), the average headway distance is about 30m, which is very close to that calculated from the predefined vehicle density in the simulation setting, i.e., 30 vehicles/km/lane. In addition, the theoretical PDF of the distance from the last hop vehicle to the nearest RSU for one delivery (through Eq. (5.18)) is further verified by Fig. 5.5(b). With 25 RSUs deployed in the network, the theoretical PDF is calculated with the parameters in the simulation setting based on Eq. (5.18). The simulated PDF is obtained from the real trace files of VISSIM. In Fig. 5.5(b), it can be seen that the simulated PDF matches well with the theoretical one, which validates the effectiveness of the theoretical analysis in Eq. (5.18). Also, according to the simulation, the average distance from the last hop vehicle to its neatest RSU is around 200m.

When the vehicle density is reduced, e.g., $\zeta = 1800$ vehicle/hour/entry, the PDF of the headway distance is shown in Fig. 5.5(c), approximately following an exponential distribution as well. And the average distance is increased to 46m. Furthermore, the PDF of the last-hop V2R distance is illustrated in Fig. 5.5(d), and the average V2R distance of the last hop is about 215m. The average V2R distance also matches with the analytical results in Eq.

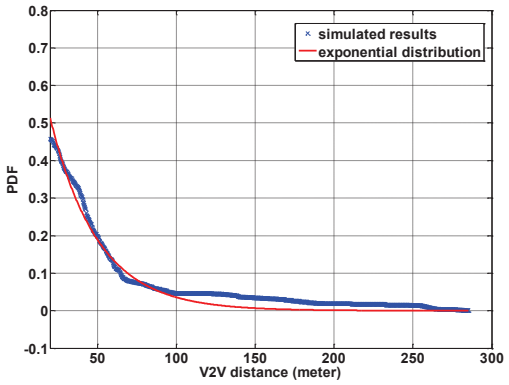

(a) The PDF of V2V distance when $\zeta = 2500$.

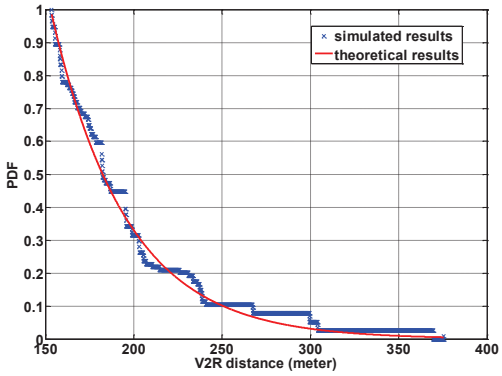

(b) The PDF of the last hop V2R distance when $\zeta = 2500$.

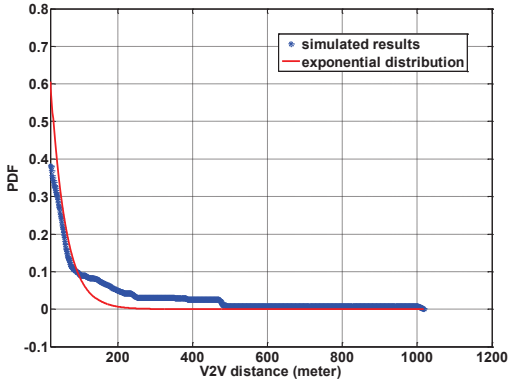

(c) The PDF of V2V distance when $\zeta = 1800$.

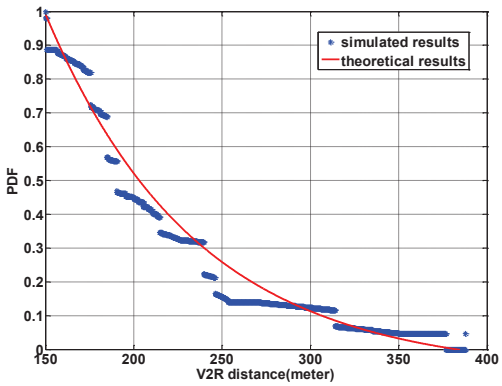

(d) The PDF of the last hop V2R distance when $\zeta = 1800$.

Figure 5.5. The PDFs of both two adjacent vehicle distance and the last hop V2R distance.

(5.18). Therefore, Fig. 5.5 validates the mobility model proposed in Section 5.2.3 as well as the analytical results of (5.18) which is derived based on the the proposed mobility model.

We then investigate the single-hop connection probability between a vehicle and its n-earest RSU and the end-to-end multi-hop transmission delay in VANETs. The results are shown in Fig. 5.6 and Fig. 5.7, respectively, under different RSU deployments (i.e., 25 or 8 RSUs are deployed in the network) and different vehicle densities (i.e., $\zeta = 2500$ vehicles/hour/entry or $\zeta = 1800$). It can be observed from Fig. 5.6 that for a given number of RSUs and ζ, the connection probability increases with larger RSU transmission range. Besides, if the RSU transmission range is fixed, larger number of RSUs and larger ζ will both

increase the single-hop connected probability but to different extents, i.e., the variation of the number of RSUs has larger impact on the connected probability than that of ζ. This can be explained as follows. As the collisions can be avoided according to the transmission model in Subsection 5.2.4, the increase of ζ will affect the connected probability only through decreasing the average U_{off} as given in Eq. (5.18). Since the average headway distances under $\zeta = 2500$ and $\zeta = 1800$ are around 30 and 50, respectively, which are relatively small compared to the RSU transmission range, the two headway distances can be viewed as in the same scaling order. As a result, the average U_{off} will not change much under the two ζ values, leading to very small gaps in the connected probabilities when the number of RSUs is fixed. On the contrary, when ζ is fixed, different numbers of RSUs will result in big difference in the average U_{off}, leading to a much larger gap.

On the other hand, it can be seen in Fig. 5.7 that the average end-to-end transmission delay decreases when the RSU transmission range, the number of RSUs or ζ increases. More interestingly, different from the single-hop connected probabilities, the transmission delay does not increase much even when the number of RSUs is largely reduced, e.g., from 25 to 8. For example, the transmission delay is around 190s with 25 RSUs and $\zeta = 2500$, and is around 240s with 8 RSUs and $\zeta = 1800$. The small change compared to the big gap of connected probability is due to the benefits of multi-hop V2V relaying. When the number of RSU largely decreases, although the single-hop connection opportunities from a vehicle to the RSU is largely reduced, the information can still be efficiently delivered to the RSU through multi-hop V2V relaying at the cost of small delay increase. In other words, the multi-hop V2V relaying increases the equivalent transmission range of a vehicle. Besides, for the considered settings, the average transmission delay is around 200s. Thus, although the transmission delay of VANETs is larger than the cellular systems, it is still tolerable for the applications of vehicle information collection compared to the decision making period (i.e., 30min). More importantly, VANETs can considerably cut down the service cost and enhance the transmission rates, which is more important for the large-volume vehicle data collection.

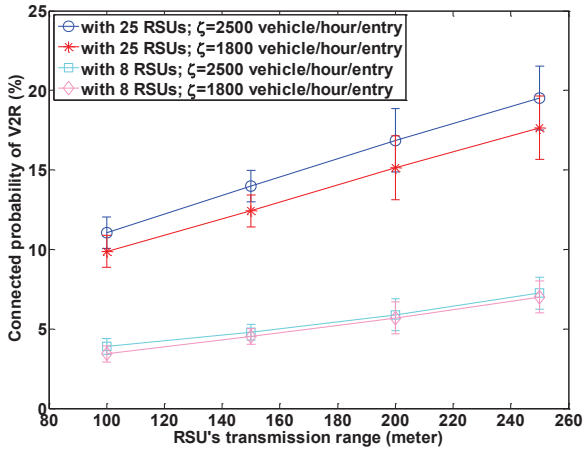

Figure 5.6. The average connected probability between a vehicle and an RSU.

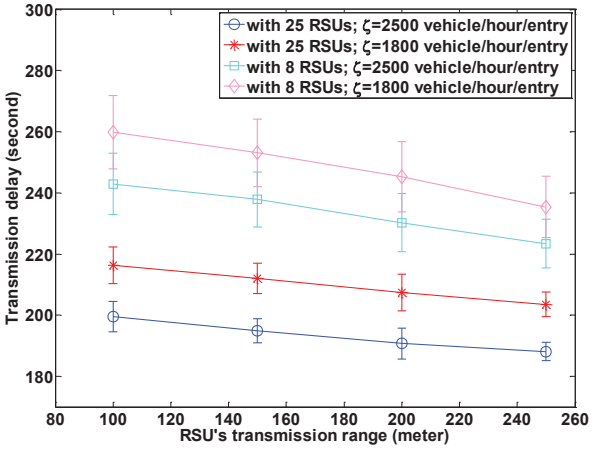

Figure 5.7. The average transmission delay for a V2R uplink.

5.5.3 Simulation Results of the Proposed Charging Strategy

In this subsection, we investigate the performance of the proposed charging strategy. As a case study, the strategy is conducted every 30mins, and the simulation results are collected every one hour. This conducted period can be set differently for different requirements, with corresponding communication infrastructure deployment. We first study the TECE performance under a weekday total-available-charging-energy (TACE) profile [103] (see Table II)

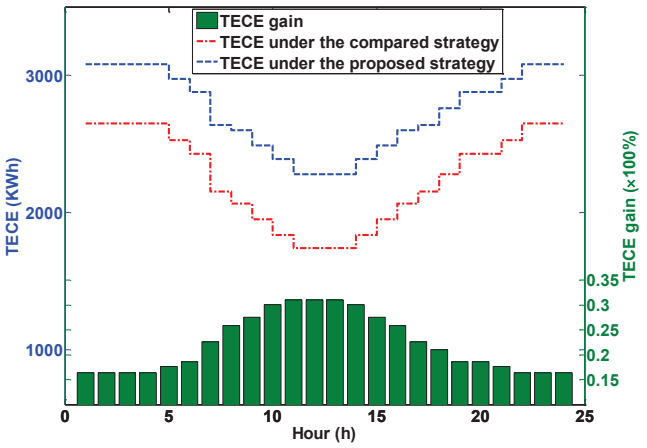

Figure 5.8. Daily TECE comparison when the total number of EVs is fixed to 1200.

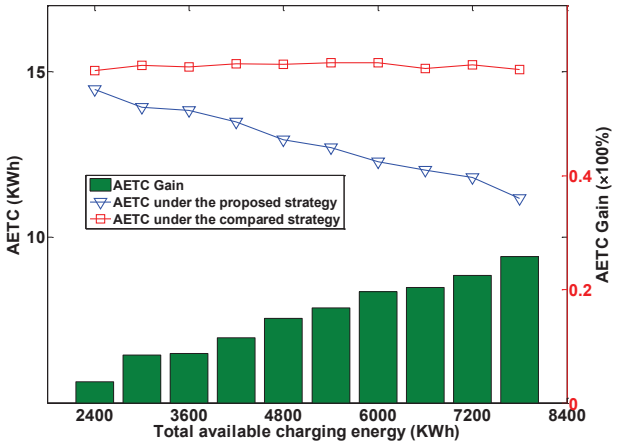

Figure 5.9. AETC comparison with increasing TACE when total number of EVs is 1200.

with fixed total number of EVs, as shown in Fig. 5.8. As we mainly focus on the behaviors of charging strategies when the overload is likely to occur, we only consider the case where the TACE is not enough to charge all the EVs in each period. It can be observed from Fig. 5.8 that for all the hours the proposed strategy can obtain larger TECE than the compared strategy. Since the compared strategy has no real-time vehicle information, the charging de-

cision is made without considering the EV mobility and the travel cost. As a result, some EVs may be dispatched to a charging station that is too far to reach based on their current battery levels, making EV batteries depleted on the way and fail to be charged. On the contrary, our strategy considers the travel cost based on the vehicle information from VANETs and dispatches the EVs only to the charging stations within their reach, thus having a larger TECE. Besides, TECE gain is from 15% to 30% for different TACE, and is larger with smaller TACE. The reason is as follows. When the TACE is smaller, the number of EVs that cannot be charged in the current period is larger. As the EVs are mobile, they will continue to consume battery energy even if they are not charged. As a result, the average initial battery level is lower in the next period, and the depletion probability if an EV is dispatched to a farther station is larger under the compared strategy. As our strategy always avoids the EV depletion situation, the gain will be larger when the TACE is smaller.

Besides, we compare the AETC under different TACE in Fig. 5.9. It can be seen that the AETC of the proposed strategy is smaller than that of the compared strategy, and the gain is larger with larger TACE. As the proposed strategy considers to reduce the AETC and thus gives preference to closer charging stations, the AETC is lower than that under the compared strategy without considering the travel cost. When the TACE is increased, each charging station can accommodate more EVs. As a result, more EVs can be dispatched to the closer charging stations under the proposed strategy, resulting in a lower AETC (i.e., a larger gain) over the compared strategy.

We further compare the number of EVs that succeed and fail in charging under different strategies, respectively, as shown in Fig. 5.10. It can be observed that compared with the existing strategy, the proposed strategy achieves a smaller total number of involved EVs (i.e., the number of successfully charged EVs plus the number of EVs that fail to be charged) but a larger number of successfully charged EVs. This observation further corroborates the explanation for Fig. 5.8. Under the proposed strategy, as the EVs tend to be assigned to the closer stations, the load assignment is less balanced than the compared strategy. Thus the total number of involved EVs is smaller under the proposed strategy. However, as some

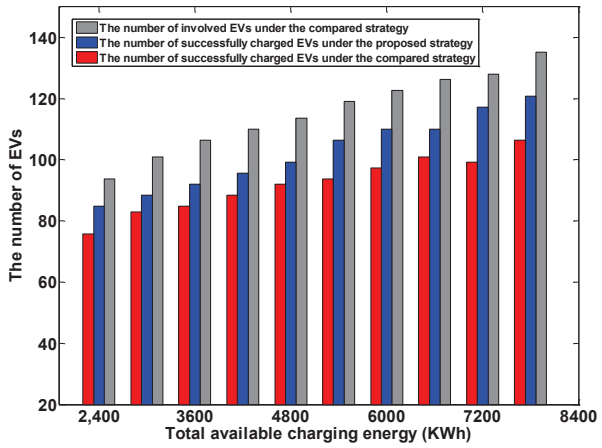

Figure 5.10. Comparison of the number of involved EVs and successfully charged EVs.

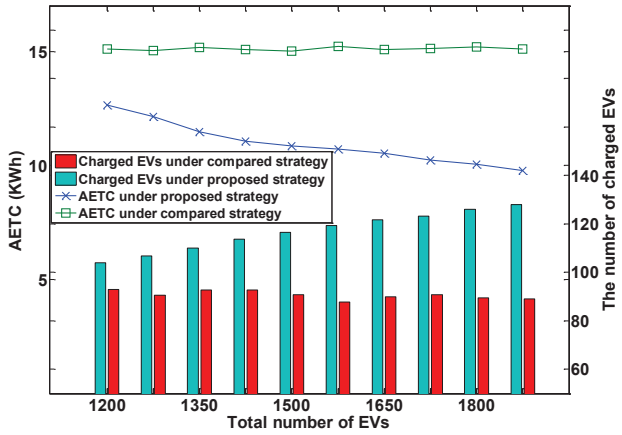

Figure 5.11. Comparison of AETC and the number of successfully charged EVs.

involved EVs' batteries may be depleted on the way under the compared strategy, the EVs that actually succeed in charging are more in the proposed strategy. Therefore, it is essential to incorporate EV mobility into the optimal charging strategy design.

Last, with fixed TACE and increasing total number of EVs, we show the comparison of the AETC performance as well as the number of successfully charged EVs in Fig. 5.11. It can be observed that when TACE is fixed and the total number of EVs increases, the AETC

of the proposed strategy decreases, and the number of successfully charged EVs increases; while both the two items remain almost unchanged under the compared strategy. As the proposed strategy considers to reduce the AETC, when the total number of EVs increases, more EVs that are closer to the charging stations are selected for charging. Thus, the AETC will decrease correspondingly. As the AETC decreases, the average battery level when the dispatched EVs arrive at the charging stations is higher, resulting in a smaller average EV charging energy. Thus more EVs can be dispatched and charged when the TACE is fixed. For the compared strategy, as it does not consider the AETC, increasing the total number of EVs has no impact on the EV selection, thus the performance remains almost unchanged.

5.6 Summary

In this chapter, considering the mobility of vehicles, with the help of vehicular communications, coordinated charging has been designed to provide efficient charging plans for EVs. The proposed charging strategy can prevent an electric power system from overloading and improve the overall energy utilization. The central philosophy of our proposed spatio-temporal coordinated charging strategy is that based on the real-time collected vehicular information, the charging requirements of the whole network can be balanced by introducing the mobility of vehicles, to increase power utilization approaching the load capacities of charging stations.

Chapter 6

Conclusions and Future Work

6.1 Conclusions

In this thesis, we evaluate the impacts of mobility on the network performance in different vehicular scenarios, i.e., pure VANETs, VANET-enhanced intelligent transportation system, and VANET-enhanced smart grid, respectively. In these scenarios, different kinds of capacities are defined, and we utilize the mobility of vehicles to improve the network throughput performance to approach the defined network capacities.

Firstly, we have analyzed the throughput capacity of VANETs for the content uploading applications in the urban area. In both the free-space propagation and non-free-space propagation environments, the achievable throughput capacity of VANETs scales as $\Theta(\frac{1}{\log n})$ decreasing with the population of vehicles n, with the number of RSUs scaling as $\Theta(\frac{n}{\log n})$. The results indicate that although more than $\Theta(\frac{n}{\log n})$ RSUs are possible to be deployed in the free-space propagation environment, the throughput cannot be greater than $\Theta(\frac{1}{\log n})$. Further, in the non-free-space propagation environment this scaling law $\Theta(\frac{1}{\log n})$ is the achievable throughput capacity as well. We have further proposed a novel two-hop forwarding scheme considering mobility diversity, to achieve that analytical throughput capacity. The simulations validate the effectiveness of the proposed scheme. The asymptotic throughput capacity in VANETs can be used as an benchmark for the real-world RSU deployment.

Secondly, we have developed a hybrid-VANET-enhanced real-time path planning for vehicles to avoid congestion and improve the vehicle-traffic throughput in an ITS. We propose a hybrid-VANET-enhanced ITS framework with functionalities of real-time traffic information collection, involving both V2V and V2R communications in VANETs and cellular communications in public transportation system. Then, a globally optimal real-time path planning algorithm is designed to improve overall spatial utilization, i.e., vehicle-traffic throughput, (to approach vehicle-traffic capacities of roads) and reduce average vehicle travel cost, by means of Lyapunov optimization. Extensive simulations have been conducted to demonstrate that the proposed path planning algorithm can achieve better performance than that without real-time path planning in terms of average moving delay as well as the adaptability to different accident durations and traffic densities.

In the third scenario of this thesis, we have incorporated the EV mobility into the EV charging and developed a VANET-enhanced coordinated EV charging strategy to improve the energy utilization (to approach load capacities of charging stations) and reduce the EV travel cost while averting the power system overloading. In specific, we first introduced a VANET-enhanced smart grid with the functionalities of real-time vehicle information collection through VANETs. Then, a predictive mobility-aware coordinated EV charging strategy was proposed to maximize the overall charging-energy-minus-travel-cost with power system overloading avoidance. Extensive simulations have been conducted to evaluate the cost incurred by the transmission delay in VANETs and demonstrate that the proposed EV charging strategy can achieve better performance than the existing strategy without considering the EV mobility and travel cost in terms of the total EV charging power, average EV travel cost and the number of successfully charged EVs.

6.2 Future Work

In future, in order to efficiently perform the applications for vehicles, there exist many challenging issues including selecting the transmission network, balancing the tradeoff between

the system technical limitations and customers' preferences, and the business revenue model for vehicles.

Network Selection for Real-time Information Delivery

In VANETs, the vehicle mobility results in intermittent V2V and V2R connections, which introduce a transmission delay and thus incur an additional travel distance (cost). While, using the cellular network for information delivery might incur additional monetary cost. Thus, by integrating both cellular networks and VANETs in the heterogeneous wireless medium, more efficient methods for message delivery can be obtained with a low-cost communication network solution, e.g., in terms of low deployment and operation costs. In such a heterogeneous wireless network, the network selection mechanism should be designed to balance a tradeoff between the travel cost due to transmission delay in VANETs and the monetary cost mainly due to cellular networks. Thus, in the future work, the design of the future wireless communication network should consider balance the VANET travel cost and the cellular network monetary cost, to make the information delivery more efficiently and economically.

Balancing the Tradeoff Between the System Technical Limitations and Preferences of Customers

Due to the mobility of vehicles, drivers usually have their own preferences for choosing a destination, e.g., a charging/swapping station. In this scenario, the preferred charging/swapping station may not be able to support any additional power loads. Thus, based on the power system overload avoidance, another charging/swapping station can be assigned to EV v charging/discharging by spatial coordination.

Since drivers prefer to maximize their preferences, there exists a tradeoff between the optimal utilization of the system (e.g., power system) and the customers' preferences. This tradeoff unveils the challenging issues of 1) how to define the preferences of individual drivers, and 2) how to balance the tradeoff between the system limitations and individual customers' preferences.

Business Revenue Model for Vehicles and Extended Large-scale Simulations

The spatial and temporal coordination introduces additional challenges. The business model established for vehicle interaction with the system should benefit both customers and system operators. Specifically, the business model should provide an incentive for drivers to use the applications designed.

In addition, we intend to find large-scale real-world vehicle traffic traces to further perform extensive simulation validations base on trace data of real-world scenarios and further digging up the implication on network design and operation.

Bibliography

[1] L. Cheng, B. E. Henty, D. D. Stancil, F. Bai, and P. Mudalige, "Mobile vehicle-to-vehicle narrow-band channel measurement and characterization of the 5.9 GHz dedicated short range communication (DSRC) frequency band," *IEEE Journal Selected Areas in Communications*, vol. 25, no. 8, pp. 1501-1516, Oct. 2007.

[2] H. T. Cheng, H. Shan, and W. Zhuang, "Infotainment and road safety service support in vehicular networking: From a communication perspective," *Mechanical Systems and Signal Processing*, vol. 25, no. 6, pp. 2020-2038, Aug. 2011.

[3] Vehicle Infrastructure Integration (VII) Program. http://www.vehicle-infrastructure.org/.

[4] http://www.nhtsa.gov/.

[5] Toyota Friend by Toyota. http://pressroom.toyota.com/releases/toyota+friend+social+network.htm.

[6] Y. Khamayseh, M. Yassein, M. Alghani, and C. Mavromoustakis, "Network Size Estimation in VANETs," *Network Protocols and Algorithms*, vol. 5, no. 3, pp. 136-152, 2013.

[7] M. Abboud, L. Jaoude, and Z. Kerbage, "Real time GPS navigation system," http://webfea-lb.fea.aub.edu.lb/proceedings/2004/SRC-ECE-27.pdf, 2004.

[8] M. Wang, H. Shan, L. X. Cai, N. Lu, X. Shen, and F. Bai, "Throughput Capacity of VANETs by Exploiting Mobility Diversity," *Proc. IEEE ICC'12*, Ottawa, Canada, June 10-15, 2012.

[9] M. Wang, H. Shan, T. H. Luan, N. Lu, R. Zhang, X. Shen, and F. Bai, "Asymptotic Throughput Capacity Analysis of VANETs Exploiting Mobility Diversity," *IEEE Trans. on Vehicular Technology*, to appear.

[10] TTI, Texas Transportation Institute: urban mobility information, 2007 Annual Urban Mobility Report. http://mobility.tamu.edu/ums.

[11] M. Papageorgiou, C. Diakaki, V. Dinopoulou, A. Kotsialos, and Y. Wang, "Review of road traffic control strategies," *Proc. The IEEE*, vol. 91, no. 12, pp. 2043-2067, 2003.

[12] T. Hunter, R. Herring, P. Abbeel, and A. Bayen, "Path and travel time inference from GPS probe vehicle data," *Proc. Neural Information Processing Systems Foundation*, Vancouver, Canada, Dec. 2009.

[13] M. Wang, H. Shan, R. Lu, R. Zhang, X. Shen, and F. Bai, "Real-Time Path Planning Based on Hybrid-VANET-Enhanced Transportation System," *IEEE Trans. on Vehicular Technology*, to appear.

[14] I. S. Bayram, G. Michailidis, M. Devetsikiotis, and F. Granelli, "Electric power allocation in a network of fast charging stations," *IEEE Journal on Selected Areas in Communications: Smart Grid Communications Series*, vol. 31, no. 7, pp. 1235-1246, Jul. 2013.

[15] TESLA Motors, [Online] Available: http://www.teslamotors.com/Pages/goelectric#.

[16] A comprehensive guide to plug-in hybrid vehicles, Hybrid Cars, [Online] Available: http://www.hybridcars.com/plug-in-hybrid-cars/#battery, 2011.

[17] Electric Power Resech Institute, [Online] Available: http://www.epri.com/Pages/Default.aspx.

[18] A. Heider and H. J. Haubrich, "Impact of wide-scale EV charging on the power suppy network," *IEE Colloqium on Electric Vehicles-A technology roadmap for the future*, vol. 6, no. 262, pp. 1-4, 1998.

[19] K. Nyns, E. Haesen, and J. Driesen, "The impact of charging plug-in hybrid electric vehicles on a residential distribution grid," *IEEE Trans. on Power System*, vol. 25, no. 1, pp. 371-380, 2010.

[20] H. Liang, B. J. Choi, W. Zhuang, and X. Shen, "Optimizing the energy delivery via V2G systems based on stochastic inventory theory," *IEEE Trans. on Smart Grid*, vol. 4, no. 4, pp. 2230-2243, 2013.

[21] P. Richardson, D. Flynn, and A. Keane, "Optimal charging of electric vehicles in low voltage distribution systems," *IEEE Trans. on Power System*, vol. 27, no. 1, pp. 268-279, 2012.

[22] J. Lopes, S. Polenz, C. Moreira, and R. Cherkaoui, "Identification of control and management strategies for LV unbalanced microgrids with plugged-in electric vehicles," *IEEE Journal of Electric Power System Research*, vol. 80, no. 8, pp. 898-906, 2010.

[23] M. Shaaban, Y. Atwa, and E. El-Saadany, "PEVs modeling and impacts mitigation in distribution networks," *IEEE Trans. on Power System*, vol. 28, no. 2, pp. 1122-1131, May 2013.

[24] D. Ban, G. Michailidis, and M. Devetsikiotis, "Demand response control for PHEV charging stations by dynamic price adjustments," *Proc. IEEE Innovative Smart Grid Technologies*, Washington DC, USA, Jan. 2012.

[25] R. C. Green, L. Wang, and M. Alam, "The impact of plug-in hybrid electric vehicles on distribution networks: a review and outlook," *Journal on Renewable and Sustainable Energy Reviews*, vol. 15, no. 1, pp. 544-553, Jan. 2011.

[26] G. T. Heydt, "The impact of electric vehicle deployment on load management strategies," *IEEE Trans. on Power Apparatus and Systems*, vol. 1, no. 144, pp. 1253-1259, 1983.

[27] M. Wang, H. Liang, R. Deng, R. Zhang, and X. Shen, "VANET based online charging strategy for electric vehicles," *Proc. IEEE GLOBECOM'13*, Atlanta, GA, USA, Dec. 2013.

[28] M. Wang, H. Liang, R. Deng, R. Zhang and X. Shen, "VANET Based Online Charging Strategy for Electric Vehicles," *Proc. IEEE Globecom'13*, Atlanta, GA, USA, Dec. 9-13, 2013.

[29] P. Gupta and P.R. Kumar, "The capacity of wireless networks," *IEEE Trans. Inform. Theory*, vol. 46, no. 1, pp. 388-404, Mar. 2000.

[30] M. Grossglauser and D. Tse, "Mobility increase the capacity of ad hoc wireless networks," *IEEE/ACM Trans. Networking*, vol. 10, no. 4, pp. 477-486, Aug. 2002.

[31] M. Neely and E. Modiano, "Capacity and delay tradeoffs for ad hoc mobile networks," *IEEE Trans. Inform. Theory*, vol. 51, no. 6, pp. 1917-1937, 2005.

[32] J. Chen, W. Xu, S. He, Y. Sun, P. Thulasiramanz, and X. Shen, "Utility-based asynchronous flow control algorithm for wireless sensor networks," *IEEE Journal Selected Areas in Communications*, vol. 28, no. 7, pp. 1116-1126, 2010.

[33] R. Dowling, A. Skabardonis, M. Carroll, and Z. Wang, "Methodology for measureing recurrent and nonrecurrent traffic congestion," *Transportation Research Record: Journal of the Transportation Research Board*, Osaka, Japan, no. 1867, pp. 60-68, 2004.

[34] M. E. Elkhatb, R. El-Shatshat, and M. Salama, "Novel coordinated voltage control for smart distribution network with DG," *IEEE Trans. on Smart Grid*, vol. 2, no. 4, pp. 598-605, 2011.

[35] P. Richardson, D. Flynn, and A. Keane, "Local versus centralized charging strategies for electric vehicles in low voltage distribution systems," *IEEE Trans. on Smart Grid*, vol. 3, no. 2, pp. 1020-1028, 2012.

[36] K. Abboud and W. Zhuang "Stochastic analysis of single-hopcommunication link in vehicular ad hoc networks," *IEEE Intelligent Transportation Systems*, vol. 15, no. 5, pp. 2297-2307, Oct. 2014.

[37] A. Abdrabou and W. Zhuang, "Probabilistic delay control and road side unit placement for vehicular ad hoc networks with disrupted connectivity," *IEEE Journal Selected Areas Communications*, vol. 29, no. 1, pp. 129-139, Jan. 2011.

[38] M. Nekoui, A. Eslami, and H. Pishro-Nik, "Scaling law for distance limited communications in vehicular ad hoc networks," *Proc. IEEE ICC*, Beijing, China, May 2008.

[39] H. Zhu, S. Chang, M. Li, K. Naik, and X. Shen, "Exploiting temporal dependency for opportunistic forwarding in urban vehicular networks," *Proc. IEEE INFOCOM*, Shanghai, China, Apr. 2011.

[40] M. Brackstone and M. McDonald, "Car-following: A historical review," *Transportation Research Part F: Psychology and Behaviour*, vol. 2, no. 4, pp. 181-196, Dec. 1999.

[41] G. Yan and S. Olariu, "A probabilistic analysis of link duration in vehicular ad hoc networks," *IEEE Trans. Intelligent Transportation Systems*, vol. 12, no. 4, pp. 1227-236, 2011.

[42] X. Chen, L. Li, and Y. Zhang, "A markov model for headway/spacing distribution of road traffic," *IEEE Trans. Intelligent Transportation Systems*, vol. 11, no. 4, pp. 773-785, Dec. 2010.

[43] P. Li, Y. Fang, and J. Li, "Throughput, delay, and mobility in wireless ad hoc networks," *Proc. IEEE INFOCOM*, San Diego, CA, Mar. 2010.

[44] M. Garetto, P. Giaccone, and E. Leonardi, "Capacity scaling in delay tolerant networks with heterogeneous mobile nodes," *Proc. ACM MobiHoc*, Montreal, QC, Canada, Sep. 2007.

[45] M. Garetto and E. Leonardi, "Restricted mobility improves delaythroughput tradeoffs in mobile ad hoc networks," *IEEE Trans. Inform. Theory*, vol. 56, no. 10, pp. 5016-5029, 2010.

[46] A. Ozgur, O. Leveque, and D. Tse, "Hierarchical cooperation achieves optimal capacity scaling in ad hoc networks," *IEEE Trans. Inform. Theory*, vol. 53, no. 10, Oct. 2007.

[47] B. Wang, J. Zhang, and L. Zheng, "Achievable rates and scaling laws of power-constrained wireless sensory relay networks," *IEEE Trans. Inform. Theory*, vol. 52, no. 9, Sep. 2006.

[48] E. Schoch, F. Kargl, M. Weber, and T. Leinmuller, "Communication patterns in VANETs," *IEEE Communications Magazine*, vol. 46, no. 11, pp. 119-125, 2008.

[49] H. Pishro-Nik, A. Ganz, and D. Ni, "The capacity of vehicular ad hoc networks," *Proc. Allerton Conference*, Allerton House, Illinois, Sep. 2007.

[50] M. Nekoui, A. Eslami, and H. Pishro-Nik, "The capacity of vehicular ad hoc networks with infrastructure," *Proc. WIOpt*, Berlin, Germany, Mar. 2008.

[51] N. Lu, H. Luan, M. Wang, X. Shen, and F. Bai, "Capacity and delay analysis for social-proximity urban vehicular networks," *Proc. IEEE INFOCOM*, Orlando, Florida, Mar. 2012.

[52] J. Herrera, D. Work, R. Herring, X. Ban, and A. Bayen, "Evaluation of traffic data obtained via GPS-enabled mobile phones: The mobiltiy century field experiment," *WORKING PAPER UCB-ITS-VWP-2009-8*, Aug. 2009.

[53] R. Herring, A. Hofleitner, and S. Amin, "Using mobile phones to forecast arterial traffic through statistical learning," *Proc. 89th Annual Meeting of Transportation Research Board*, Washington D.C., US, Jan. 2010.

[54] J. Jariyasunant, D. Work, B. Kerkez, R. Sengupta, S. Glaser, and A. Bayen, "Mobile transit trip planning with real-time data," *Proc. Transportation Research Board 89th Annual Meeting*, Washington DC, US, Jan. 2010.

[55] J. Chen and A. M. Bayen, "Traffic flow reconstruction using mobile sensors and loop detector data," *Proc. Transportation Research Board 87th Annual Meeting*, Washington DC, US, Jan. 2008.

[56] A. Skabardonis and N. Geroliminis, "Real-time monitoring and control on signalized arterials," *IEEE Journal of Intelligent Transportation Systems: Technology, Planning, and Operations*, vol. 12, no. 2, pp. 64-74, 2008.

[57] H. Liu, A. Danczyk, R. Brewer, and R. Starr, "Evaluation of cell phone traffic data in minnesota," *Transportation Research Record*, vol. 2086, no. 1, pp. 1-7, Dec. 2008.

[58] B. Hoh, M. Gruteser, and R. Herring, "Virtual trip lines for distributed privacy-preserving traffic monitoring," *Proc. 6th Annual International Conference on Mobile Systems, Applications and Services*, Breckenridge, US, June 2008.

[59] H.T. Cheng, H. Shan, and W. Zhuang, "Infotainment and road safety service support in vehicular networking: From a communication perspective," *Mechanical Systems and Signal Processing, Special Issue on Integrated Vehicle Dynamics*, vol. 25, no. 6, pp. 2020-2038, Aug. 2011.

[60] J. Zhao and G. Cao, "VADD: Vehicle-assisted data delivery in vehicular ad hoc networks," *Proc. IEEE INFOCOM*, Barcelon, Spain, Apr. 2006.

[61] T. H. Luan, X. Ling, and X. Shen, "Provisioning QoS controlled media access in vehicular to infrastructure communications," *AD HOC Networks*, vol. 10, no. 2, pp. 231-242, 2012.

[62] C. Xu, F. Zhao, J. Guan, and G. Muntean, "QoE-driven user-centric VoD services in urban multihomed P2P-based vehicular networks," *IEEE Trans. on Vehicular Technology*, vol. 62, no. 5, pp. 2273-2289, 2013.

[63] L. Zhou, Y. Zhang, K. Song, W. Jing, and A. Vasilakos, "Distributed media services in P2P-based vehicular networks," *IEEE Trans. on Vehicular Technology*, vol. 60, no. 2, pp. 692-703, 2011.

[64] A. Khosroshahi, P. Keshavarzi, Z. KoozehKanani, and J. Sobhi, "Acquiring real time traffic information using VANET and dynamic route guidance," *Proc. IEEE Computing, Control and Industrial Engineering*, Wuhan, China, Aug. 2011.

[65] P. Chen, Y. Guo, and W. Chen, "Fuel-saving navigation system in VANETs," *Proc. IEEE Vehicular Technology Conference*, Ottawa, Canada, Sept. 2010.

[66] M. Kimra, S. Inoue, Y. Taoda, T. Dohi, Y. Kakuda, "A novel method based on VANET for alleviating traffic congestion in urban transportations," *Proc. Autonomous Decentralized Systems*, Mexica City, Mexico, Mar. 2013.

[67] T. Schouwenaars, B. Moor, E. Feron, and J. How, "Mixed integer programming for multi-vehicle path planning," *Proc. European Control Conferencce*, Porto, Portugal, Sept. 2001.

[68] K. Mets, T. Verschueren, W. Haerick, C. Develder, and F. Turck, "Optimizing smart energy control strategies for plug-in hybrid electric vehicle charging," *Proc. IEEE Network Operations and Management Symposium Workshops*, Osaka, Apr. 2010.

[69] K. Clement, E. Haesen, and J. Driesen, "Coordinated charging of multiple plug-in hybrid electric vehicles in residential distribution grids," *Proc. IEEE Power Systems Conference and Exposition*, Seattle, WA, Mar. 2009.

[70] L. Kelly, "Probabilistic modeling of plug-in hybrid electric vehicle impacts on distribution networks in British Columbia," M. S. thesis, Dept. Mech. Eng., Univ. Victoria, Victoria, BC, Canada, 2009.

[71] S. Bae and A. Kwasinski, "Spatial and temporal model of electric vehicle charging demand," *IEEE Trans. on Smart Grid*, vol. 3, no. 1, pp. 394-403, 2012.

[72] K. Lee, J. Lee, Y. Yi, I. Rhee, and S. Chong, "Mobile data offloading: how much can wifi deliver?" *Proc. ACM Co-NEXT*, New York, USA, Nov. 2010.

[73] N. Lu, N. Zhang, N. Cheng, X. Shen, J. Mark, and F. Bai, "Vehicles meet infrastructure: toward capacity-cost tradeoffs for vehicular access networks," *IEEE Trans. on Intelligent Transportation Systems*, vol. 14, no. 3, pp. 1266-1277, 2013.

[74] M. Wang, H. Shan, L. X. Cai, N. Lu, X. Shen, and F. Bai, "Throughput capacity of VANETs by exploiting mobility diversity," *Proc. IEEE ICC'12*, Ottawa, Canada, June 2012.

[75] N. Lu, T. Luan, M. Wang, X. Shen, and F. Bai, "Bounds of asymptotic performance limits of social-proximity vehicular networks," *IEEE/ACM Trans. on Networking*, to appear.

[76] P. Bratanov and E. Bonek, "Mobility model of vehicle-borne terminals in urban cellular systems," *IEEE Trans. Vehicular Technology*, vol. 52, no. 4, July 2003.

[77] J. G. Andrews, R. K. Ganti, N. Jindal, M. Haenggi, and S. Weber, "A primer on spatial modeling and analysis in wireless networks," *IEEE Communications Magazine*, vol. 48, no. 11, pp. 156-163, Nov. 2010.

[78] C. Avin, Z. Lotker, F. Pasquale, and Y. Pignolet, "A note uniform power connectivity in the SINR model," *Proc. ALGOSENSORS*, Rhodes, Greece, July. 2009, pp. 116-127.

[79] R. Corless, G. Gonnet, D. Hare, D. Jeffrey, and D. Knuth, "On the Lambert W function," *Adv. Comput. Math.*, vol. 5, pp. 329-359, 1996.

[80] M. Rousan, A. AIAli, and K. Darwish, "GSM-based mobile tele-monitoring and management system for inter-cities public transportations," *Proc. IEEE International Conference on Industrial Technology*, Hammamet, Tunisia, Dec. 2004.

[81] T. Schoepflin and D. Dailey, "Dynamic camera calibration of roadside traffic management cameras for vehicle speed estimation," *IEEE Trans. on Interlligent Transportation Systems,* vol. 4, no. 2, pp. 90-98, 2003.

[82] S. Dornbush and A. Joshi, "Streetsmart traffic: Discovering and dissemination automobile congestion using VANETs," *IEEE Vehicular Technology Conference,* Dublin, Apr. 2007.

[83] A. Abdrabou and W. Zhuang, "Probabilistic delay control and road side unit placement for vehicular ad hoc netowrks with disrupted connectivity," *IEEE Journal on Selected Areas in Communications*, vol. 29, no. 1, pp. 129-139, Jan. 2011.

[84] A. May, "Traffic flow fundamentals," *Prentice Hall*, 1990.

[85] N. Wisitpongphan, F. Bai, P. Mudalige, V. Sadekar, and O. Tonguz, "Routing in sparse vehicular ad hoc networks", *IEEE Journal on Selected Areas in Communications*, vol. 25, no. 8, pp. 1538-1556, Oct. 2007.

[86] *Highway Capacity Manual (2000)*, Transportation Research Board, National Research Council, *Washington, D.C.*, 2000.

[87] H. Liang, B. J. Choi, W. Zhuang, and X. Shen, "Optimizing the energy delivery via V2G systems based on stochastic inventory theory," *IEEE Trans. on Smart Grid*, vol. 4, no. 4, pp. 2230-2243, 2013.

[88] M. Neely, *Stochastic network optimization with application to communication and queueing systems,* Morgan and Claypool Publishers, 2010.

[89] L. Georgiadis, M. Neely, and L. Tassiulas, "Resource allocation and crosslayer control in wireless networks," *Foundations and Trends in Networking,* vol. 1, no. 1, pp. 1-149, 2006.

[90] R. Urgaonkar, U. C. Kozat, K. Igarashi, and M. Neely, "Dynamic resource allocation and power management in virtualized data centers," *IEEE Network Operations and Management Symposium*, Osaka, Japan, Apr. 2010.

[91] S. Boyd and L. Vandenberghe, *Convex Optimization,* Cambridge, U.K., Cambridge Univ. Press, 2004.

[92] http://vision-traffic.ptvgroup.com/en-uk/products/ptv-vissim/.

[93] R. Guha and W. Chen, "A distributed traffic navigation system using vehicular communication," *IEEE Vehiculat Networking Conference*, Tokyo, Japan, Oct. 2009.

[94] O. Hafez, "Some aspects of microgrid planning and optimal distribution operation in the presence of electric vehicles," M. S. thesis, Dept. Electrical and Computer Eng., Univ. Waterloo, Waterloo, ON, Canada, 2011.

[95] R. Nelson, "Power requirements for batteries in hybrid electric vehicles", *IEEE Journal of Power Source*, vol. 91, no. 1, pp. 2-26, Nov. 2000.

[96] IEEE WG, *IEEE 802.11p/D2.01, Draft Amendement to Part 11: Wireless Medium Access Control (MAC) and Physical Layer (PHY) specifications: Wireless Access in Vehicular Environments*, Mar. 2007.

[97] R. Deng, Z. Yang, J. Chen, and M. Chow, "Load scheduling with price uncertainty and temporally-coupled constraints in smart grids," *IEEE Trans. on Power Systems*, 2014, to appear.

[98] R. Deng, Z. Yang, J. Chen, N. Asr, and M. Chow, "Residential energy consumption scheduling: A coupled-constraint game approach," *IEEE Trans. on Smart Grid*, 2014, to appear.

[99] M. Abboud, L. Jaoude, and Z. Kerbage, Real time GPS navigation system, http://webfea-lb.fea.aub.edu.lb/proceedings/2004/SRC-ECE-27.pdf, 2004.

[100] A. Geoffrion, "Lagrangean relaxation for integer programming," *Mathematical Programming Study*, vol. 2, pp. 82-114, 1974.

[101] M. Duran and I. Grossmann, "An outer-approximation algorithm for a class of mixed-integer nonlinear programs," *Mathematical Programming*, vol. 36, no. 3, pp. 307-339, 1986.

[102] P. Bonami, L. Biegler, A. Conn, G. Cornuejols, I. Grossmann, C. Laird, J. Lee, A. Lodi, F. Margot, N. Sawaya, and A. Wachter, "An algorithmic framework for convex mixed integer nonlinear programs," *Journal of Discrete Optimization*, vol. 5, no. 2, pp. 186-204, 2008.

[103] C. Norén and J. Pyrko, "Typical load shapes for Swedish schools and hotels," *Energy and Buildings*, vol. 28, no. 2, pp. 145-157, 1998.

[104] R. Wiedemann, "Modeling of RTI-elements on multi-lane roads," *Proc. Drive Conference*, Brussels, Belgium, Feb. 1991.

Related Publications

Journal Papers

1. **M. Wang**, H. Shan, T. H. Luan, N. Lu, R. Zhang, X. Shen, and F. Bai, "Asymptotic Throughput Capacity Analysis of VANETs Exploiting Mobility Diversity," *IEEE Trans. on Vehicular Technology*, to appear.

2. **M. Wang**, H. Shan, R. Lu, R. Zhang, X. Shen, and F. Bai, "Real-Time Path Planning Based on Hybrid-VANET-Enhanced Transportation System," *IEEE Trans. on Vehicular Technology*, to appear.

3. **M. Wang**, M. Ismail, X. Shen, E. Serpedin, and K. Qaraqe, "Spatial and Temporal Online Charging/Discharging Coordination for Mobile PEVs," *IEEE Wireless Communications Magazine*, to appear.

4. **M. Wang**, H. Liang, R. Zhang, R. Deng, and X. Shen, "Mobility-Aware Coordinated Charging for Electric Vehicles in VANET-Enhanced Smart Grid," *IEEE J. Selected Areas of Communications*, vol. 32, no. 7, pp. 1344-1360, July 2014.

5. **M. Wang**, M. Ismail, R. Zhang, X. Shen, E. Serpedin, and K. Qaraqe, "Spatio-Temporal Coordinate V2V Fast Charging Strategy for Mobile GEVs via Price Control," *IEEE J. Selected Areas of Communications*, under review.

6. **M. Wang**, Q. Shen, R. Zhang, H. Liang, X. Shen, "Vehicle-Density Based Adaptive MAC for High Throughput in Drive-Thru Networks," *IEEE Internet of Things Journal*, vol. 1, no. 6, pp. 533-543, Dec. 2014.

7. N. Lu, T. H. Luan, **M. Wang**, X. Shen and F. Bai, "Bounds of Asymptotic Performance Limits of Social-Proximity Vehicular Networks," *IEEE/ACM Trans. on Networking*, vol. 22, no. 3, pp. 812-825, June 2014.

8. R. Zhang, Z. Zheng, **M. Wang**, X. Shen, and L. Xie, "Equivalent Capacity in Carrier Aggregation-Based LTE-A Systems: A Probabilistic Analysis," *IEEE Trans. on Wireless Communications*, vol. 13, no. 11, pp. 6444-6460, 2014.

9. R. Zhang, **M. Wang**, X. Shen, and L. Xie, "Probabilistic analysis on QoS Provisioning for Internet of Things in LTE-A Heterogeneous Networks with Partial Spectrum Usage," *IEEE Internet of Things over LTE/LTE-A networks*, under review.

Conference Papers

1. R. Zhang, **M. Wang**, L. Cai, Z. Zheng, X. Shen, and L. Xie, "Modeling and Analysis of a MAC Protocol for LTE-U Co-existing with Wi-Fi," *Proc. IEEE Globecom'15*, under review.

2. **M. Wang**, M. Ismail, R. Zhang, X. Shen, E. Serpedin, and K. A. Qaraqe, "A Semi-Distributed V2V Fast Charging Strategy based on Price Control," *Proc. IEEE Globecom'14*, (**Best paper awards**), Austin, USA, Dec.8-12, 2014.

3. R. Zhang, **M. Wang**, Z. Zheng, X. Shen, and L. Xie, "Stochastic Geometric Performance Analysis for Carrier Aggregation in LTE-A Systems," *Proc. IEEE ICC'14*, Sydney, Australia, June 10-14, 2014.

4. R. Zhang, **M. Wang**, Z. Zheng, X. Shen, and L. Xie, "Cross-Layer Carrier Selection and Power Control for LTE-A Uplink with Carrier Aggregation," *Proc. IEEE Globecom'13*, Atlanta, GA, USA, Dec. 9-13, 2013.

5. R. Zhang, Z. Zheng, **M. Wang**, X. Shen, and L. Xie, "Equivalent Capacity Analysis of LTE-Advanced Systems with Carrier Aggregation," *Proc. IEEE ICC'13*, Budapest, Hungary, June 9-13, 2013.

6. **M. Wang**, H. Liang, R. Deng, R. Zhang and X. Shen, "VANET Based Online Charging Strategy for Electric Vehicles," *Proc. IEEE Globecom'13*, Atlanta, GA, USA, Dec. 9-13, 2013.

7. **M. Wang**, H. Shan, L. X. Cai, N. Lu, X. Shen, and F. Bai, "Throughput Capacity of VANETs by Exploiting Mobility Diversity," *Proc. IEEE ICC'12*, Ottawa, Canada, June 10-15, 2012.

8. N. Lu, T. H. Luan, **M. Wang**, X. Shen, and F. Bai, "Capacity and Delay Analysis for Social-Proximity Urban Vehicular Networks," *Proc. IEEE INFOCOM'12*, Orlando, Florida, USA, March 25-30, 2012.

Vita

Miao Wang received her B.Sc. degree from Beijing University of Posts and Telecommunications and M.Sc. degree from Beihang University, Beijing, China, in 2007 and 2010, respectively. She is currently working toward the Ph.D. degree with the Department of Electrical and Computer Engineering, University of Waterloo, Waterloo, ON, Canada. Her current research interests include the capacity and delay analysis in vehicular networks and electrical vehicle charging control in smart grids.